Hard X-ray imaging with Synchrotron Radiation

Giuliana Tromba

SYnchrotron **R**adiation for **ME**dical **P**hysics (SYRMEP) beamline

Elettra - Sincrotrone Trieste

I on-line edition of the
International School on Synchrotron Radiation
"Gilberto Vlaic":
Fundamentals, Methods and Applications

SOCIETA' ITALIANA DI LUCE DI SINCROTRONE

Elettra Sincrotrone Trieste

Outline

- Potentials and advantages of SR for hard X-ray imaging
- SR based techniques
  - K-Edge subtraction imaging
  - *Phase sensitive (phase contrast)* techniques
- Dynamic and multiscale imaging and tomography
- Some applications (biomedicine, biology, materials science, cultural heritage)

Advantages of SR for hard X-ray imaging

Monochromaticity allows for:

- *optimization* of X-ray energy according to the specific case under study (dose reduction)
- quantitative CT evaluations
- no beam hardening
- convenient use of contrast agent (**K-edge subtraction imaging**)

Spatial coherence

- Phase contrast overcomes the limitation of conventional radiology (it enables the applications of ***phase contrast techniques)***
- It brings to a dose reduction
- Improved contrast resolution, edges enhancement
- Use of phase retrieval algorithms to separate phase from absorption contribution

High fluxes

- Short exposure time
- Dynamic studies….

Collimation

- parallel beams, scatter reduction
- beam shaping (micro-beams)

Elettra Sincrotrone Trieste

SR X-rays imaging techniques

1) K-Edge Subtraction (KES) imaging

<u>Reference:</u>

K-edge subtraction synchrotron X-ray imaging in bio-medical research
W.Thomlinson, H.Ellaume, L.Porra, P.Suortti

Phys Med 2018 May;49:58-76. doi: 10.1016/j.ejmp.2018.04.389.

The paper reviews the development of the KES techniques and technology as applied to bio-medical imaging from the early low-power tube sources of X-rays to the latest high-power synchrotron sources.

<u>Exploiting the monochromaticity of SR…</u>

K-Edge Subtraction (KES) Imaging

1. Contrast agent: Iodine, or Gadolinium, etc.
2. Two Images are acquired: just Above (A) and just Below (B) the K-edge of Contrast agent
3. From image processing : Iodine and Tissue images can be separated

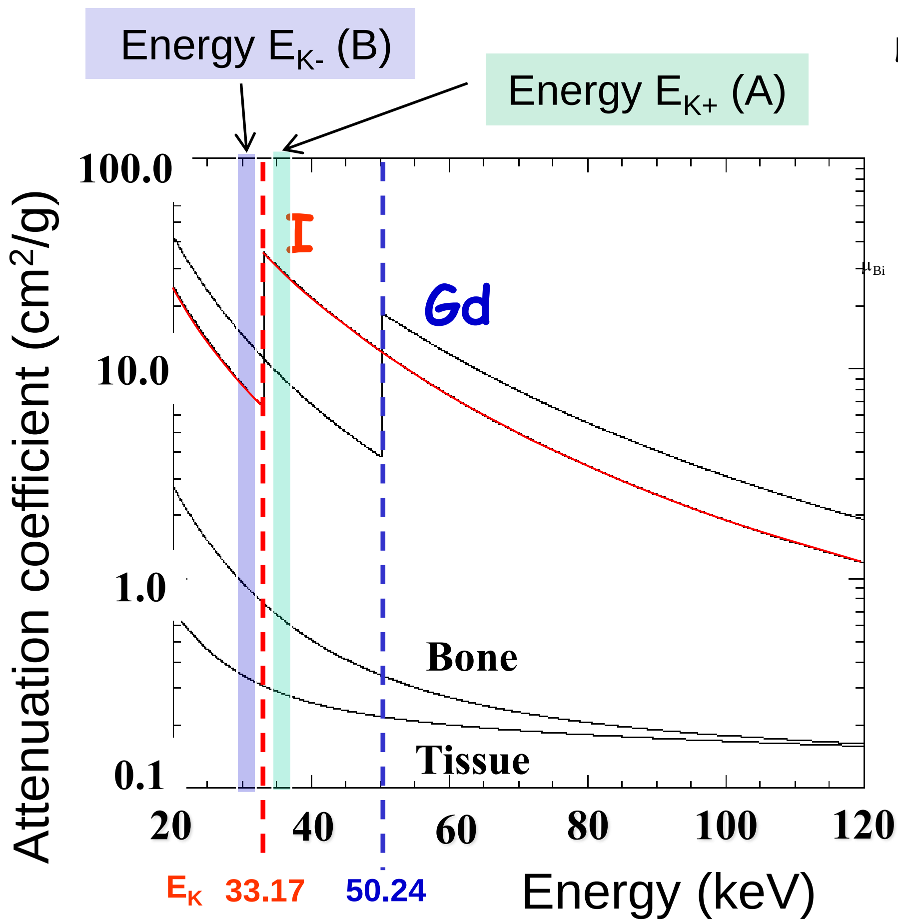

μ_{xy} : Attenuation coefficients : x = energies (A or B), y = material (tissue (t) or iodine (i)).

$$x_i = \frac{\mu_{Bi} \ln(A) - \mu_{Ai} \ln(B)}{\mu_{Bi}\,\mu_{At} - \mu_{Ai}\,\mu_{Bt}}$$

$$x_t = \frac{\mu_{Bi} \ln(A) - \mu_{Ai} \ln(B)}{\mu_{Bi}\,\mu_{At} + \mu_{Ai}\,\mu_{Bt}}$$

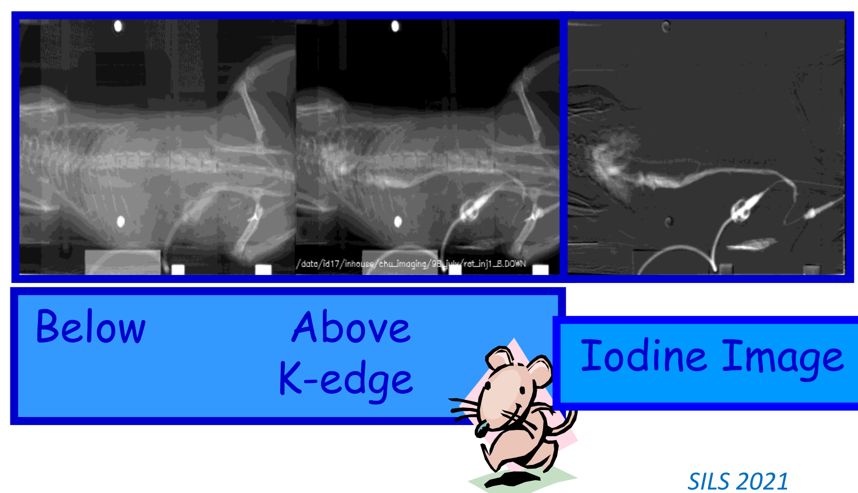

Bronchography - CT imaging at ESRF

Dual Line Ge Detector

w: 150 mm, 350 μm pitch, beam thickness 700 μm

Used contrast agent: Xenon (gas)

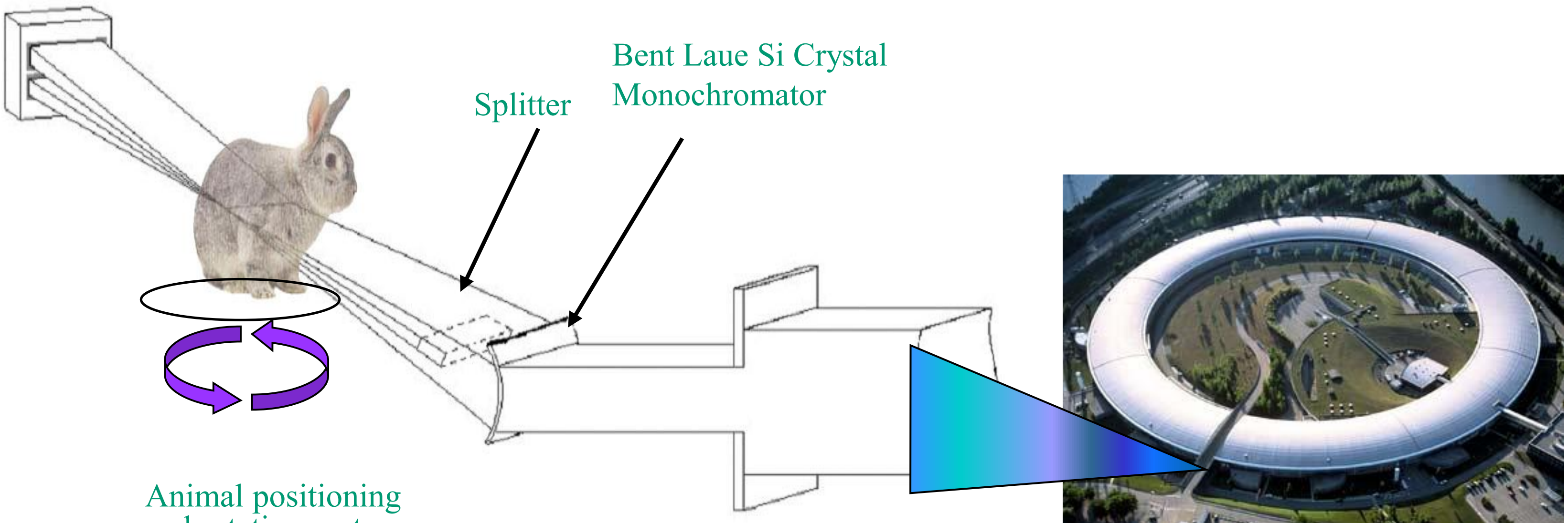

Image Processing

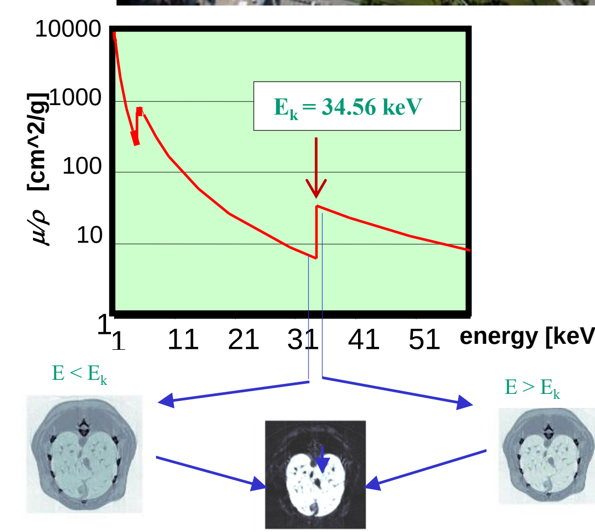

Projection Images
In Vivo Rabbit Lung
Xenon K-edge Imaging

Lung ventilation studies
Presence of ventilation heterogeneities

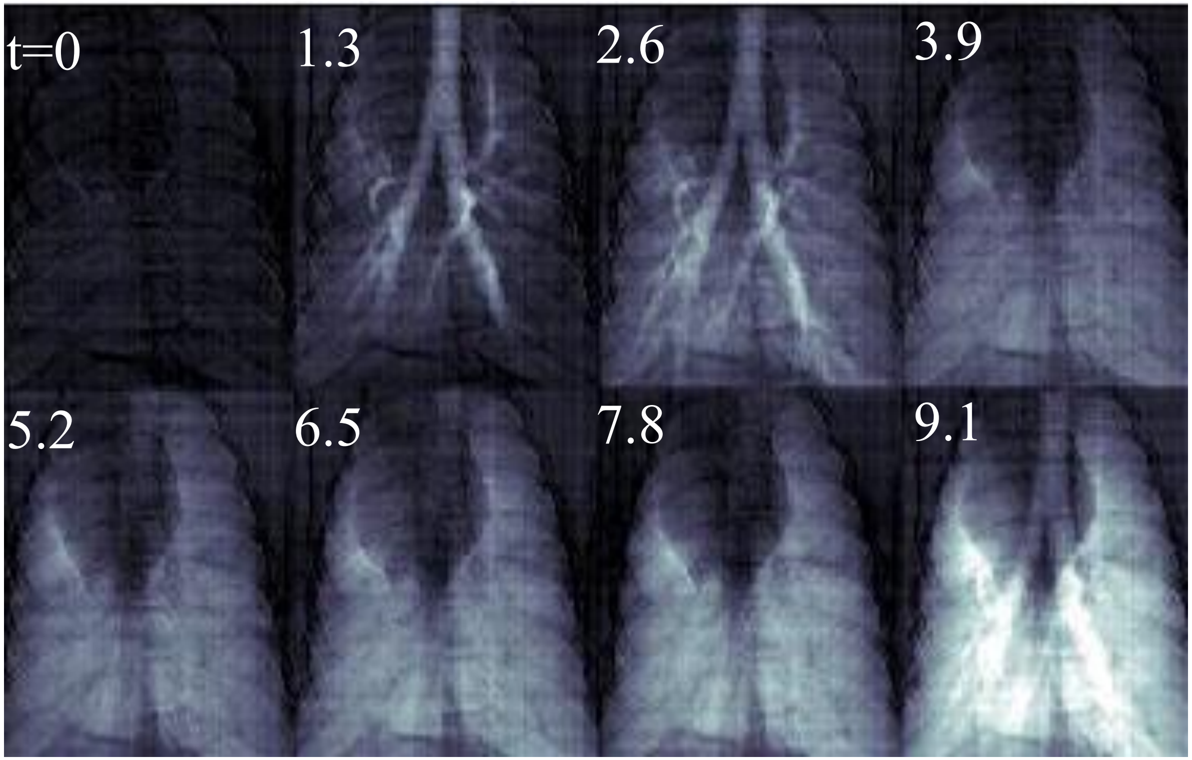

Time between images = 1.3 sec

Courtesy of A.Bravin (ESRF)

Effects on lungs ventilation induced by different treatments on healthy or asthmatic animals

KES CT studies have been carried out to evaluate allergic reactions induced by ovalbumine in a rabbit **rabbit model**. These allergic reactions were compared with asthma reactions caused by non-specific drug provocation (Methacholine, Mch).

Mch caused **airway narrowing** mainly on the central large airways, while ovalbumine induces **a predominantly peripheral and heterogeneous lung response**.

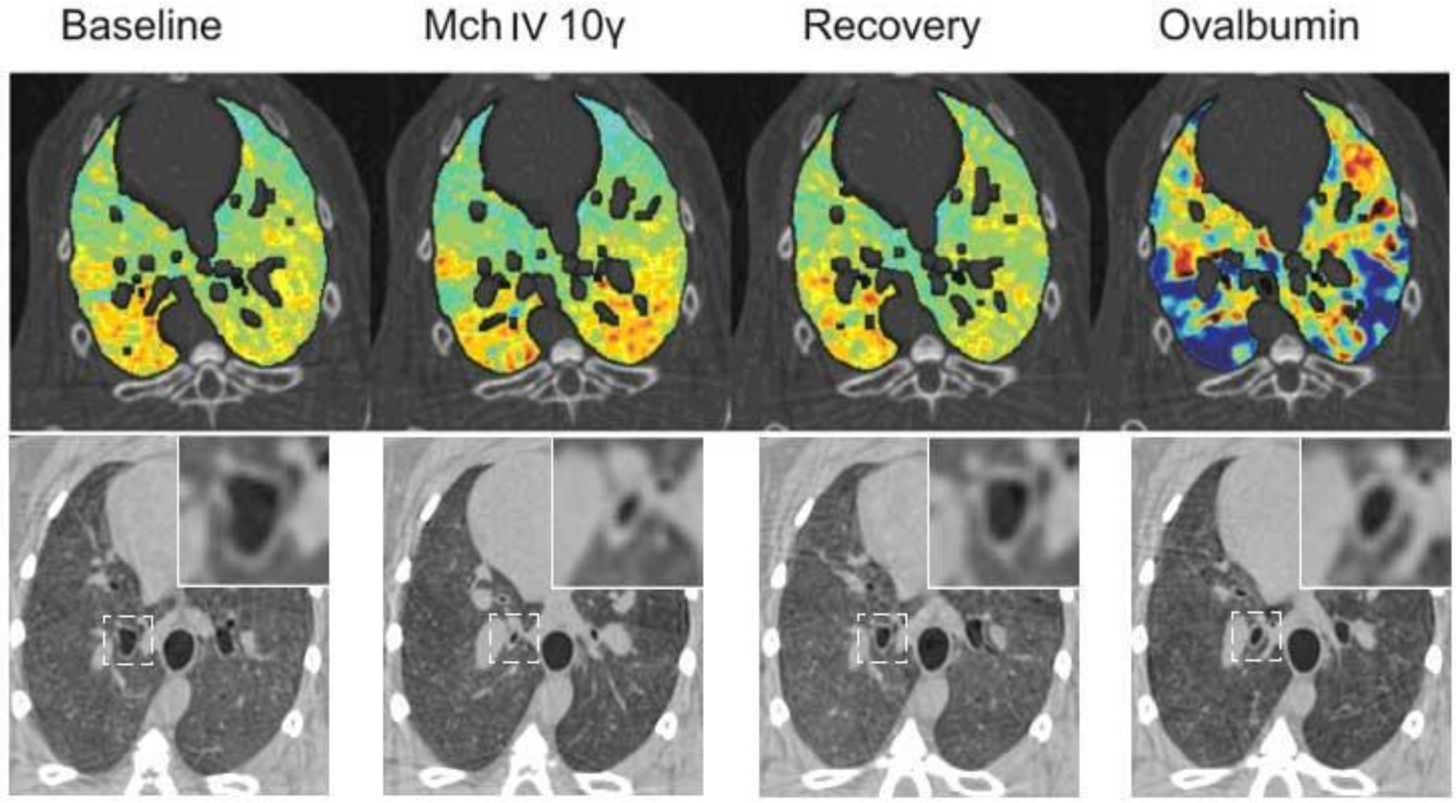

Upper part: **images of specific ventilation** in a sensitized rabbit at baseline, during Mch infusion, upon recovery and after Ovalbumine allergen provocation. Lower part: **absorption CT slices** showing changes in the central airway cross-sectional area at the different experimental stages in one representative animal. Magnifications of the indicated square areas are shown in the right-upper corners.

 Bayat S. et al:, Am J Respir Crit Care Med.180(4) (2009). *Courtesy of S.Bayat (INSERM-Univ. Grenoble)*

Study of aerosol particle deposition on in-vivo rabbits- quantitative imaging of contrast agents.

- To evaluate the inhaled **aerosol particle distribution and targeting** in the lung, knowledge of **regional deposition**, **lung morphology** and **regional ventilation**, is needed
- KES imaging was used to quantitatively map the regional deposition of **iodine labelled aerosol particles**
- 2 X-ray beams tuned at slightly different energies above and below the K-edge, of **Xe (34.6 keV)** or **Iodine (33.2 keV)**
- Two CT scans are simultaneously acquired during the **inhalation of stable Xe gas** or **iodine-stained aerosol particles**. The density due to the contrast element (**Xe, I**) can be separated from that of tissue, in each image.
- **"Xe-density" or "I-density" images allow the direct quantitative measurement of these elements within the airways.**
- **A "tissue-density" image obtained from the same data allows the assessment of lung morphology.**

Iodine Aerosol Deposition on *In Vivo* Rabbit

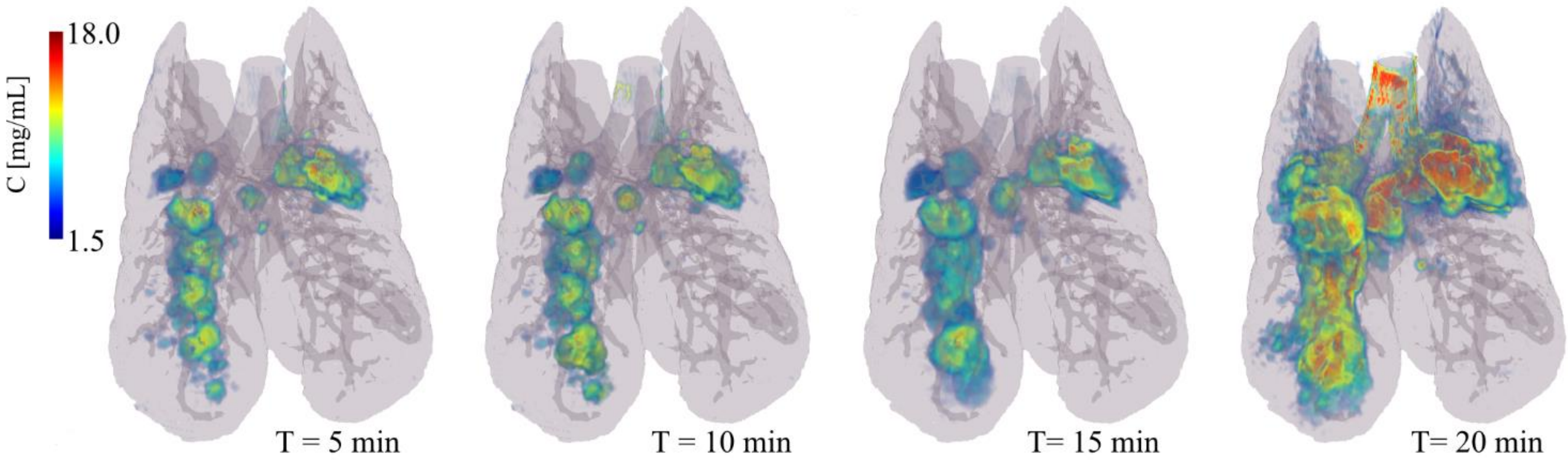

- Aerosol particles with 3 µm mass median aerodynamic diameter -> inhomogenous deposition !
- Comprehensive technique for studying biodistribution of inhaled drugs/pollutants

Courtesy of S.Bayat (INSERM-Univ. Grenoble)

 Porra L. et al. Scientific Reports. 2018:8:3519 DOI:10.1038/s41598-018-20986-x

Elettra
Sincrotrone
Trieste

2 - *Phase – sensitive* imaging techniques

Reference:

An overview of the evolution and key features of various hard X-ray PHC methods in connection with translation to a wide range of imaging applications can be found in the paper:

On the evolution and relative merits of hard X-ray phase-contrast imaging methods

S. W. Wilkins, Ya. I. Nesterets, T. E. Gureyev, S. C. Mayo, A. Pogany and A. W. Stevenson

Phil. Trans. R. Soc. A 2014 **372**, 20130021, published 27 January 2014

Exploiting the spatial coherence of SR…

Phase sensitive techniques (PHase Contrast (PHC) imaging)

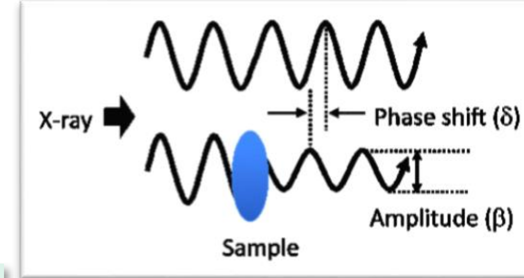

- Conventional imaging relies on **X-ray absorption**
- Phase contrast imaging is based on the detection of **phase shifts** occurring to X-rays crossing the sample

Complex refractive index: $n = 1-\delta+i\beta$, $\beta << \delta$
Linear attenuation of X-rays: $\mu = 4\pi\beta/\lambda$ (λ = X-ray wavelength)
Transmitted beam intensity: $I = I_0\, e^{-\mu t}$ (I_0 = incident intensity) - **absorption contrast**
Phase shifts: $\phi = -2\pi\delta t/\lambda$ (t=sample thickness)- **phase contrast**

Propagation based imaging (PBI) - Simplest approach – no optical element needed.Contrast arises from interference among parts of the wave front differently deviated (or phase shifted) by the sample.
Edge enhancement effects, different regimes according to the selected sample-to-detector distance.

PHC regimes

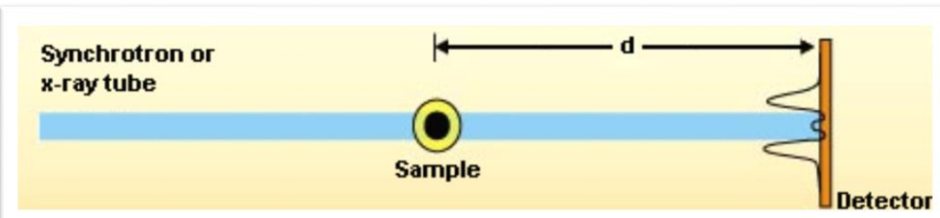

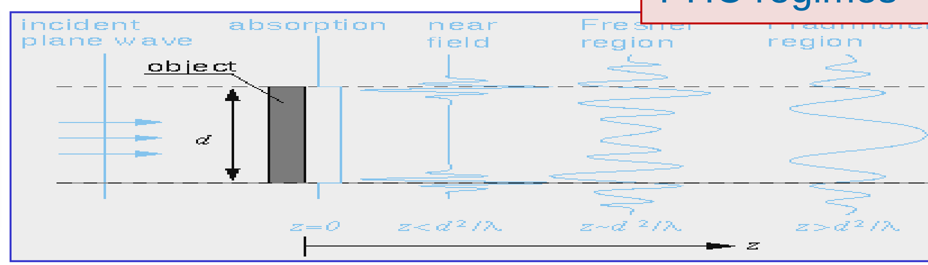

Absorption (z = 0)

Near field (z = 50 cm)

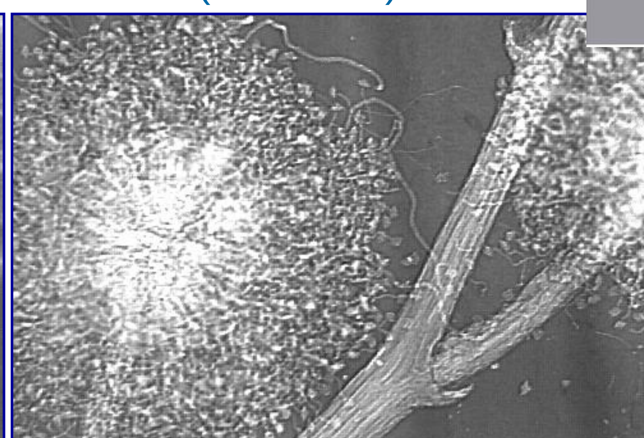

Edge enhancements effects – trend with X-ray energy

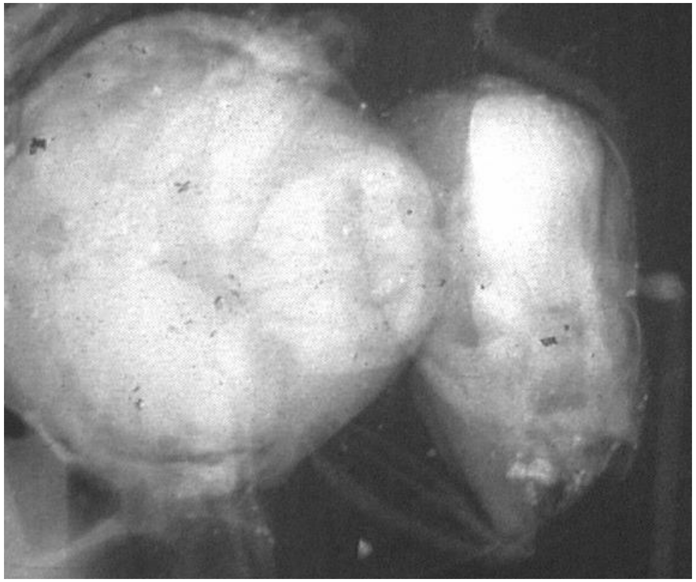

10 keV

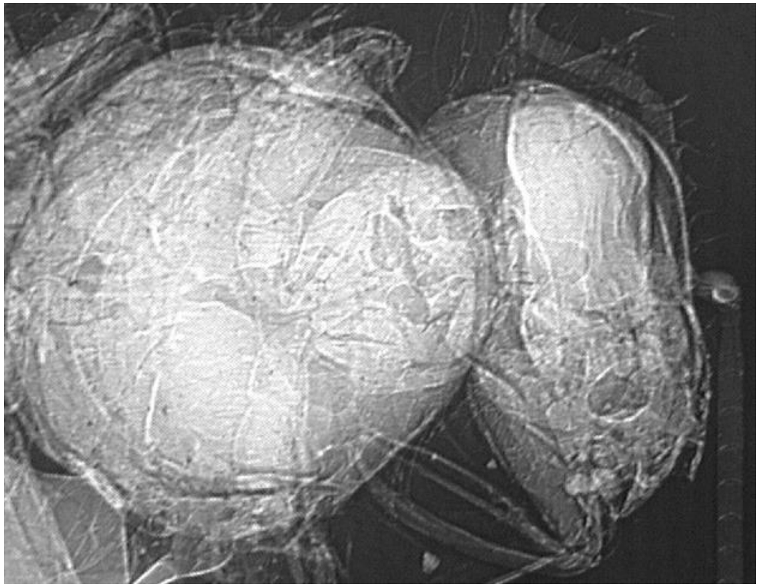

Absorption

Phase Contrast

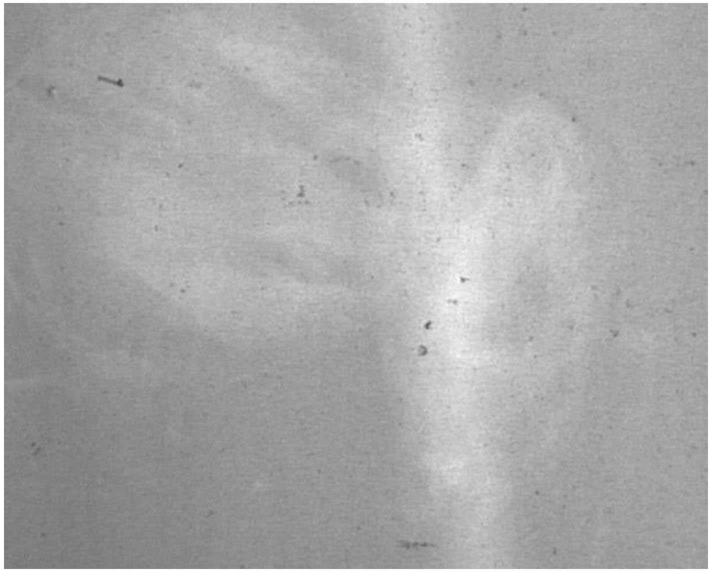

20 keV

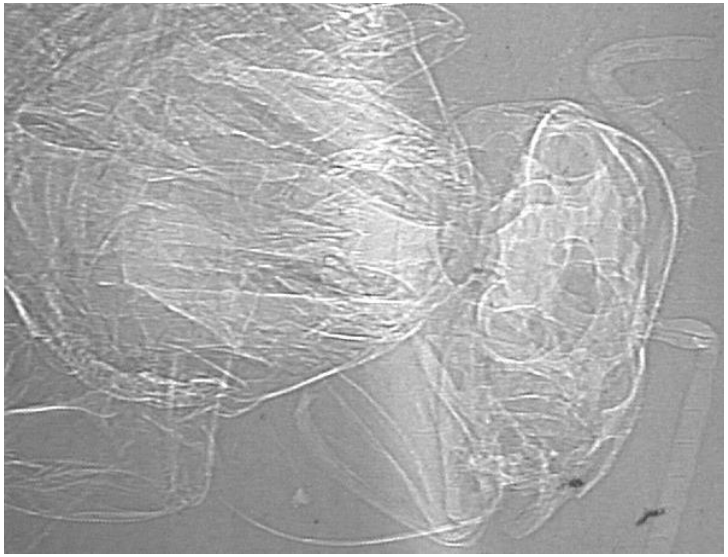

Elettra Sincrotrone Trieste

Edge enhancement effect and use of phase retrieval algorithms

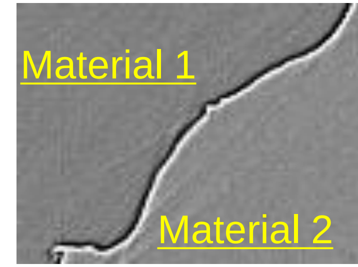

Edge between two materials with negligible absorption

An “edge” image obtained by PBI imaging does not resolve unambiguously the structure of the imaged sample

Complex refractive index: $n = 1 - \delta + i\beta$

phase

attenuation

Instead of “edge contrast” we would like “area contrast” (ideally a map of δ)
The approach to get the “area contrast” is called *phase retrieval* and two main approches exist:

- **Holotomography** - (P. Cloetens et al., ESRF) - quantitative approach with identification of material components, it requires multiple distances acquisition
- **Single-distance** – approximated, working on homogeneus materials in the near field conditions has the advantage to require acquisition at one distance (D. Paganin – Monash Univ.) – preferable for biomedical imaging

Edge contrast – PHC

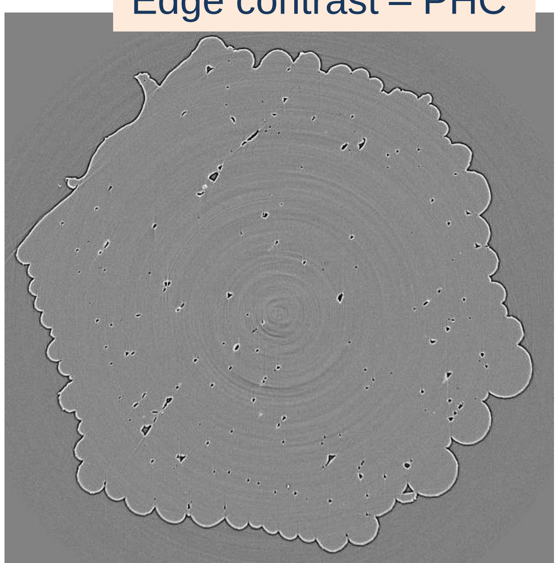

Typical edge enhancement features of PHC

Area contrast

Application of phase retrieval (Single distance algorithm)

*Paganin D., et al., J Microsc **206**, 33–40 (2002).*

P. Cloetens et al., Appl. Phys. Lett. 75, 2912 (1999)

Elettra Sincrotrone Trieste

PHC imaging: other approaches

Methods exploiting the particle nature of photons – measure of X-ray refraction angles

Analyzer Based Imaging
Use of perfect crystals to select angular directions of X-rays exiting the sample

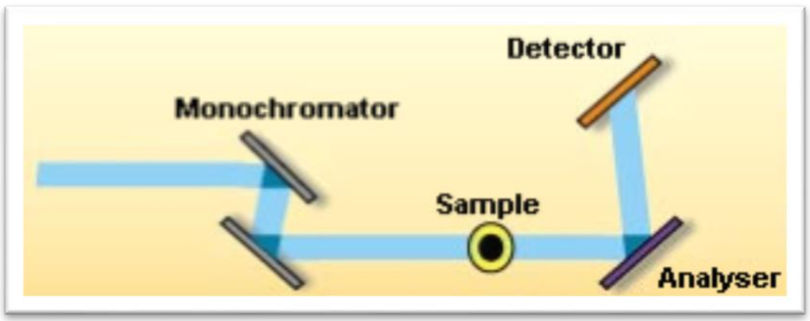

Coded Apertures
Use of coded apertures (masks) to select refraction angles

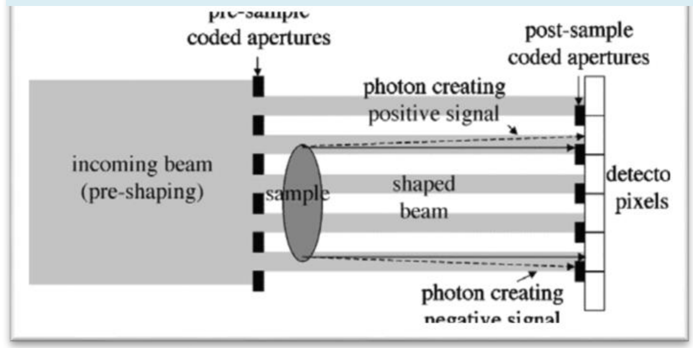

Interferometric approaches - waves are superimposed in order to extract information - direct measure of phase shifts introduced by the sample

Crystal Interferometry

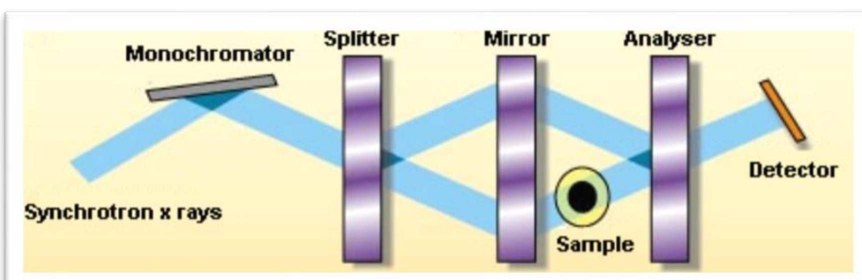

Grating interferometry

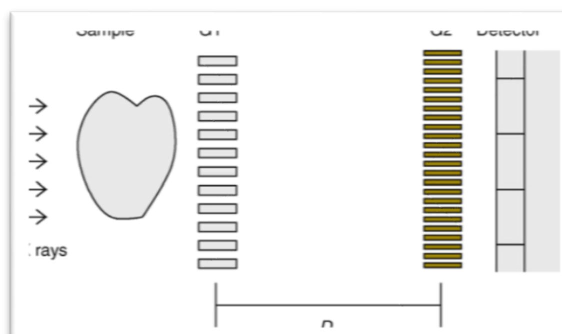

Analyzer Based Imaging (ABI)

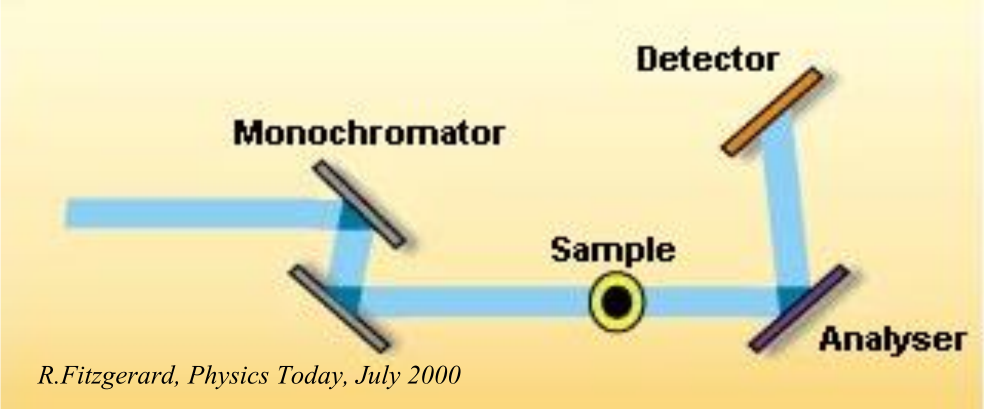

- A perfect crystal is used as an angular filter to select angular emission of X-rays. The filtering function is the rocking curve (FWHM: 1-20 μrad)
- Image formation with ABI is sensitive to a variation of δ in the sample. Indeed, **refraction angle is roughly proportional to the gradient of δ**
- Analyzer and monochromator aligned -> X-ray scattered by more than some tens μrad are rejected
- Small misalignments -> investigation of phase shift effects
- With greater misalignments the primary beam is almost totally rejected and pure refraction images are obtained
- Sensitive to $\nabla\Phi(x,y)$
- The technique requires the beam monochromaticity.

Podurets K. M. et al., Sov. Phys. Tech. Phys. 34(6), 1989
V. N. Ingal and E. A. Beliaevskaya, J. Phys. D: Appl. Phys. 28, 1995
Chapman D et al., Phys. Med. Biol. 42, 1997

Elettra Sincrotrone Trieste

ABI images for different analyzer positions

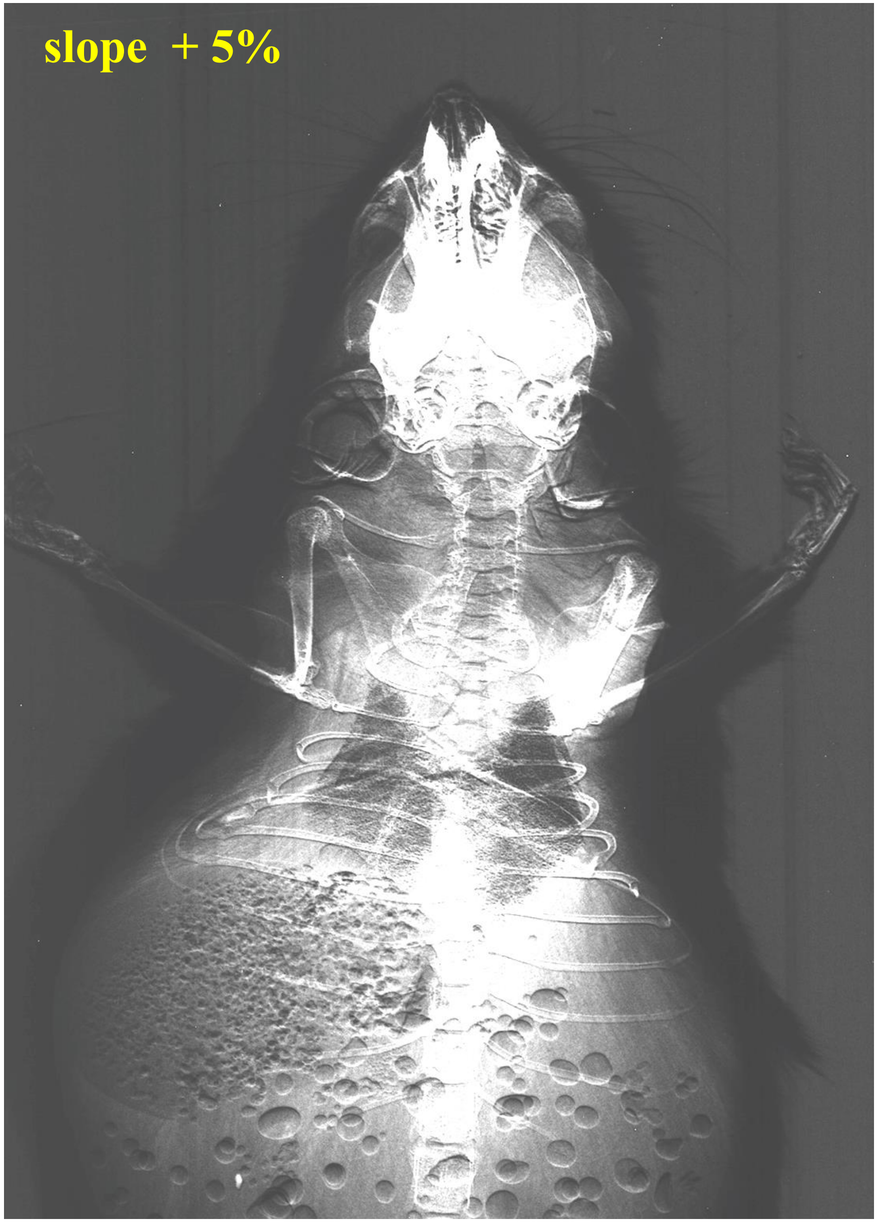

ABI image manipulation (original algorithm)

I_L

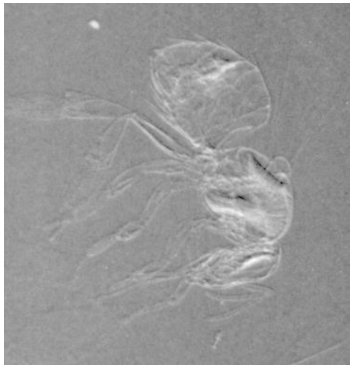

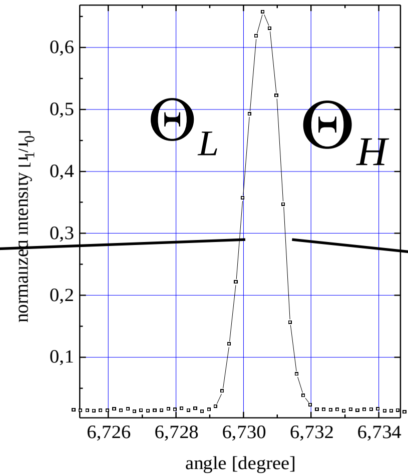

I_H

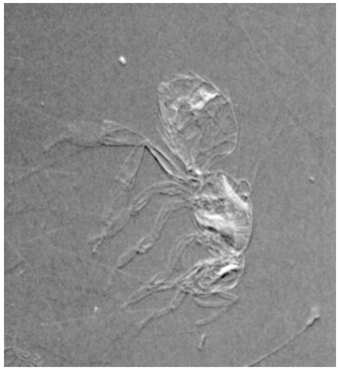

Linear approximation of rocking curve at half values (I_R and I_L)

$$I_L = I_R\left(R(\Theta_L) + \frac{\partial R}{\partial \Theta}(\Theta_L)\Delta\Theta_z \right)$$

$$I_H = I_R\left(R(\Theta_H) + \frac{\partial R}{\partial \Theta}(\Theta_H)\Delta\Theta_z \right)$$

Θ_Z = refraction Image

I_R = apparent absorption image (absorption+extinction)

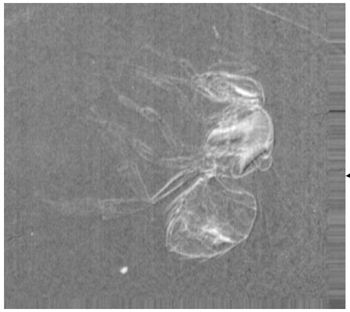

Apparent Absorption Image

$$I_R = \frac{I_L \cdot \left.\frac{dR}{d\Theta}\right|_{\Theta_H} - I_H \cdot \left.\frac{dR}{d\Theta}\right|_{\Theta_L}}{R(\Theta_L)\cdot \left.\frac{dR}{d\Theta}\right|_{\Theta_H} - R(\Theta_H)\cdot \left.\frac{dR}{d\Theta}\right|_{\Theta_L}}$$

$$\Theta_Z = \frac{I_H \cdot R(\Theta_L) - I_L \cdot R(\Theta_H)}{I_L \cdot \left.\frac{dR}{d\Theta}\right|_{\Theta_H} - I_H \cdot \left.\frac{dR}{d\Theta}\right|_{\Theta_L}}$$

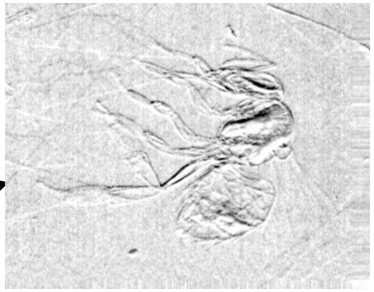

Refraction Image

Ref: Chapman et al, Phys.Med.Biol, 42,1997

Apparent absorption and refraction images

Apparent absorption

Refraction image

Computed micro-Tomography setup

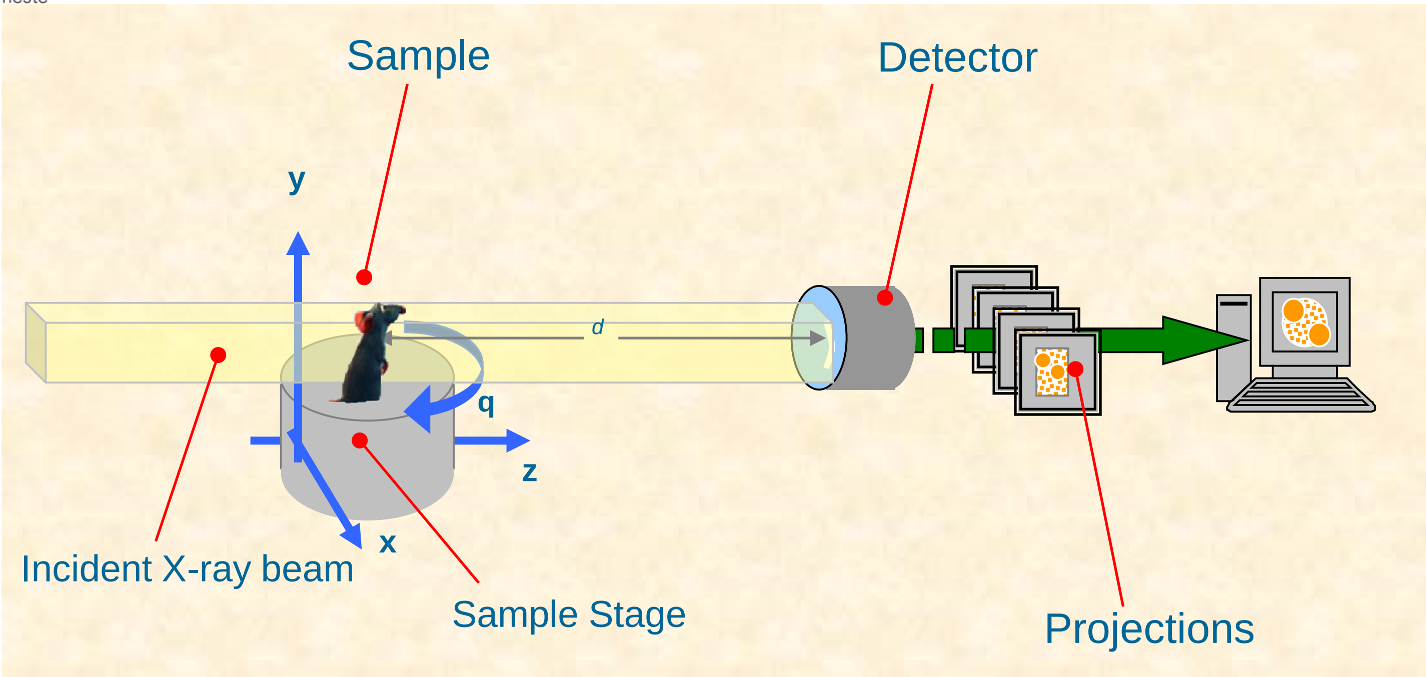

- *In material science: not destructive tool to study the **internal features** of the sample*
  - It dose not require any sample preparation
  - the sample can be after studied by other experimental techniques, or submitted to several treatments (mechanical, thermal, etc...)
  - access to quantitative information on the *density maps* of the irradiated volumes
- *In biomedical imaging: suited for in vivo imaging on small animals (taking into consideration the radiation dose!!)*

- Projections are elaborated using the Filtered Back Projection algorithm (*Herman,* 1980) to reconstruct multiple slices of the sample under study
- Phase retrieval pre-processing algorithms can be applied to decouple phase from absorption
- Slices are stacked to create volumes and rendered for visualization
- Volumes can be elaborated by custom adapted Digital Image Processing procedures

Elettra Sincrotrone Trieste

Reconstructed slices can be used to visualize the inner structure of the sample and extract quantitative parameters

University of Bologna
Physics Department

ISTITUTI ORTOPEDICI RIZZOLI

10 cm

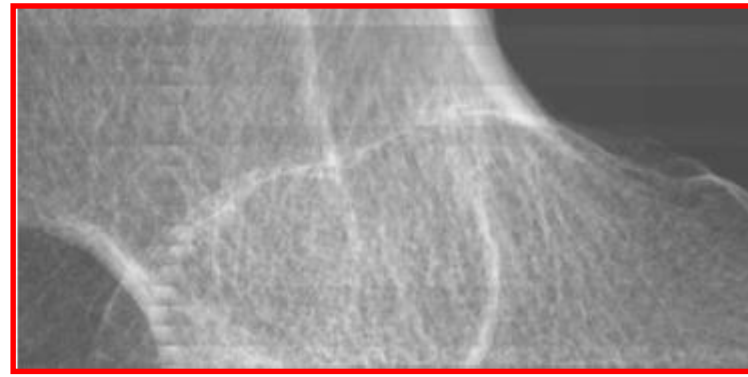

E = 34 keV

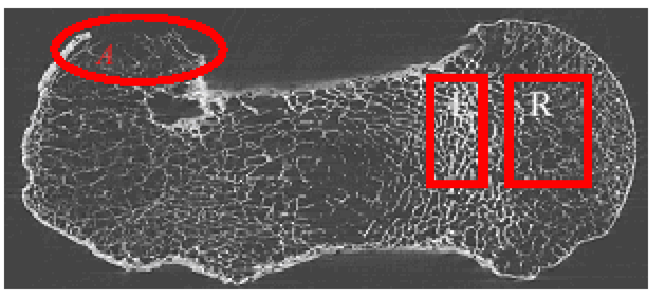

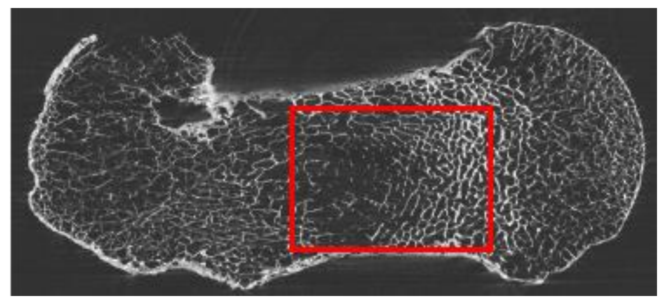

	BV/TV [%]	Tb.Th [μm]	Tb.N [mm^{-1}]	Tb.Sp [μm]
Left ROI	21.4±0.3	167±2	1.28±0.03	610±20
Right ROI	13.8±0.2	120±1	1.17±0.02	740±10

	BV/TV [%]	Tb.Th [μm]	Tb.N [mm^{-1}]	Tb.Sp [μm]
Big ROI	17.5±0.2	122±2	1.44±0.02	576±8

LEGENDA:
BV/TV – Bone Volume/Tissue Volume
Tb.Th – Trabecular thickness
Tb.N – Trabecular Number
Tb.Sp – Trabecular Space

A. Pasini et al., Proceedings of IEEE NSS/MIC 2004 Annual meeting, Rome, Italy

Application of K-Edge subtraction and Phase contrast imaging:

- Mapping metal intake in plants

PHC and K-edge imaging: Mapping of the metal intake in plants by X-ray micro-radiography and tomography

- **Accumulation of metals**, such as **Cu, Zn, As, Cd, Pb, Hg**, **in the environment** is a high health risk because of the possibility for these elements to be transferred to living organisms through fresh water or vegetables.

- **Among the different solutions**, a frequently used **method** is **phytoremediation**: it consists in the removal of contaminants by means of their absorption and accumulation in roots and leaves of plants, specially cultivated for this purpose and then harvested. Also transgenic plants have been obtained, with higher accumulation properties.

- **To face these problems**: detection of contaminants, comparison of accumulation properties of the various plants, mapping of possible biological structures accumulating specific metals within a tissue.

- We used **dual-energy micro-radiography** taking advantage of the highly-monochromatic, large-field synchrotron radiation to detect the heavy-metal accumulation in 2D and 3D biological samples.

J. Kaiser et al., Eur. Phys. J. D 32, 113–118 (2005)

Mapping of the metal intake in plants by dual energy micro-CT

***Dyplotaxis erucoides* root grown in 2% $CuSO_4$ solution**

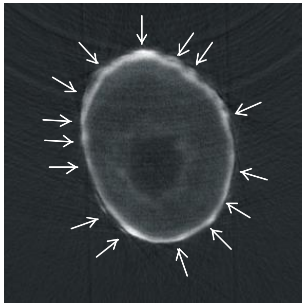

E = 9.05 and 8.90 keV

difference

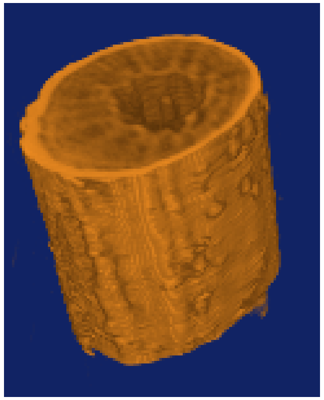

h = 1 mm

∅ ca. 3 mm

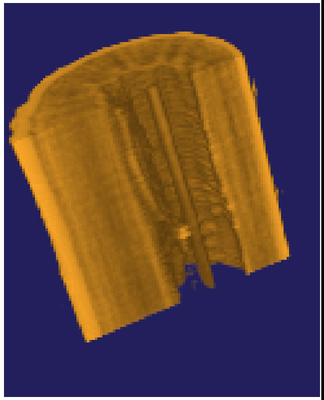

3D rendering

***Helianthuus annuus* leaf treated in a 10 mM $PbSO_4$ solution**

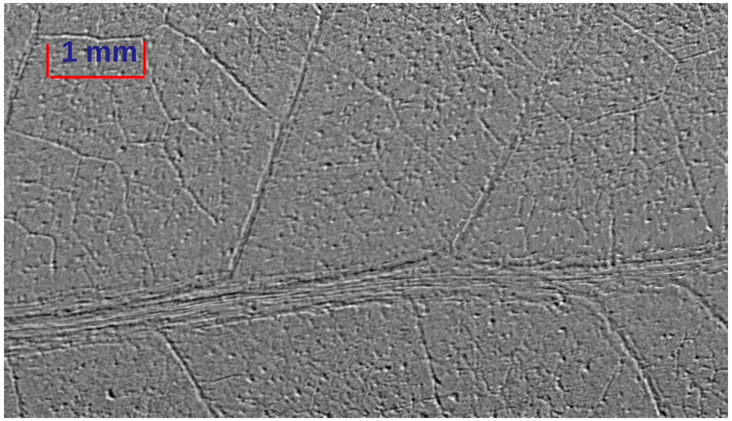

E = 13.150 and 12.975 keV

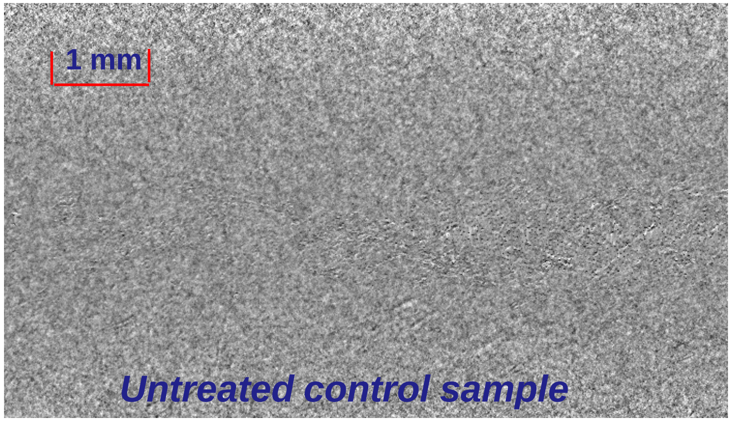

J. Kaiser et al., Eur. Phys. J. D 32, 113–118 (2005)

Pb detection by dual energy and phase contrast imaging in Helianthus annuus leaf

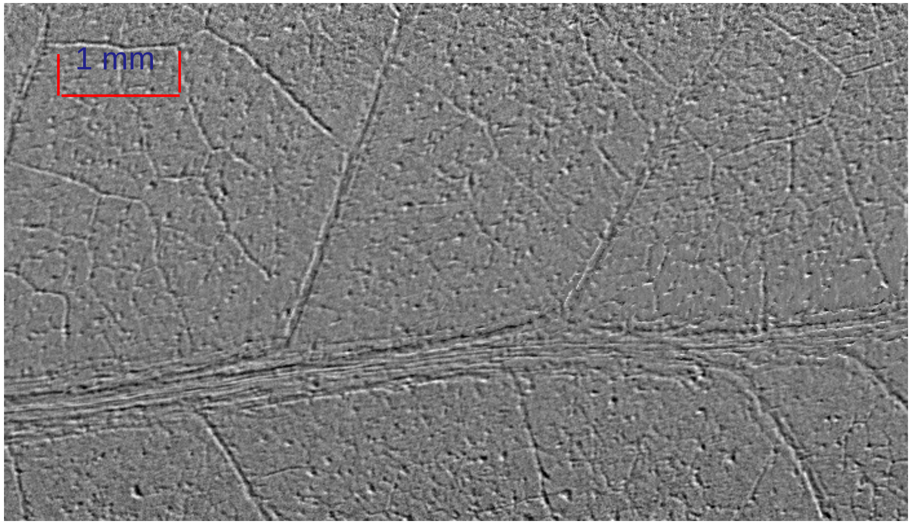

10 mM $PbSO_4$ treated sample

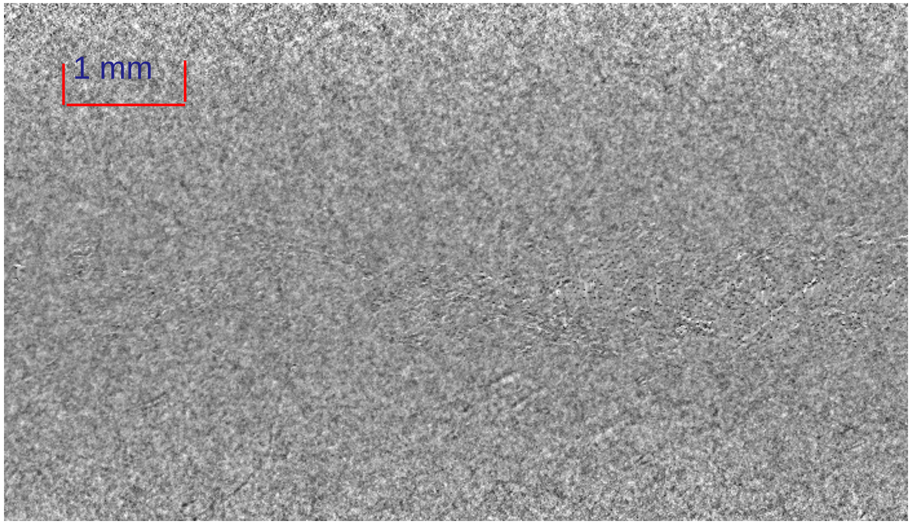

Untreated control sample

E = 13.150 and 12.975 keV

D =168cm

J. Kaiser et al., Eur. Phys. J. D 32, 113–118 (2005)

Cu detection by dual energy and phase contrast imaging in Phaseolus vulgaris leaf

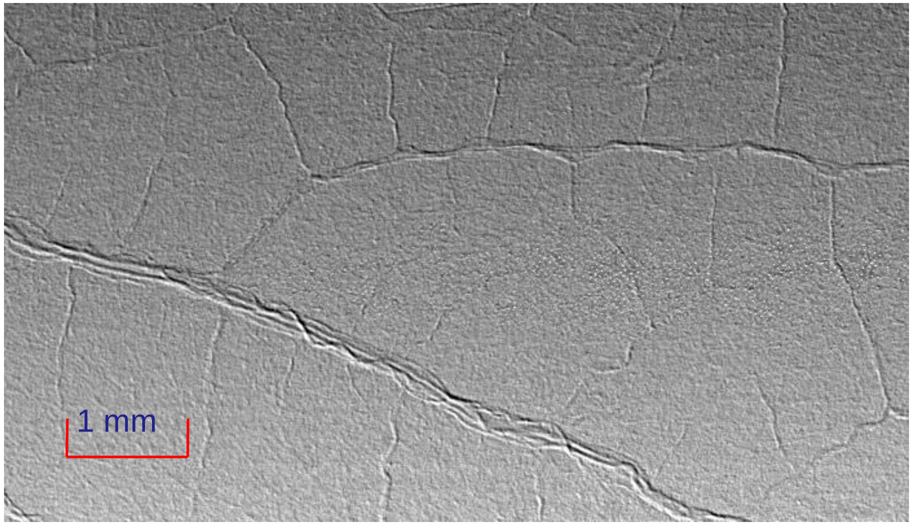

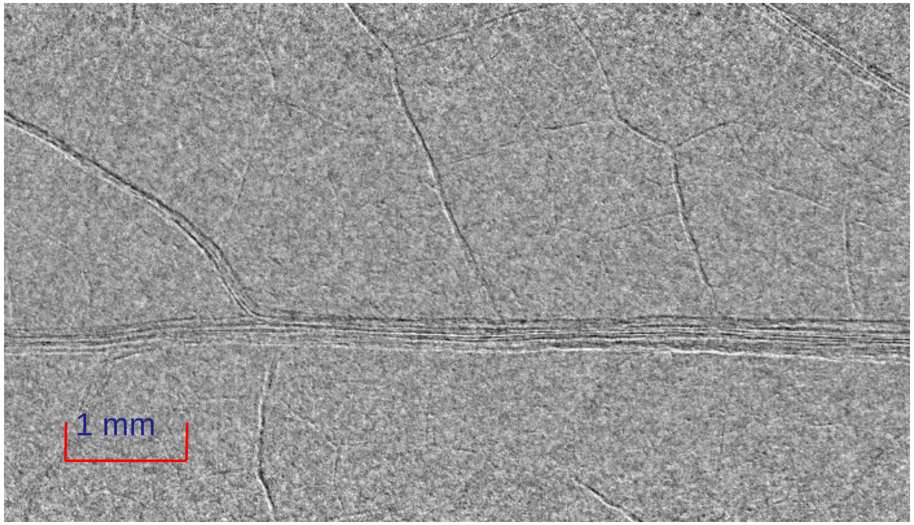

15 days 10 mM $CuSO_4$ treated samples: ethanol-fixed compared with air dried

E = 9.05 and 8.90 keV

d = 35 cm

J. Kaiser et al., Eur. Phys. J. D 32, 113–118 (2005)

Elettra Sincrotrone Trieste

VYSOKÉ UČENÍ TECHNICKÉ V BRNĚ

Cu detection by dual energy absorption imaging in Phaseolus vulgaris leaf

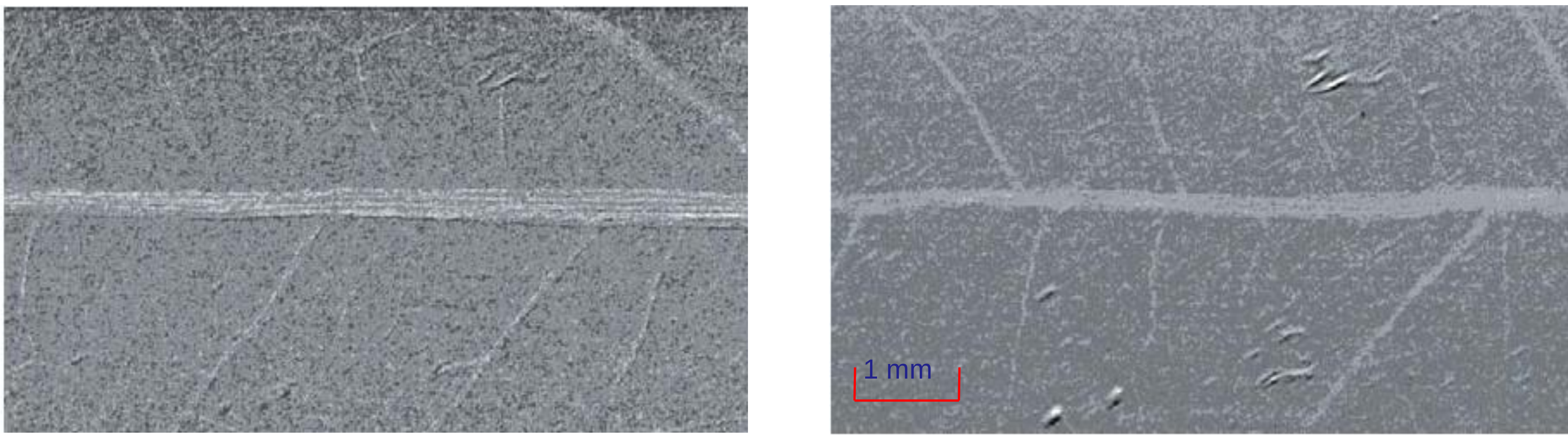

15 days 10 mM $CuSO_4$ treated samples: ethanol-fixed compared with air dried

E = 9.05 and 8.90 keV

d = 2 cm (absorption)

J. Kaiser et al., Eur. Phys. J. D 32, 113–118 (2005)

Applications of phase sensitive techniques

High resolution Phase Contrast imaging

- “In vitro” imaging: high resolution morphological studies (es. micro-CT studies of tissues, organs, biomaterials - virtual histology)
  High resolution required, main limitation is radiation damage

- Virtual histology
  - Breast lesions
  - Imaging of atherosclerotic plaques (PBI and GI)
- PBI potentials in tissues visualization
- Use of staining and Phase Retrieval algorithm
- Dose reduction with PHC Imaging
- Imaging wood, plants and seeds

Virtual histology of breast malignant lesions

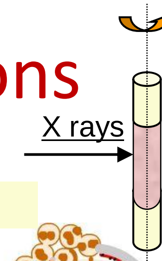

Use of high resolution microCT as complementary tool of histology

- Unstained sample embedded in paraffine (3-4 mm)
- White/pink scan, 0.9-1.2 µm pixel size
- sample-detector dist. = 19 cm, application of PHR

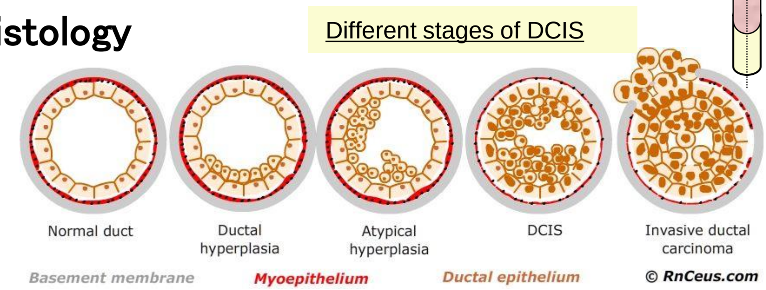

In situ cribriform Ductal Carcinoma (DCIS)

a) classical histological slice stained with haematoxylin and eosin, b) µCT slice

https://cdn.knightlab.com/libs/juxtapose/latest/embed/index.html?uid=cb428a40-d914-11e7-b263-0edaf8f81e27

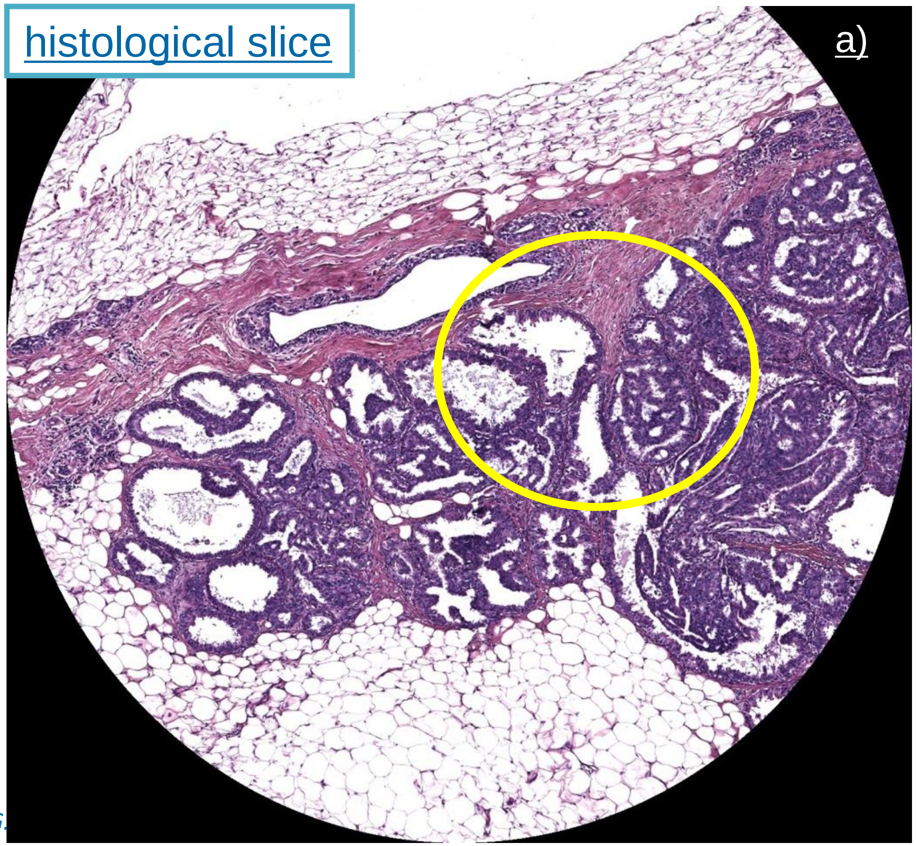

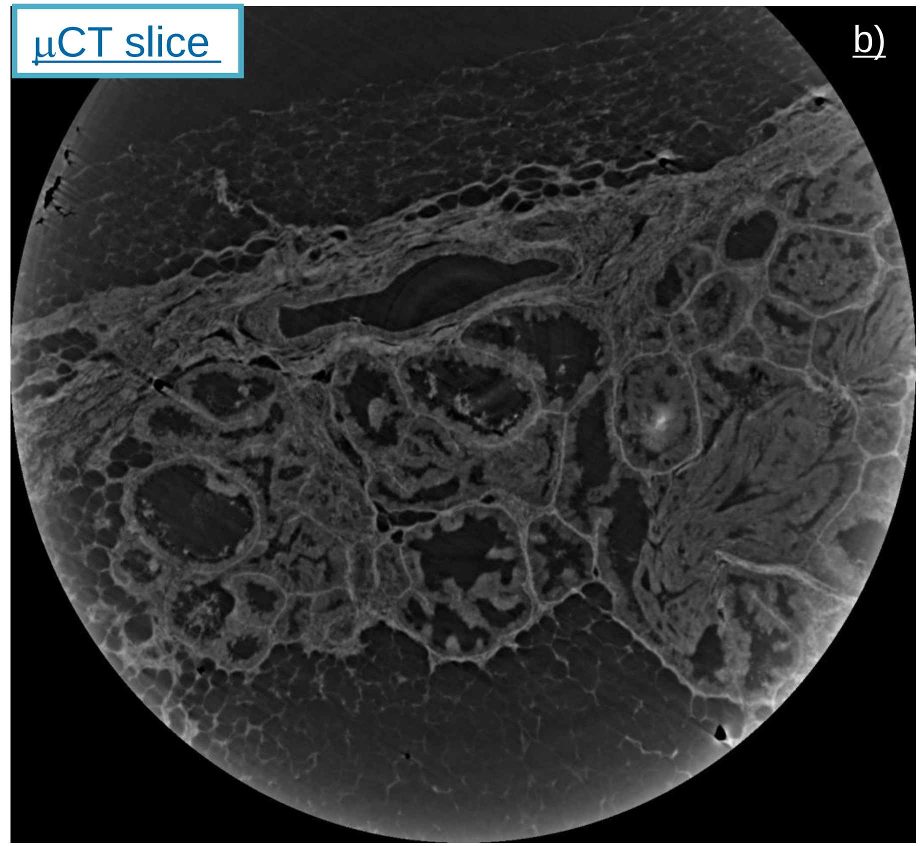

Breast malignant lesion: duct detail

histological slice - detail

μCT slice - detail

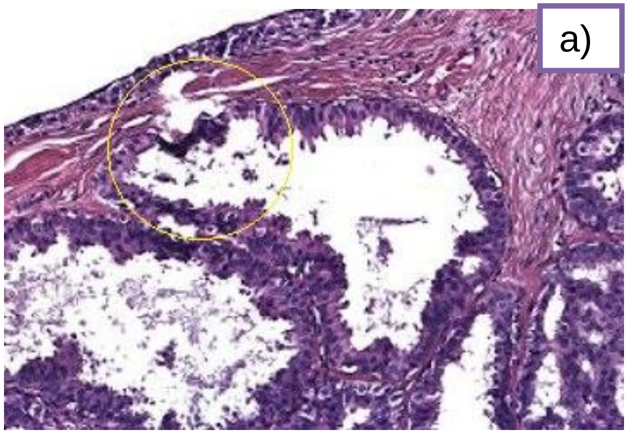

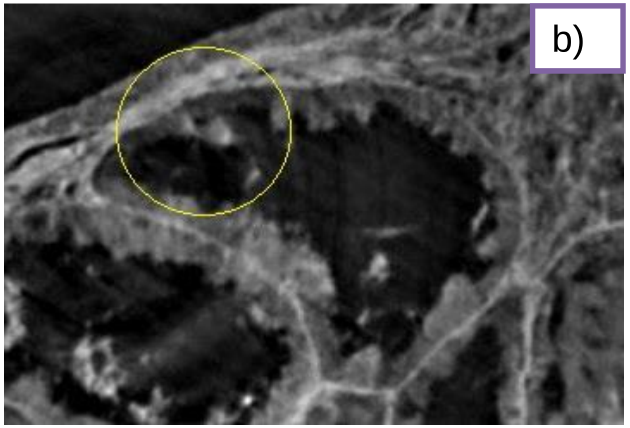

Close-up of a duct including micro-calcifications (yellow circle). On μCT image (b) calcifications are well visible, on the histology image (a) they are completely lost due to the cutting process causing an hyperchromasia (dark purple zone inside the circle).

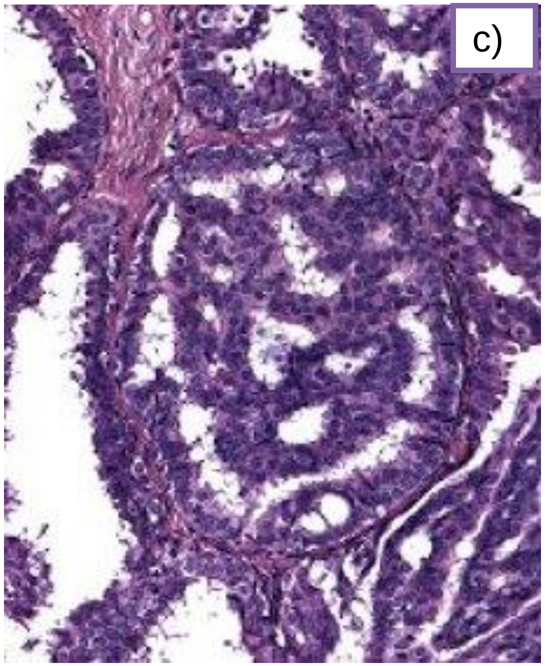

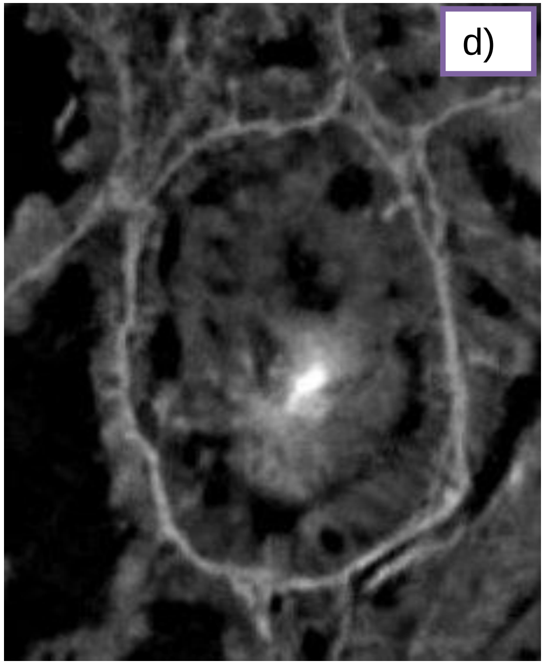

Duct with typical cribriform features. Basement membrane and calcification better visible in in d)

PBI μCT can be helpful for:

- deciding the cutting orientation of the histology
- evaluate presence of microcalcifications
- highlight interfaces (membranes, etc.)

Virtual histology: visualizing atherosclerosis plaques in mice using PBI

Animal model: atherosclerotic mouse

Apolipoprotein E-deficient (apo) mouse (deficient transgenic mice demonstrates a strong tendency to develop hyper-cholesterolemia)

Aim: evaluate the capability of **µ**CT to highlight the formation of atherosclerotic plaques in normal and Apo mice - All mice were fed with a high fat diet for 70 days.

Combination of soft tissue staining by phosphotungstic acid (PTA)* and sample embedding in paraffin or agarose gel allows direct overlay of **µ**CT data sets and microscopy after immunochemical staining

(A) Virtual cut through a volume rendering- Details of the anatomical structures: the right atrium (ra), the left atrium (la), the right and left ventricle (rv, lv), some coronary arteries (ca), the aorta (a) and the aortic valve (white arrow head) and the pulmonary artery (pa). The PTA staining allows for identification of the orientation of the muscle fibre bundles**. (B) Detailed view of the PTA stained right ventricle shown in (A)**. The position and orientation of the virtual cut section shown here is indicated by the line 'B' in panel (A). **(C) Image of the right ventricle area of an unstained heart**, it shows no contrast apart from a difference between fatty and soft-tissue.

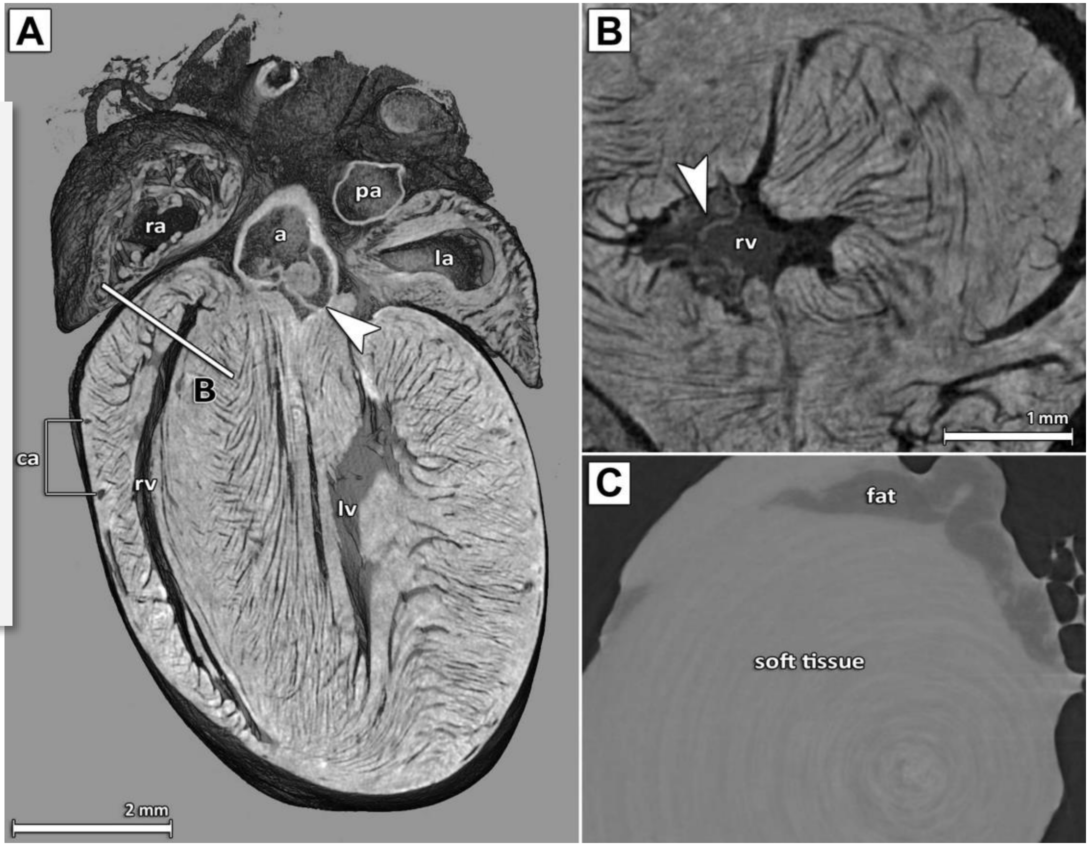

*B.Metscher, BMC Physiology 2009,

Dullin C et al., PLoS ONE 12(2): e0170597 (2017)

Comparing CT slice with histology

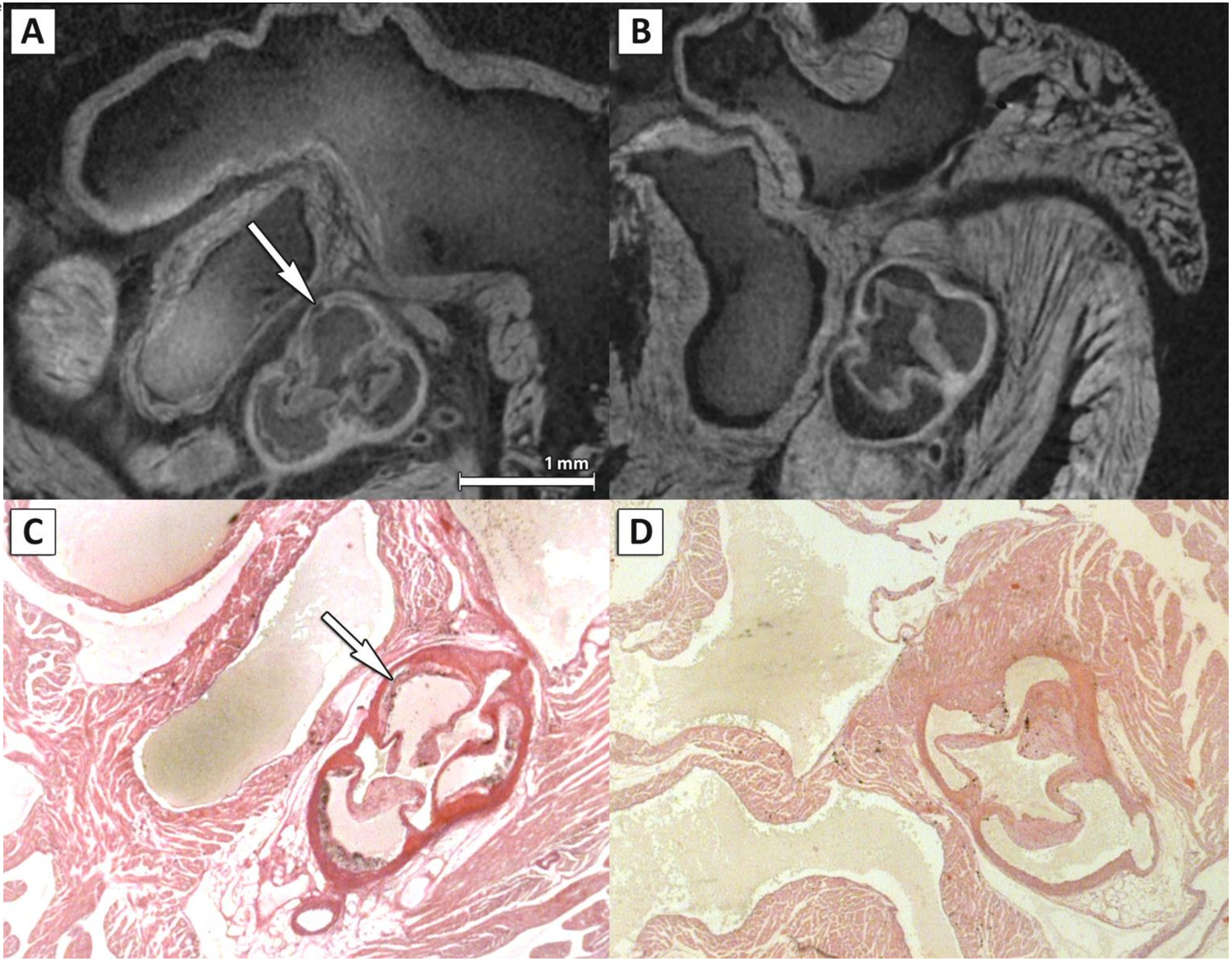

no additional shrinkage or distortion by re-embedding the tissue in resin

Dullin C et al., PLoS ONE 12(2): e0170597 (2017)

Dose reduction with PBI Imaging using Phase Retrieval

•The phase shift signal (δ) is much stronger than the absorption signal (β) signal -> This means that phase retrieval (PHR) should allow for significant dose reduction

Magnified mouse lung tissue reconstructions as a function of propagation distance and exposure time

- ❖ Single distance PHR has been employed.
- ❖ Raw reconstruction dominated by noise at short distance, particularly at 1 and 10 ms exp time
- ❖ Substantial improvement is visible with application of PHR even at 0.16 m
- ❖ PHR removes the halo artefacts and greatly suppresses noise without losing visibility of the microscopic alveoli, even for the 1 ms exp.
- ❖ At larger distances the image quality appears remarkably consistent across all exposure settings, despite the dose varying by a factor 300.
- ❖ Analysis confirmed by quantitative evaluation of SNR

Image dimensions: 3.83 mm × 3.83 mm.

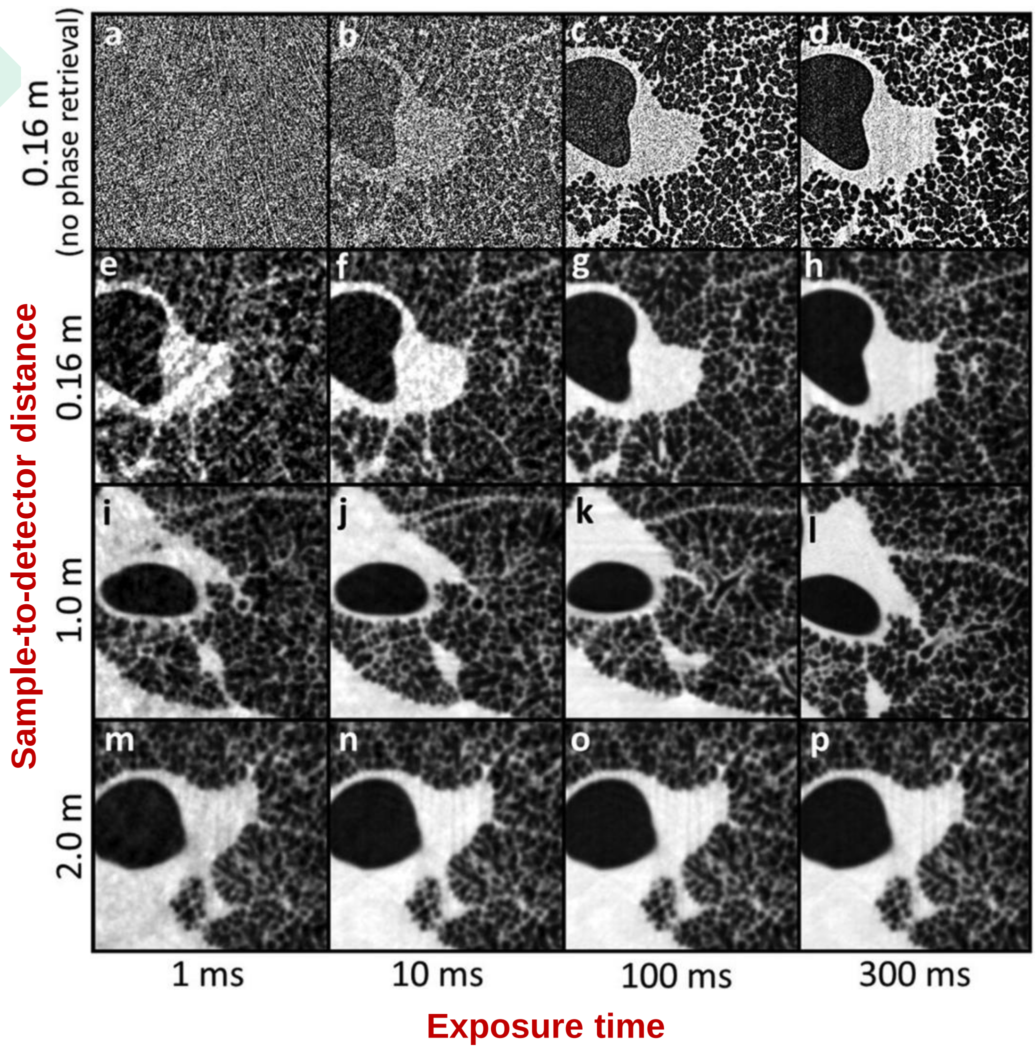

M.J.Kitchen et al., Sci.Rep. | 7: 15953 | (2017).
*Paganin, D., et al. J Microsc **206**, 33–40 (2002).*

Use of staining and Phase Retrieval algorithm - Imaging of PTA stained mouse heart embedded in paraffin

Elettra Sincrotrone Trieste

Standard FBP reconstruction

Application of Phase retrieval algorithm

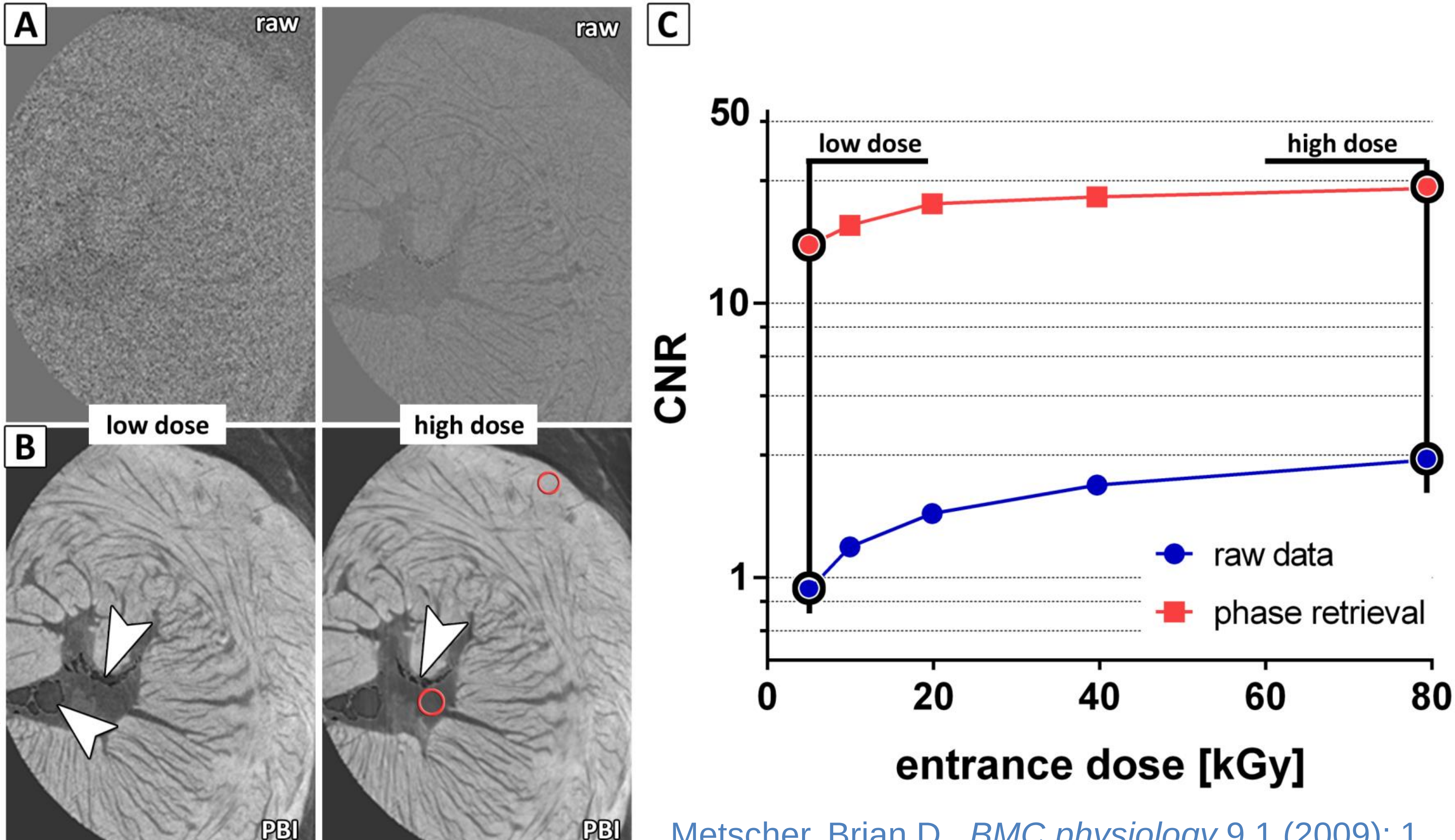

Metscher, Brian D. *BMC physiology* 9.1 (2009): 1

PBI + phase retrieval dramatically **increases** contrast-to-noise ratio in PTA stained mouse hearts -> possible **dose reduction** or **shorter acquisition times**

M.Saccomanno et al., J. Synchrotron Rad. (2018). 25

Study of 3D-cell distribution in regenerating muscle skeletal system with PB µCT

- Use PB µCT to evaluate the process of muscular and skeletal structures grow and regeneration. A developing salamander (Pleurodeles waltl) limb– a key model organism for vertebrate regeneration studies – has been used to evaluate tissue differentiation and quantitative analysis of the 3D-cell distribution.

M. Tesařová et al., Scientific Reports, 8 (2018) 14145

- Animal larvas stained with PTA
- White beam, Av. energy = 20 keV
- Detector used: SCMOS, pixel size = 1.05 µm, 1000 projections acquired over a total scan angle of 180˚

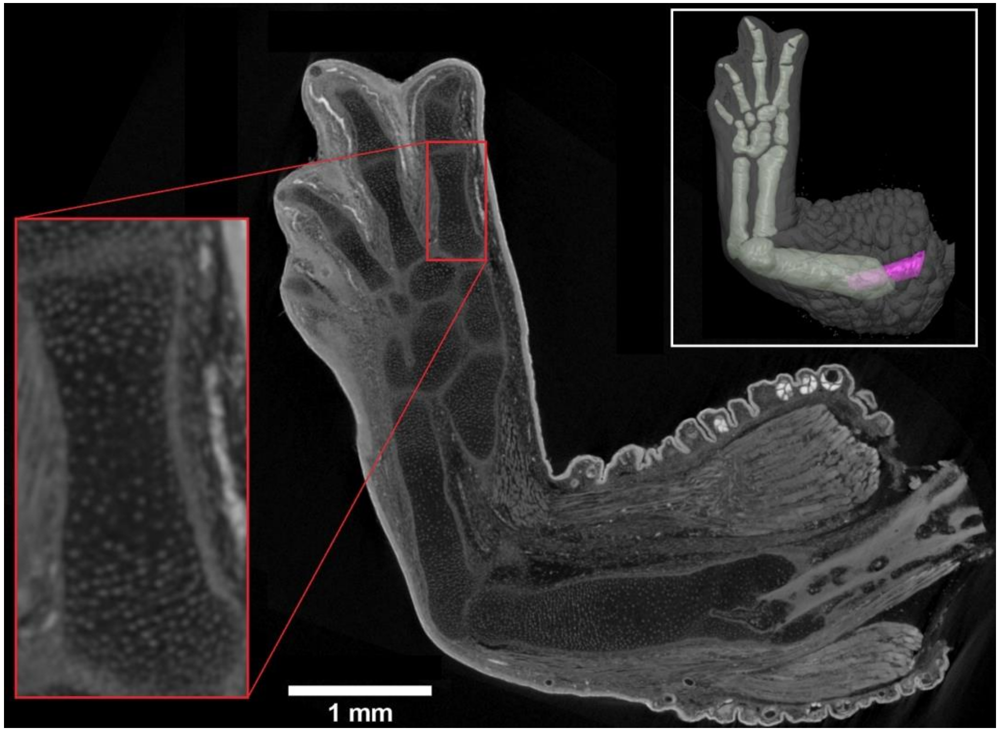

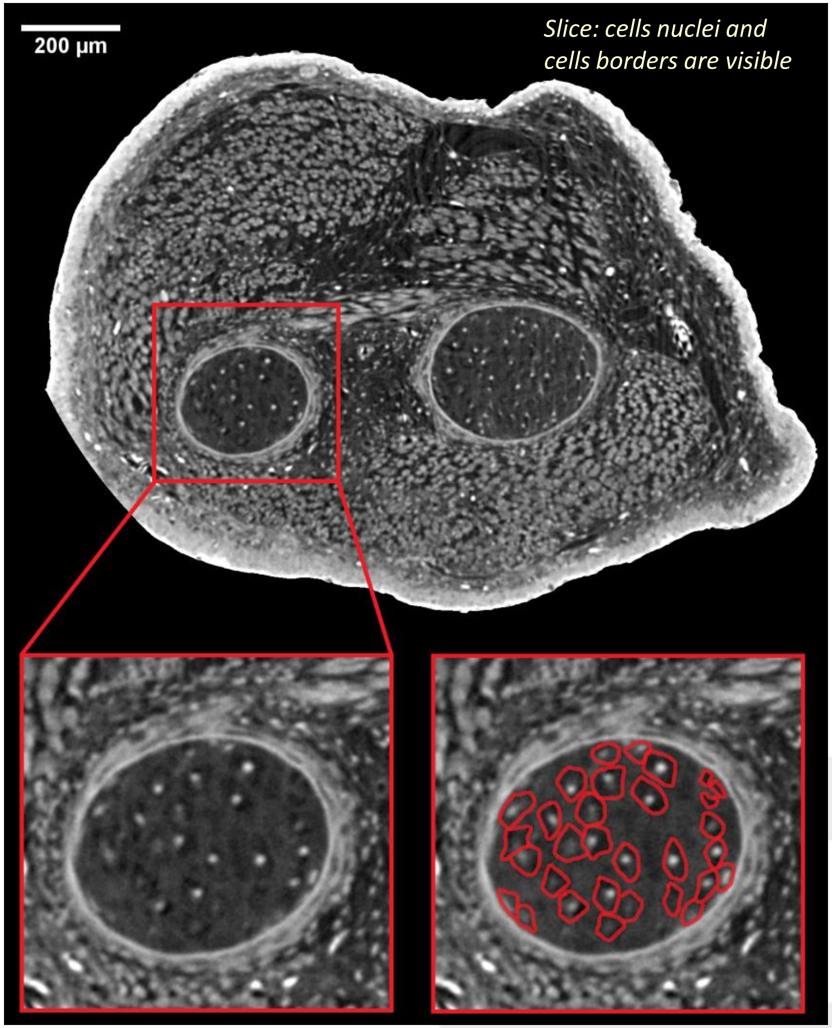

MEDICAL UNIVERSITY OF VIENNA

CEITEC

Karolinska Institutet

Elettra Sincrotrone Trieste

Sample tissues segmentation

Elettra Sincrotrone Trieste

Cartilage (light blue), muscle fibers (red), skin epithelium (yellow)

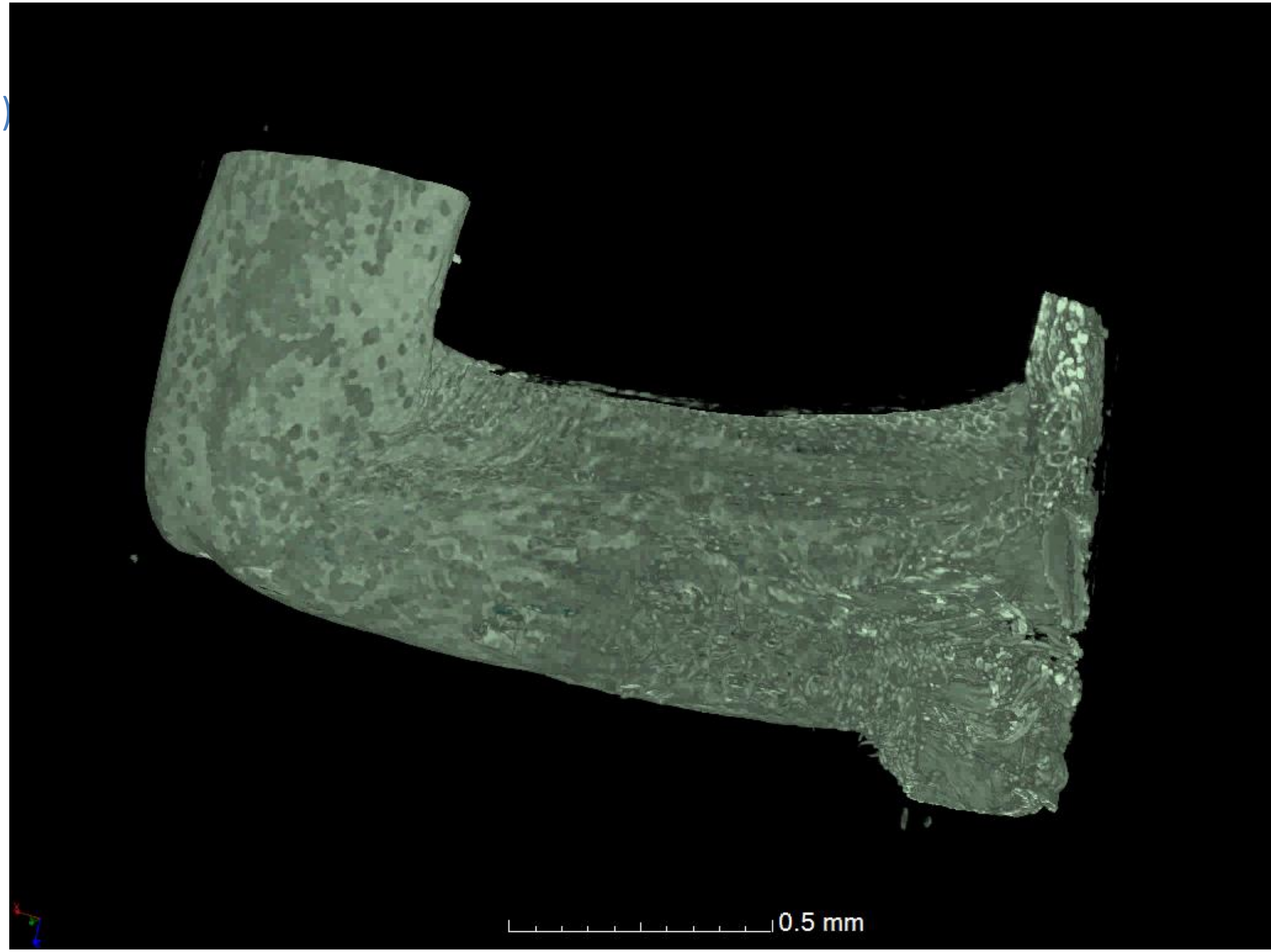

Effective use of PB modality with phase retrieval and use of staining

- Cells distributions and quantitative analysis on cells polarizations in the muscle-cartilage tissue
- A 3D model describing the cells growth process can be accessed

M. Tesařová et al., Scientific Reports, 8 (2018) 14145

Archeological vs. recent oak

Archaeological oak

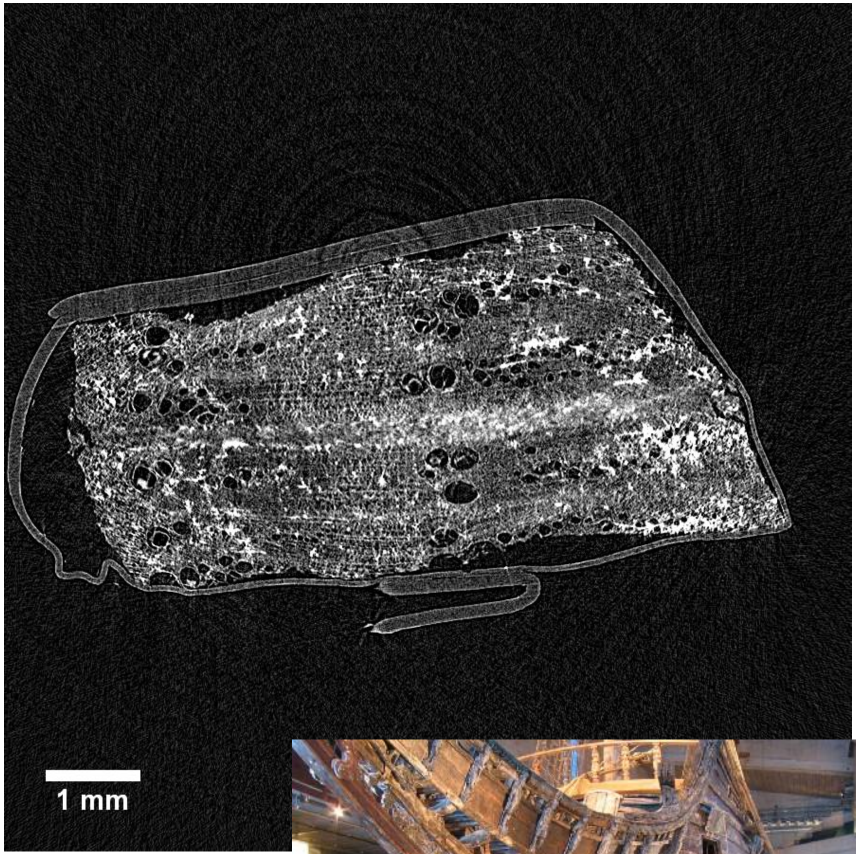

Recent oak

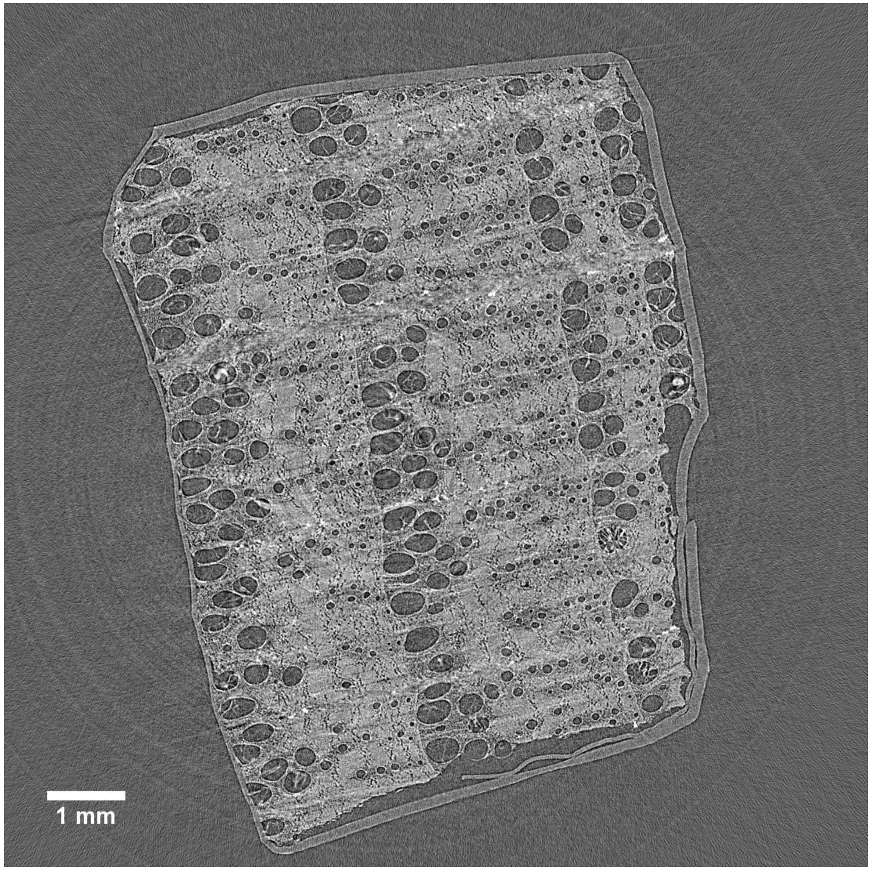

E = 15 keV

Università degli Studi di Firenze

Courtesy of N.Sodini

Phase contrast microCT for the study of plants response to drought conditions

- PHC is particularly capable to detect air/tissue interfaces. In botany this property can be efficiently applied to study the response of plants to **drought conditions**.
- The vulnerability to **drought-induced xylem embolism** of ***Laurus nobilis***, ***Acer pseudoplatanus*** and ***Fagus sylvatica* plants** has been studied at SYRMEP
- The study aimed at real-time observations of **xylem conduits in main organs** (stem, roots and leaves) during progressive plant dehydration.
- Using the micro-CT technique, it was possible to study intact seedlings and compare vulnerability patterns within single plants.
- The theoretical loss of stem hydraulic conductivity calculated from micro-CT observations can be compared with classical hydraulic measurements performed on seedling stems.

Laurus nobilis

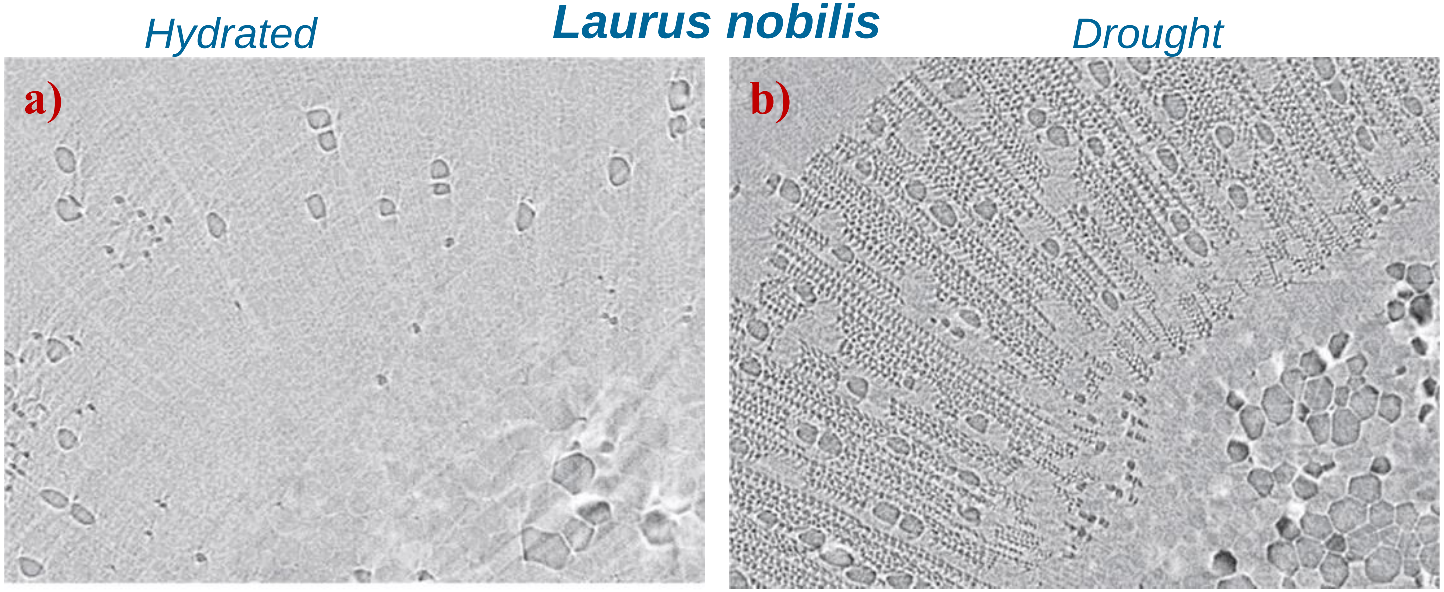

(a) stem with a xylem pressure (Ψ_{xyl}) = -0.11 MPa; **(b)** a second shoot dehydrated to Ψ_{xyl} = -3.3 MPa.
(Ψ_{xyl} is referred to water pressure with respect to distilled water)

A.Nardini et al, New Phytologist (2016), doi: 10.1111/nph.14245

Varying drought conditions….

Acer pseudoplatanus

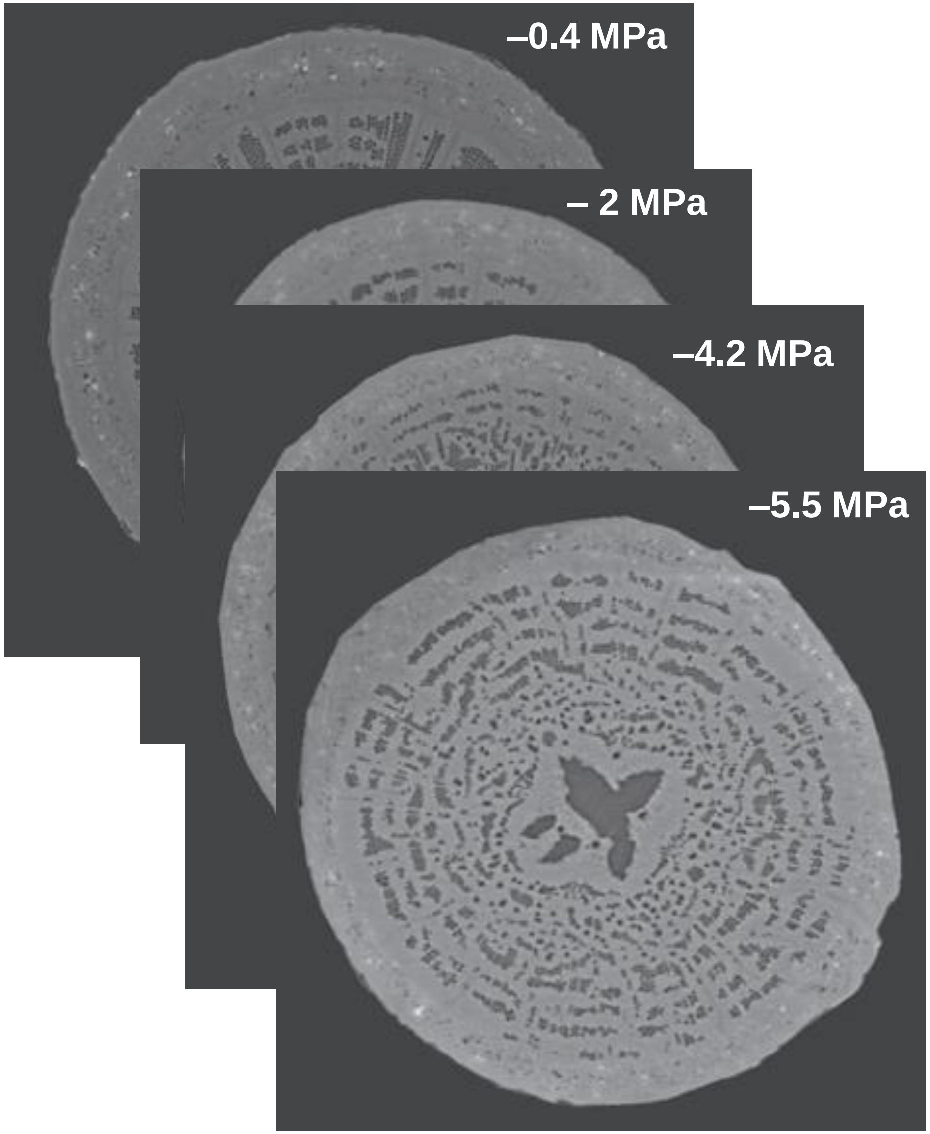

Fagus sylvatica

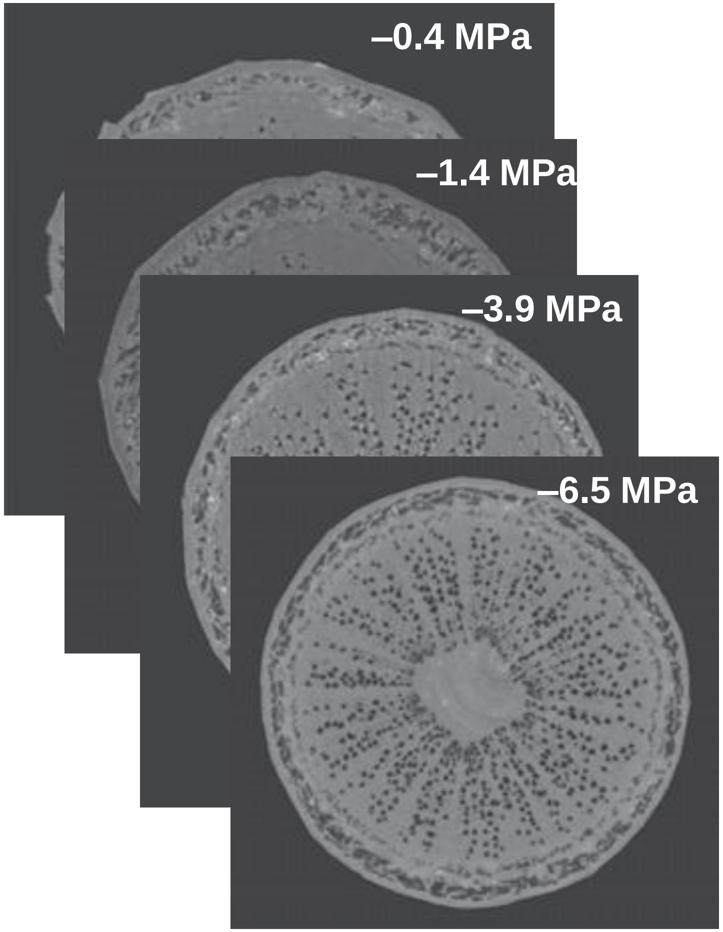

Morphology of ... Phase retrieval vs
...e ...ection

Elettra

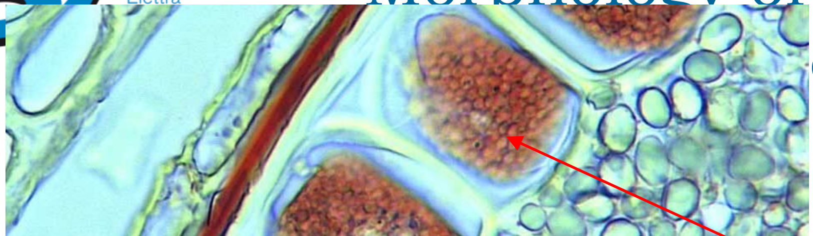

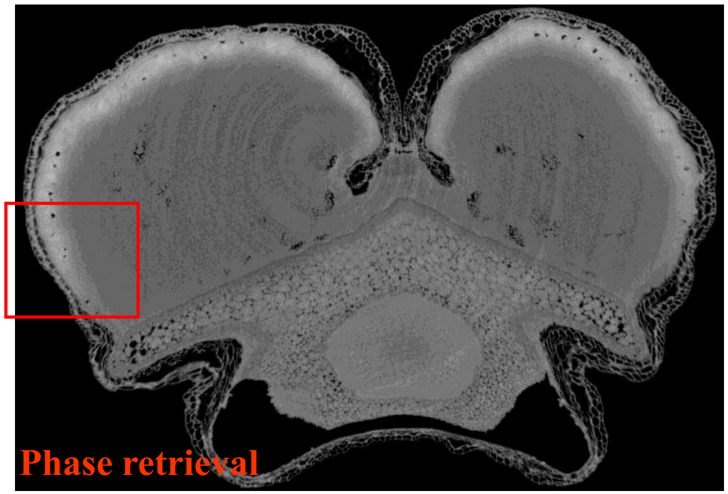

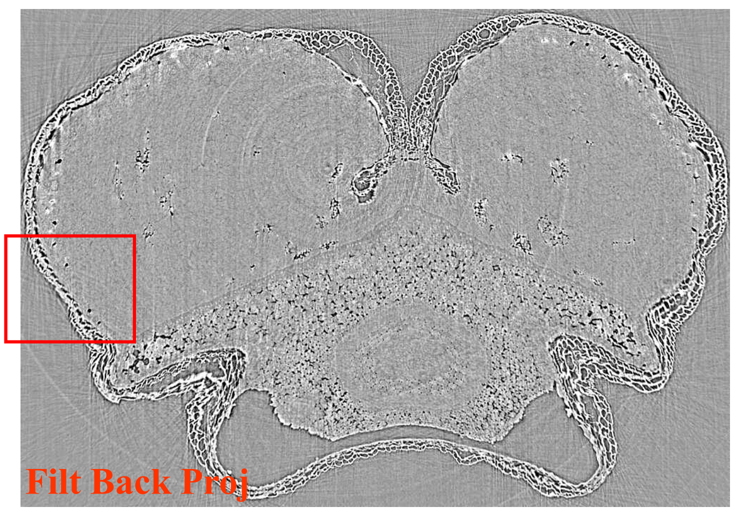

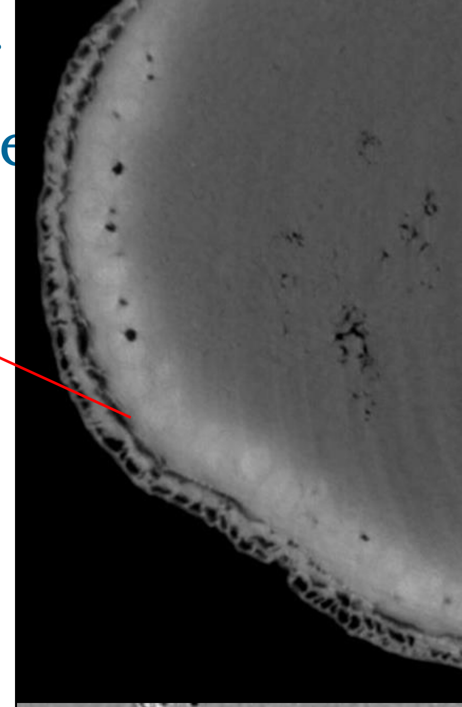

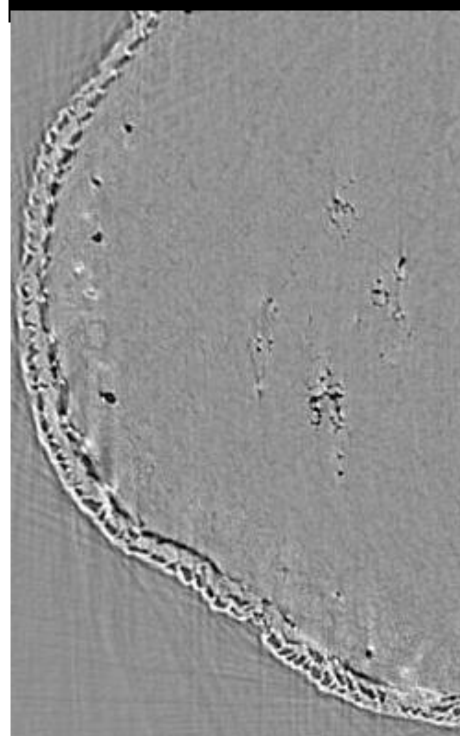

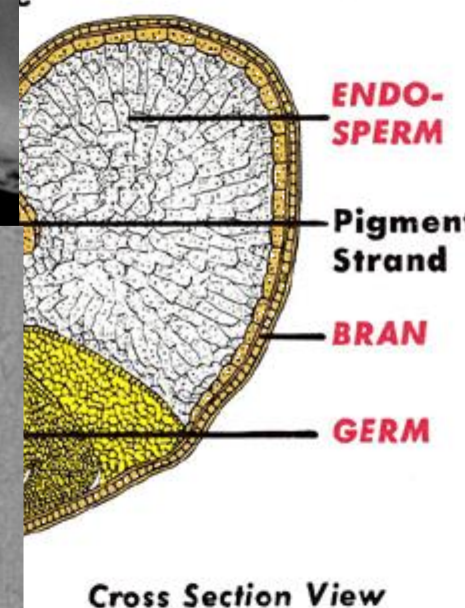

Univerza v Ljubljani
Biotehniška fakulteta

Courtesy of M.Regvar

Courtesy of S. Mohammadi

Application to cultural Heritage: Peter Herresthal and his Giovanni Battista Guadagnini (1753)

N. Sodini,et al., Journal of Cultural Heritage, 13 (2012) S44–S49

Work at the experimental hutch

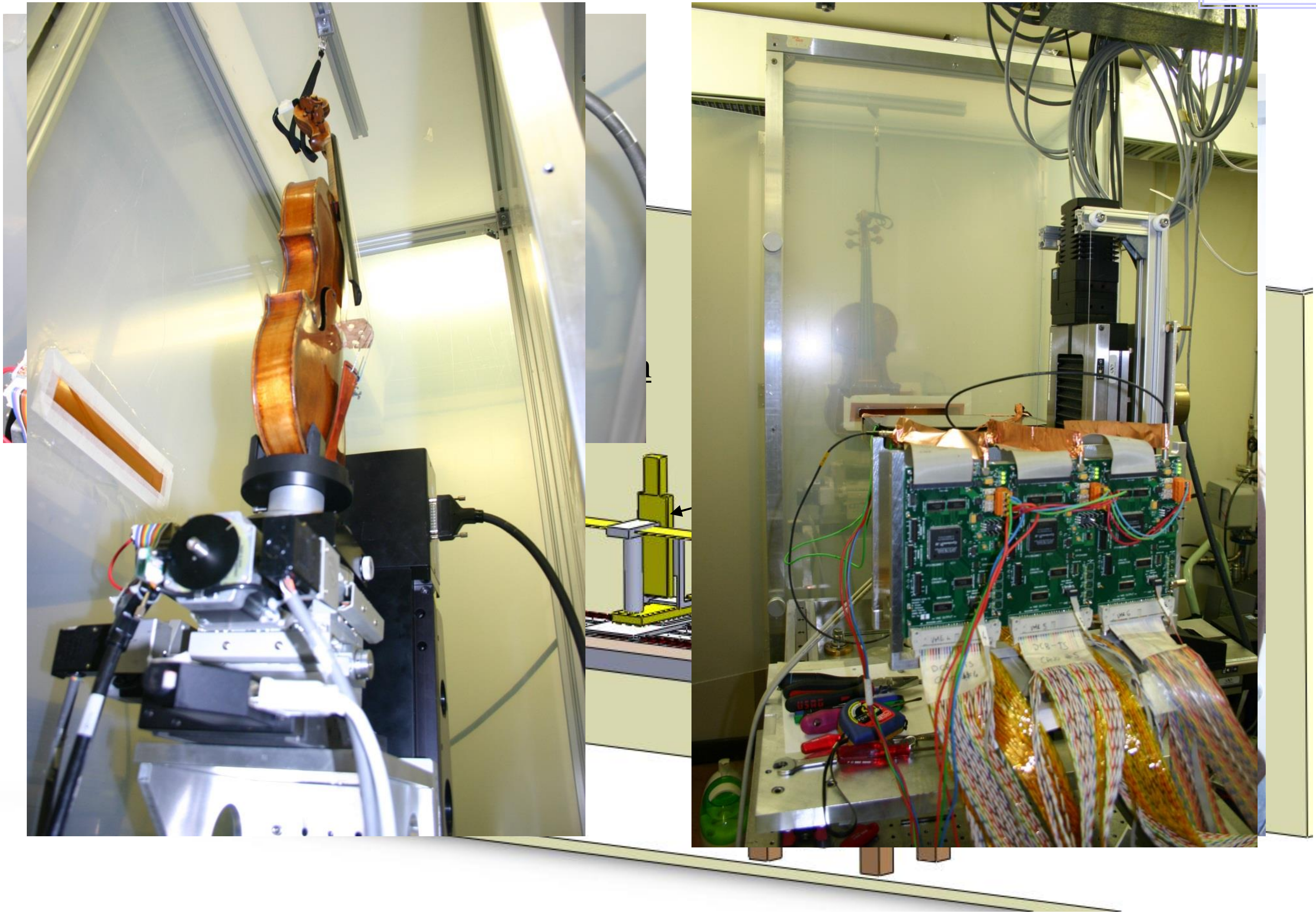

State-of-the-art clinical instrument of the Azienda Ospedaliera – University of Trieste

pixel size ca. 500 mm

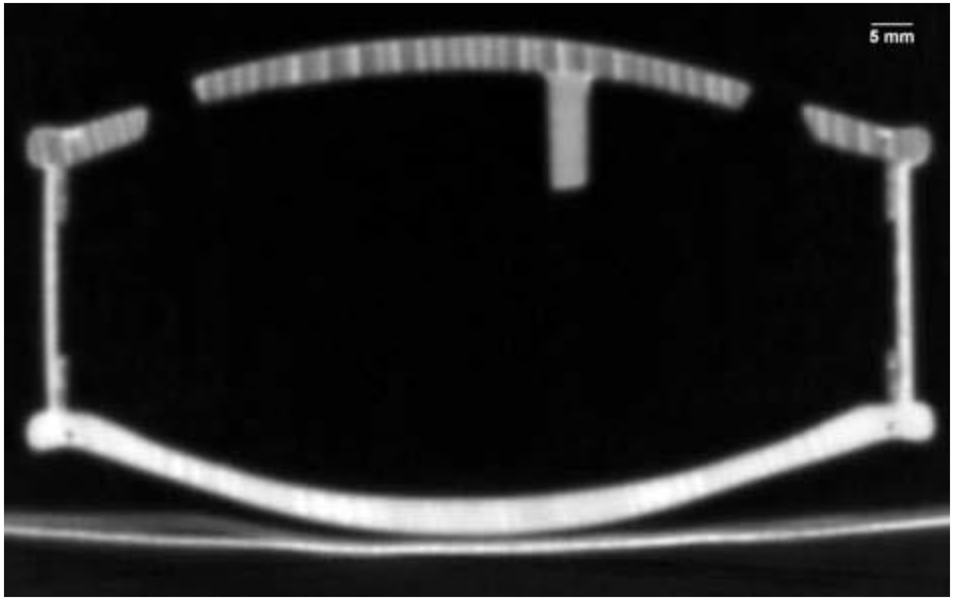

SYRMEP beamline@Elettra

pixel size = 50 mm

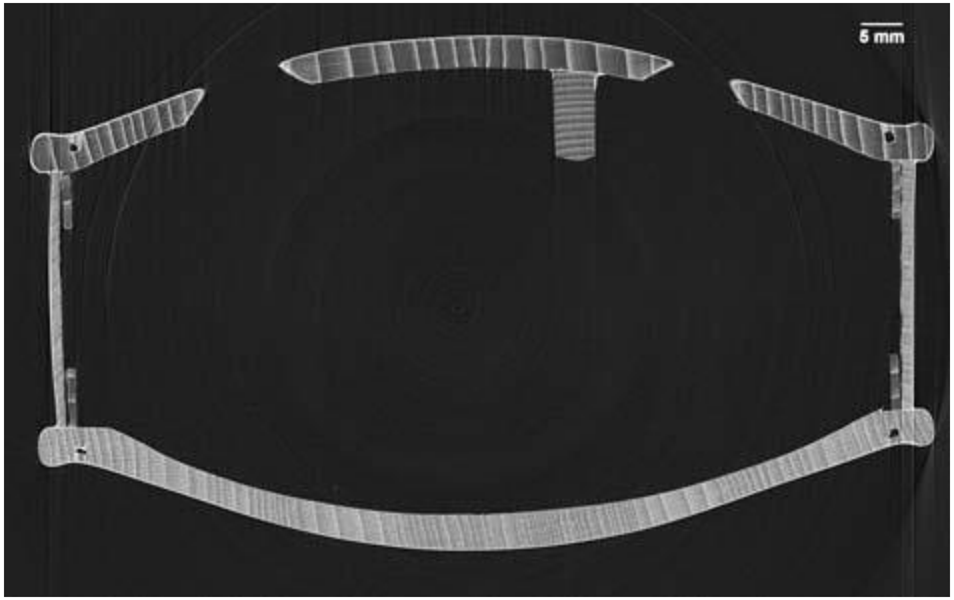

L. Rigon et al., e-Preservation Science, 7 (2010) 71-77.

The planar image

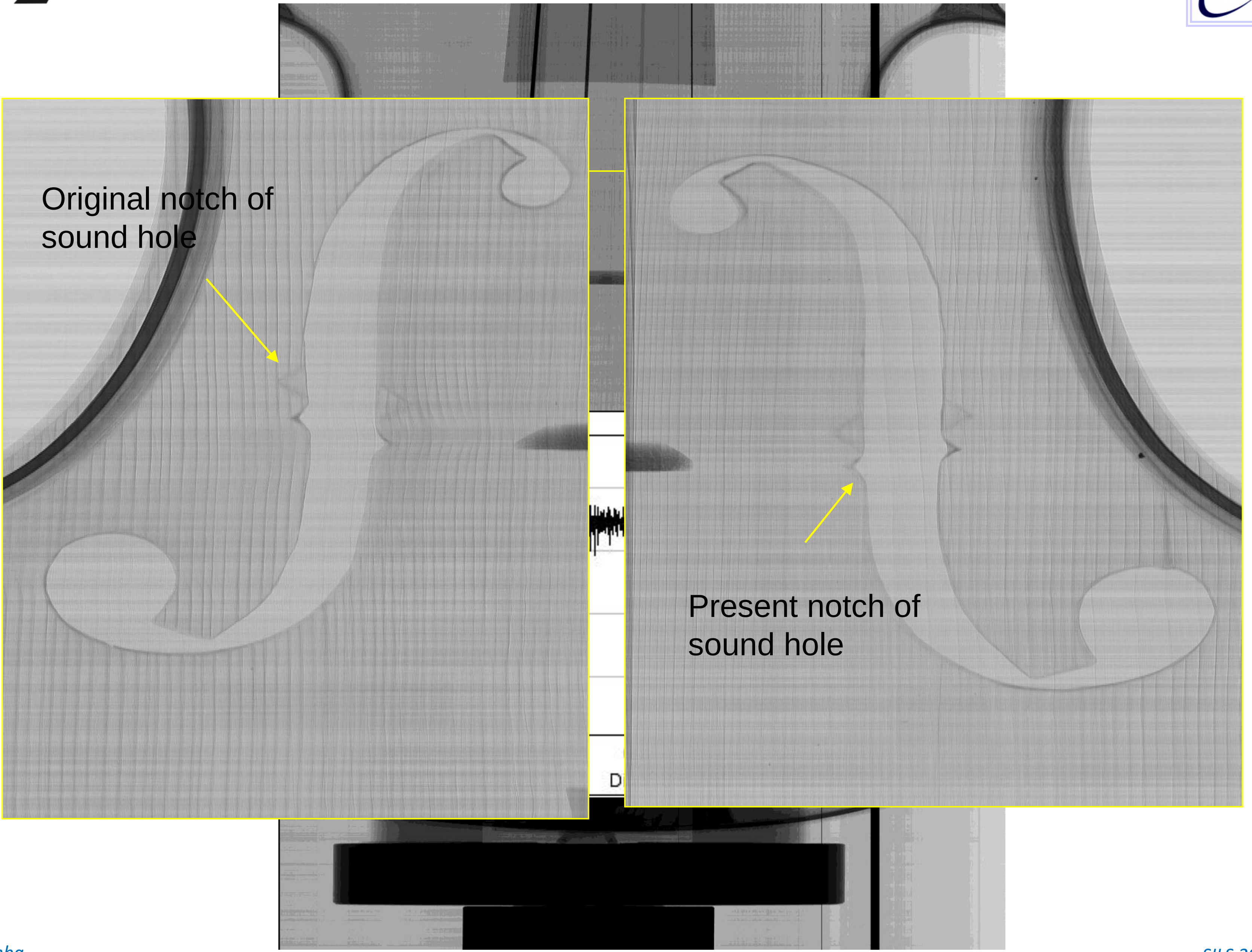

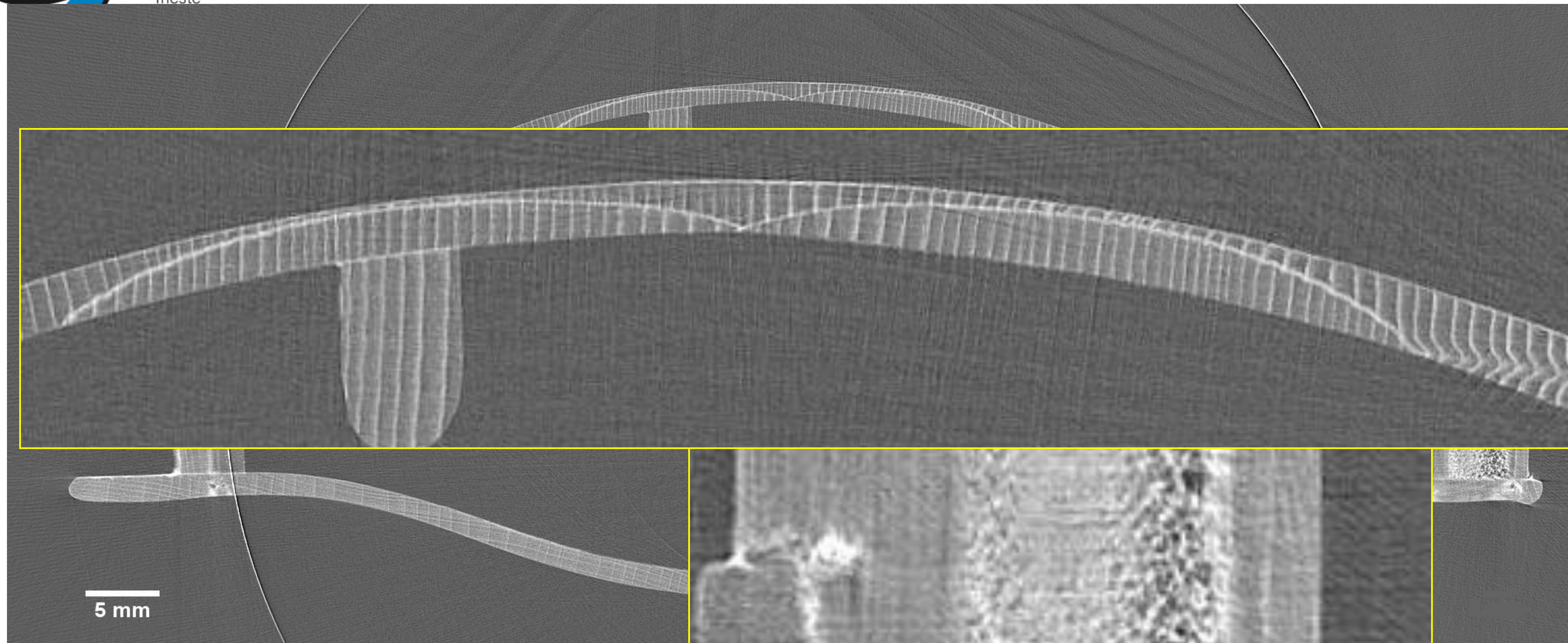

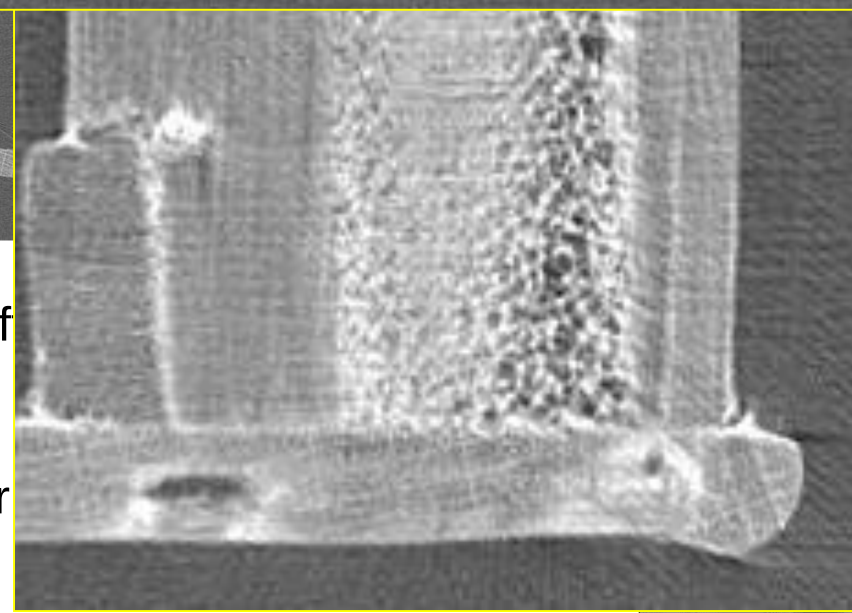

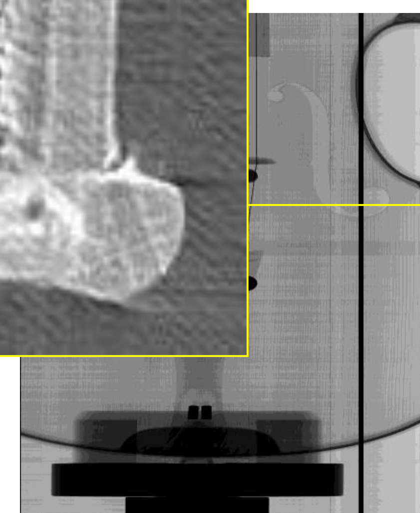

- Reinforcement patch on the lef
- Presence of filling compound
- Woodworm between the corner
- glue on the right corner block
- Good quality patches on the top plate

Non-destructive study of fossil inclusions in opaque amber using PB imaging

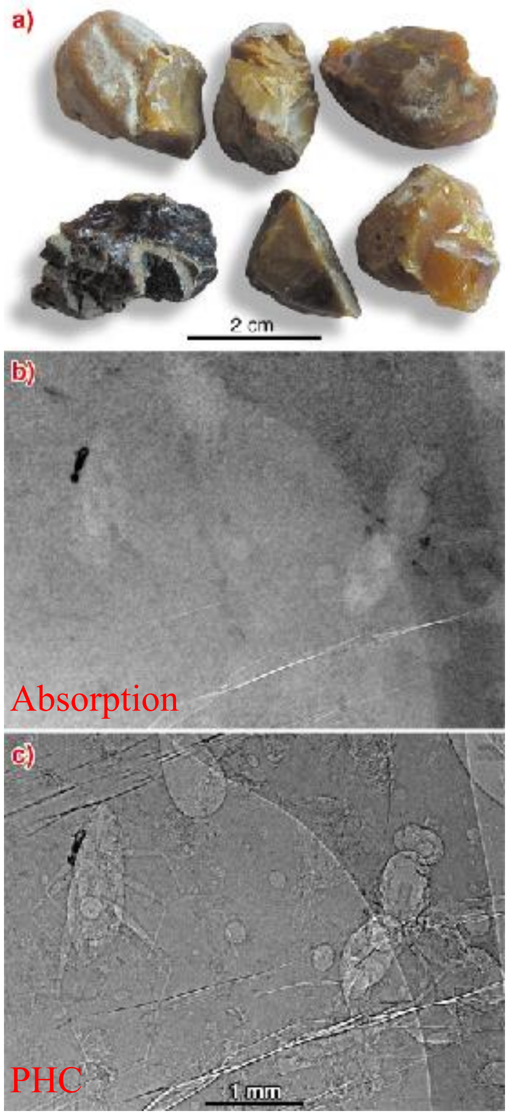

- Amber is a plant fossil resin that dates from the Carboniferous period (~ 300/350 million years ago) to the present day.
- It can contain fossil organisms that are generally in an excellent state of preservation.
- The study of these organisms permits to evaluate the paleoenvironments conditions and to get information about the evolution of groups that are relatively rare in the fossil record, such as insects and spiders
- Finding the precise location of organisms embedded in the opaque amber was impossible using conventional methods (b)

P. Tafforeau et al., Applied Physics A, 195-202 (2006)

Segmentation and volume rendering

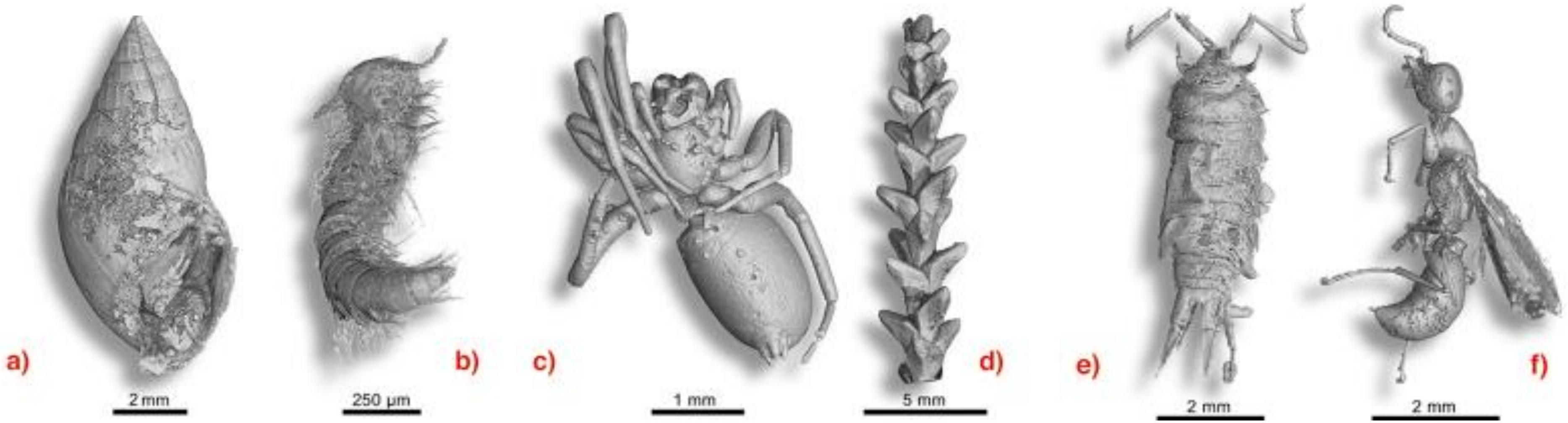

- The use of phase contrast retrieval algorithm allow to virtually extract each detail from the background
- PHC works also on ‘hard materials’, dramatically increasing the image contrast

P. Tafforeau et al., Applied Physics A, 195-202 (2006)

Elettra
Sincrotrone
Trieste

Volume rendering of a varroa (the bee's mite, yesterday experiment)

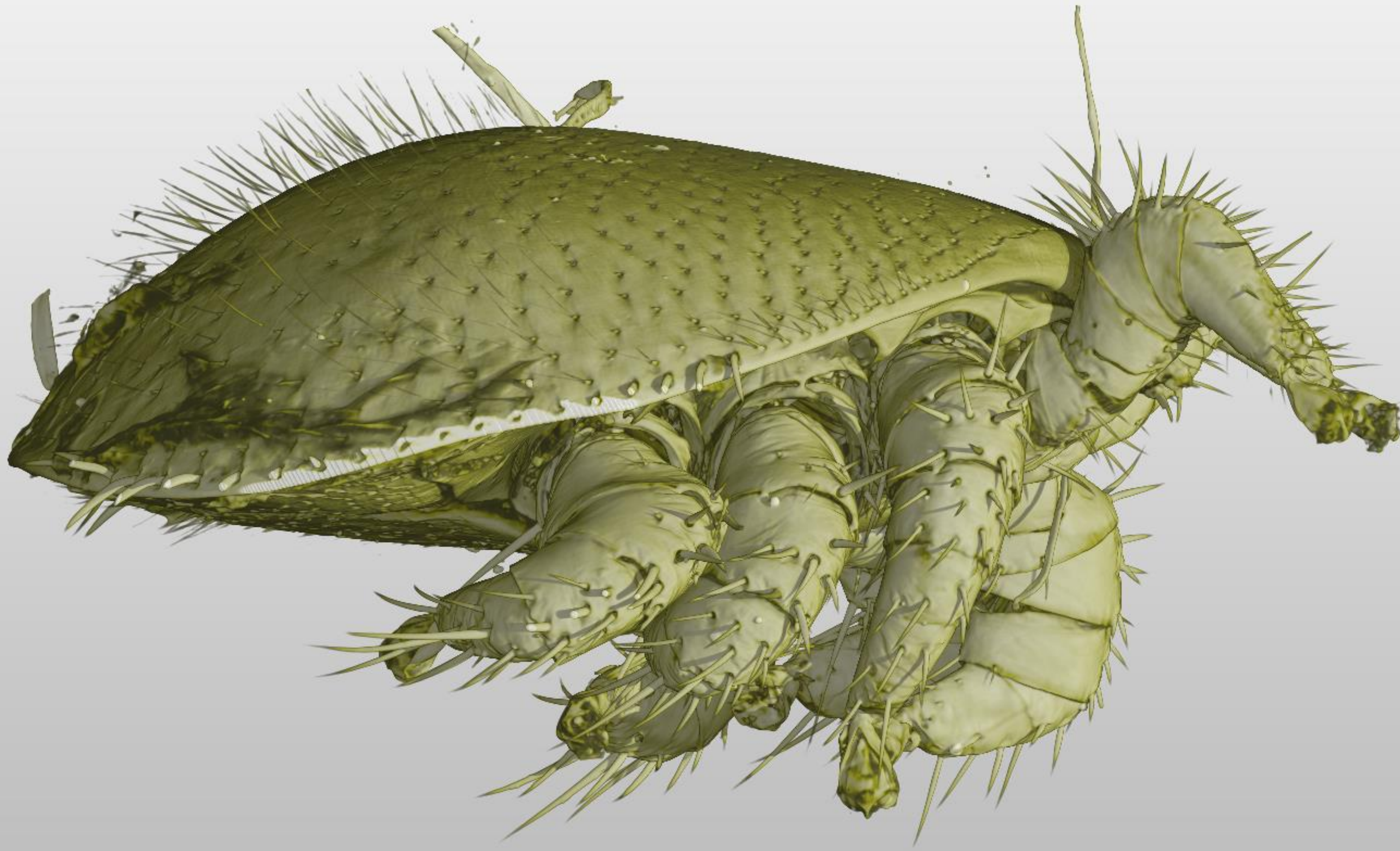

Pre-clinical imaging

- Imaging of small animals, tissues and organs: applied for different purposes in the development of ***animal models*** *(ex vivo, in-vivo)*
  Research protocols, pixel size: 4.5 - 9 µm (ex-vivo) up to 100 µm (in-vivo).

  - Lungs imaging: 2D and 3D, structure and function
  - Imaging of brain

2D dynamic Imaging of lungs Function & morphology (I)

- Animal model: rabbit pups
- Imaged pups with PBI, either before the first breath (fetus) and at fixed intervals after birth (up to 2h)

Effects of Ventilation on Lung Liquid Clearance at Birth

Aim: to observe lung aeration on a breath-by-breath basis.

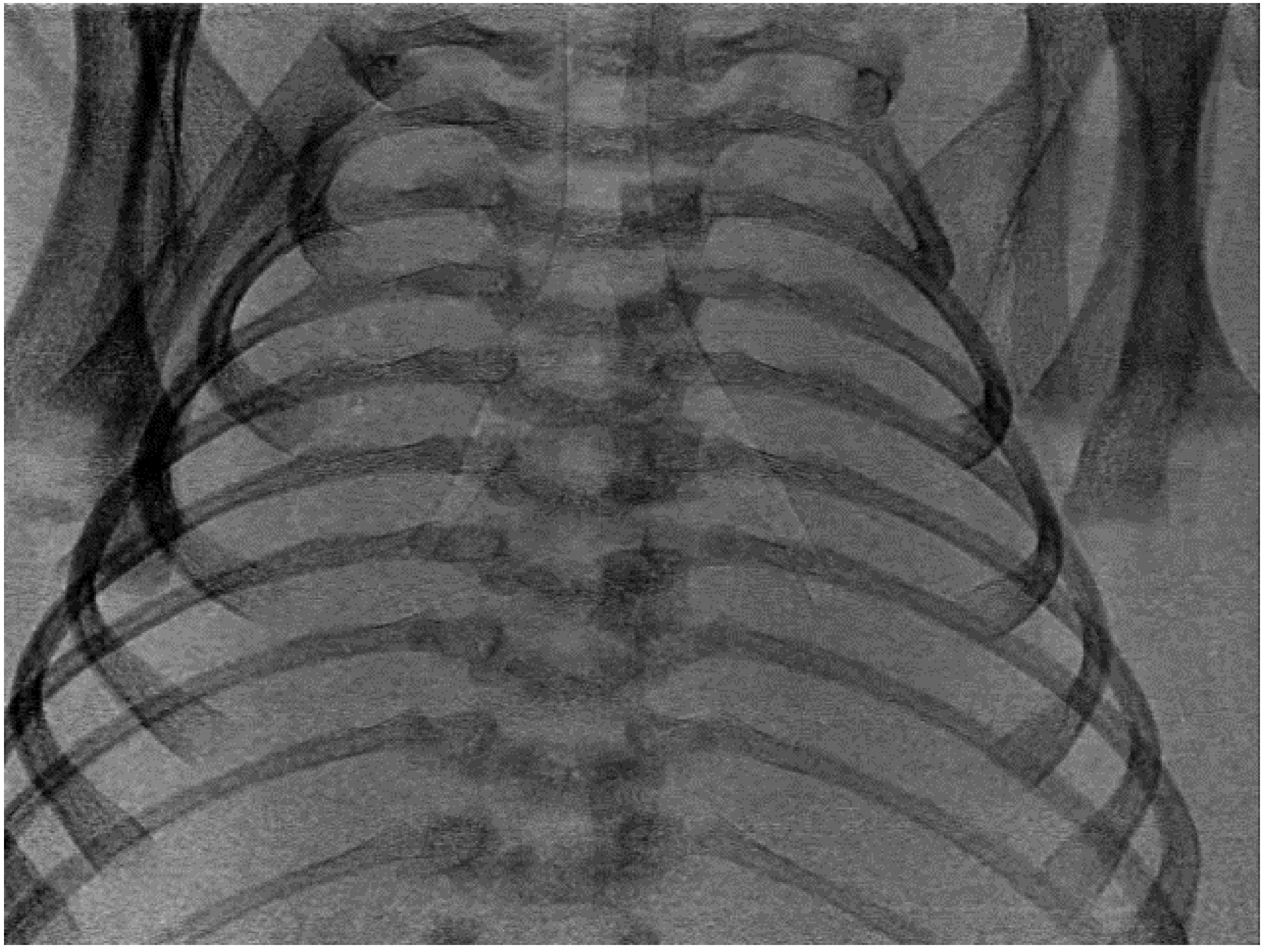

Exp. time: 80 ms
Interval: 0.8 s
Skin Dose: ~ 0.15mGy/f
Pixel Size: 22.5 µm
E = 25 keV

Kitchen, M. J., et al., Phys. Med. Biol., 53(21), 6065-77 (2008).

Elettra
Sincrotrone
Trieste

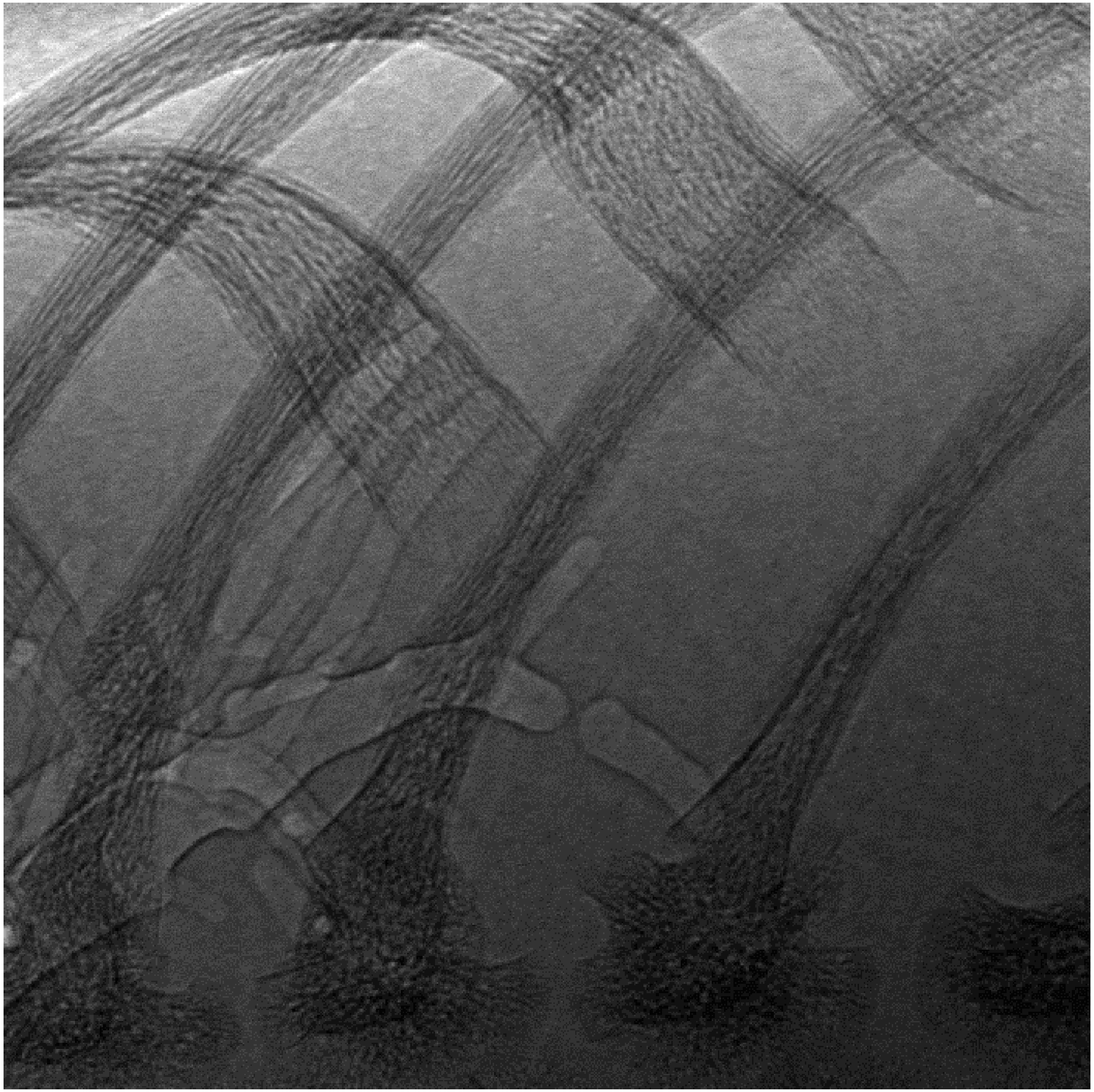

PBI potentials in tissues visualization II - Imaging of inflammation in asthmatic mice

- Animal model of allergic asthma induced by ovalbumin based on balb/c mice
- Murine Alveolar Macrophage Cells stained with Barium sulfate (Guerbet, F)
- Macrophages adminstered to the animals intra tracheally 48 hours after asthma induction

No PHR

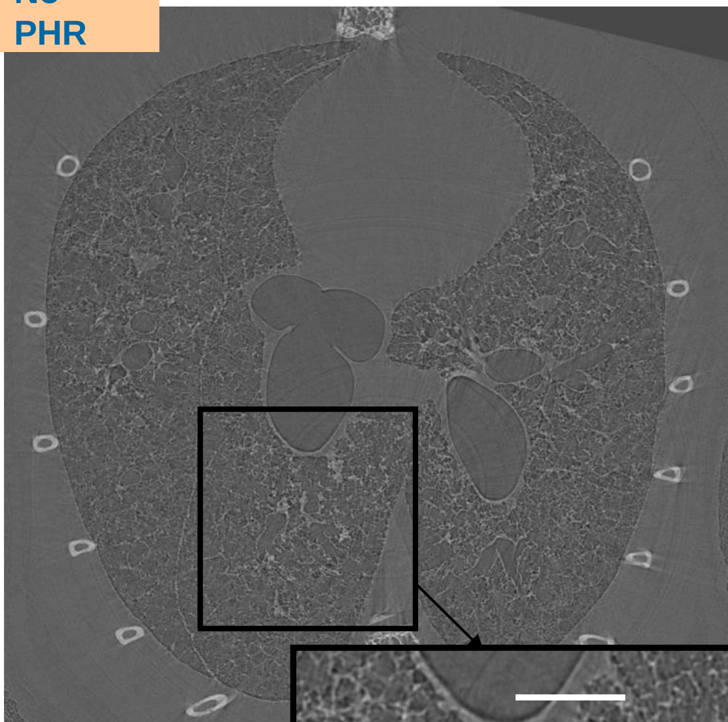

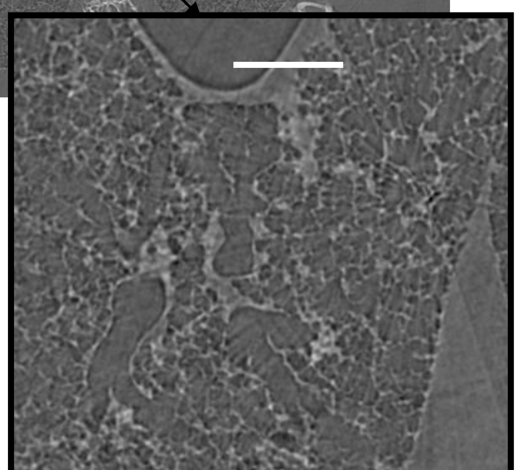

Lung slice

E=22 keV
PHC dist = 30 cm
Pixel size = 9 µm

Clear separation of tissue, Ba and bones signals with PHR

PHR (single dist.)

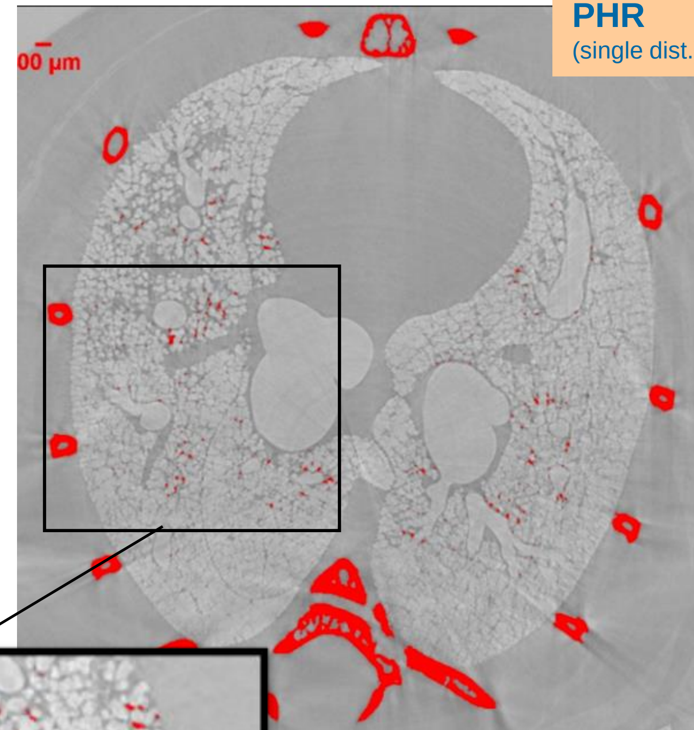

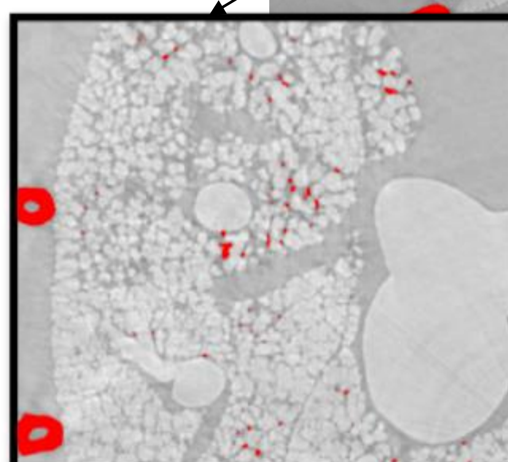

Bones
Barium

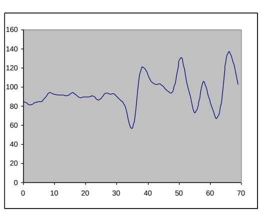

Edge enhancement effects due to PHC

C. Dullin et al, J. of Synchrotron Radiation 22(1) (2015)

Visualization of labeled macrophages

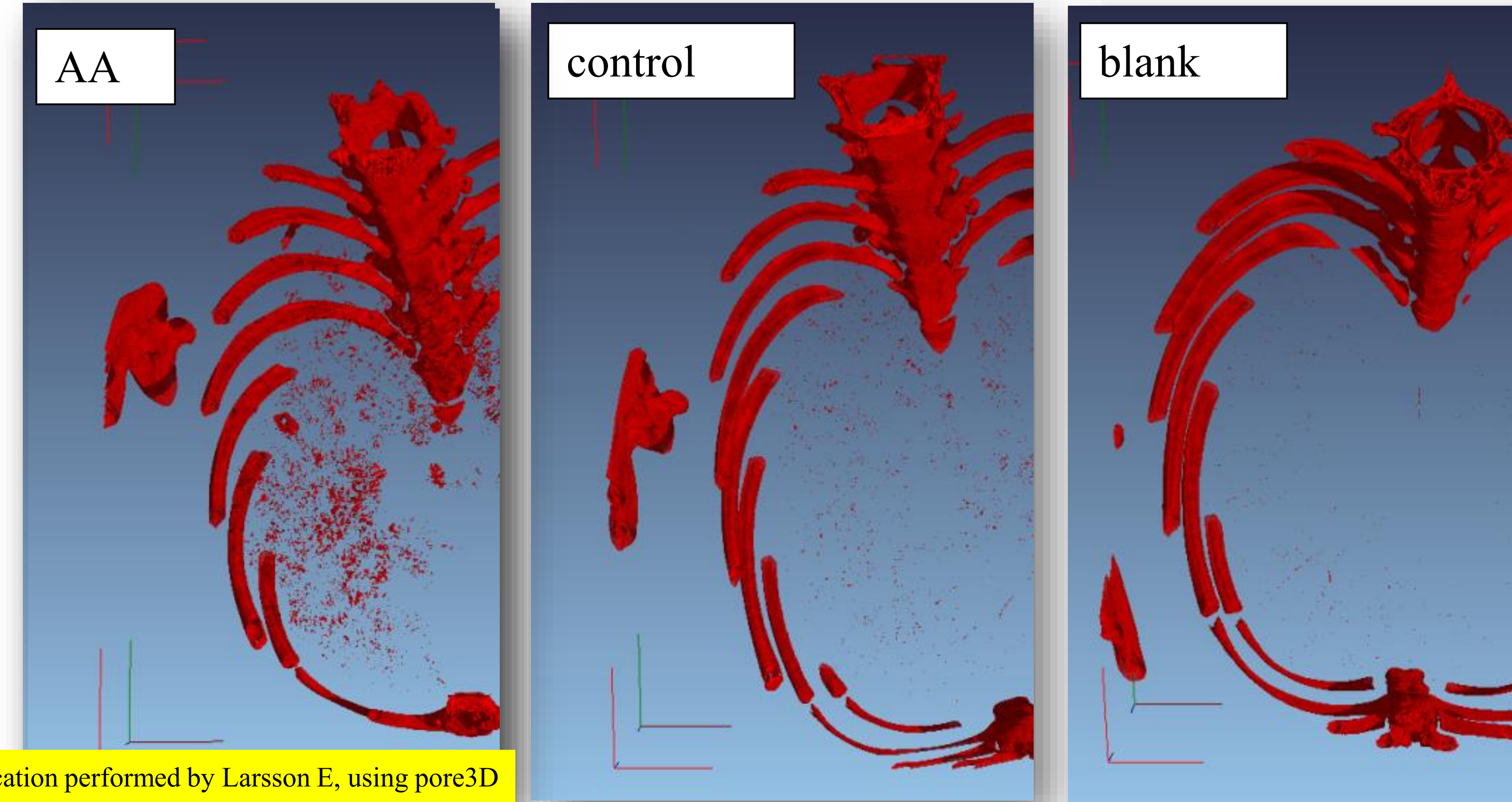

Quantification performed by Larsson E, using pore3D

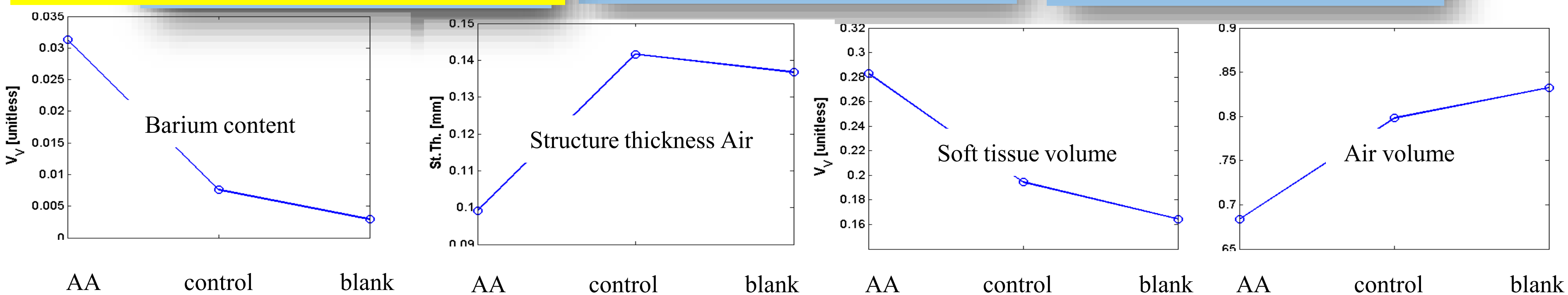

C. Dullin et al, J. of Synchrotron Radiation 22(1) (2015)

VOI of soft lung tissue

Soft Tissue (green), Macrophages with barium (red), Medial axis/skeleton (blue)

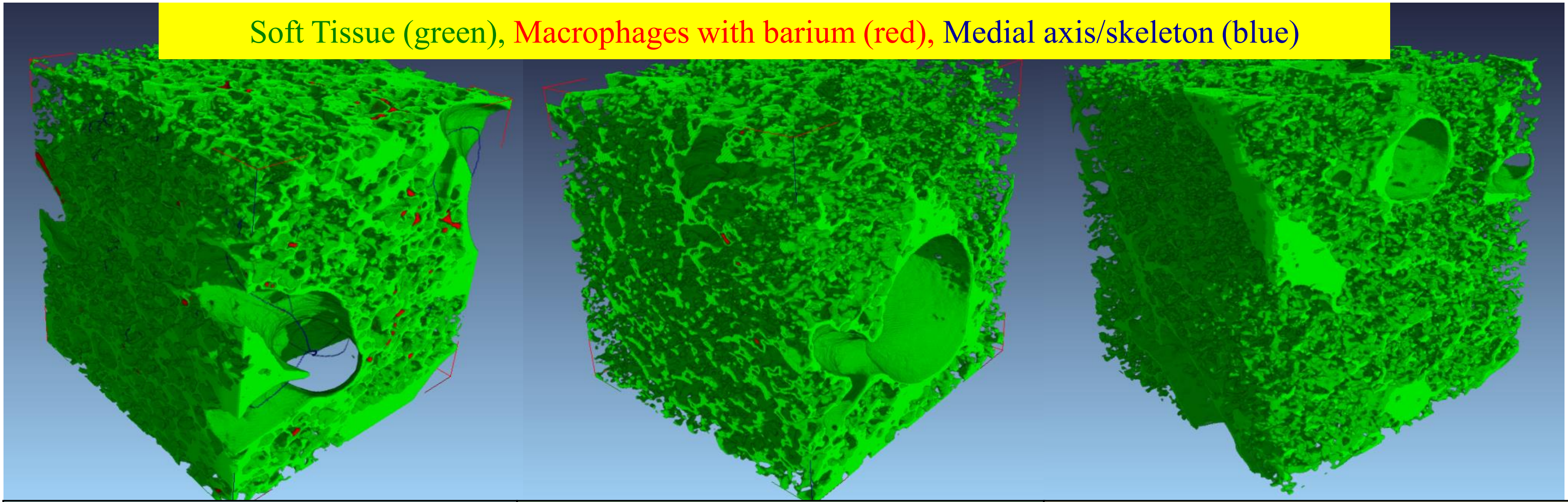

a) asthmatic mouse treated with macrophages labeled by Barium	b) healthy mouse treated with macrophages labeled by Barium	c) control: healthy mouse untreated (no Barium)

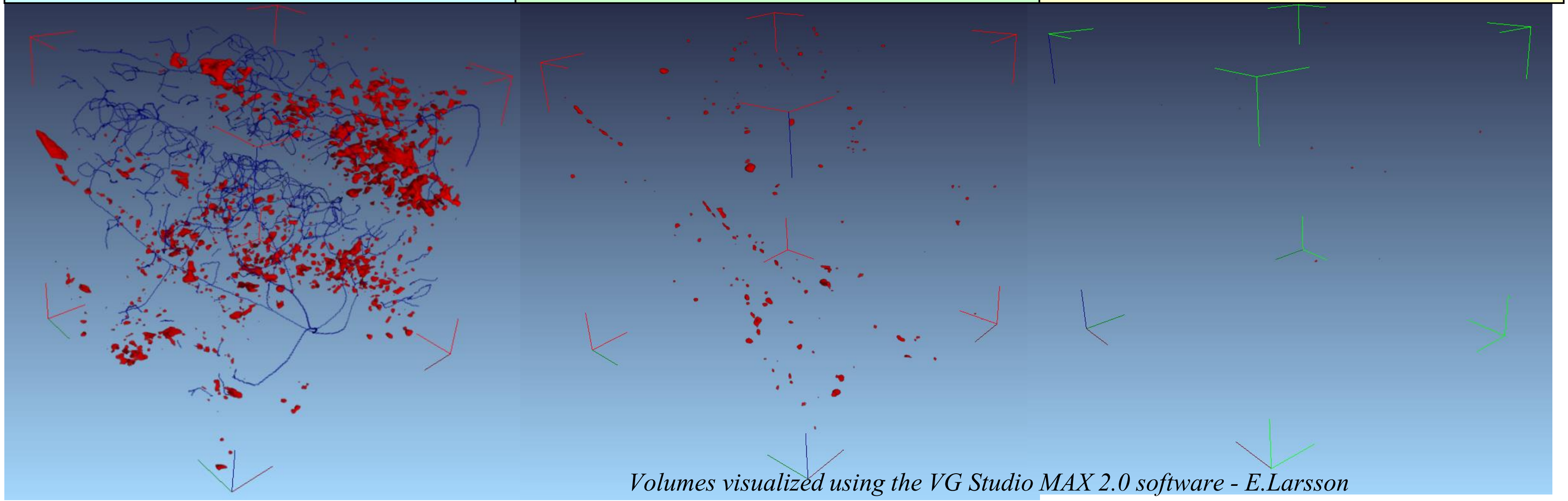

Volumes visualized using the VG Studio MAX 2.0 software - E.Larsson

Cell tracking brain tumors in rats

C6 glioma cells were cultured and some of the cultures were exposed to colloidal **Gold Nano Particles** (GNP) for 22 hrs.

Cells were implanted into the brain of adult male Wistar rats with animal under anesthesia.

The animals were sacrificed two weeks later.

The detection of labeled cells is **enhanced by the higher absorption of gold** with respect to tissue and by PHC effects.

Aims for cell tracking:

- to monitor the dynamic of tumour growth
- to follow the migration of tumour cells
- to understand the metastasis spread dynamic

E = 24 keV

Num. proj. = 720, Pixel size =14µm

3D rendering of 3 mm height skull portion

A1 and A2: Tumor with 300,000 cells – not labelled

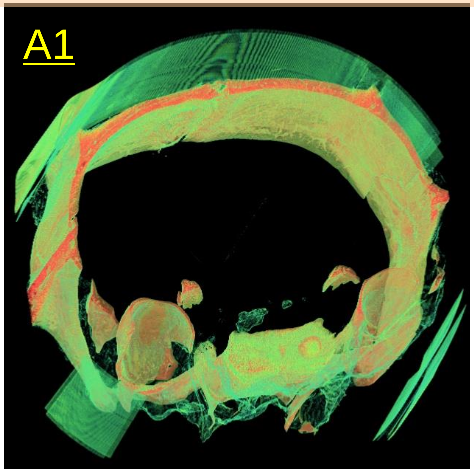

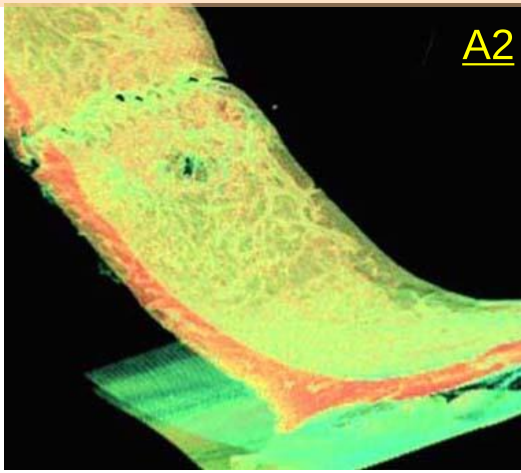

B 1 and B 2: Tumor with 300,000 colloidal gold-loaded cells

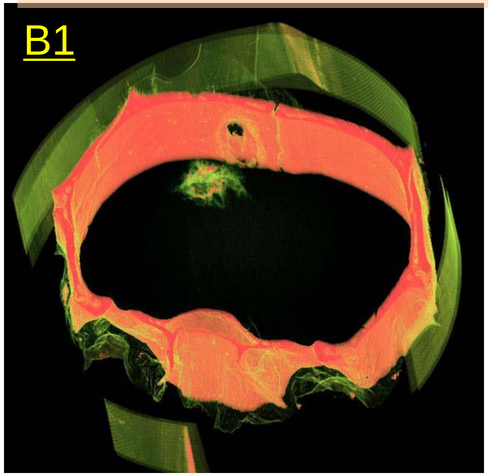

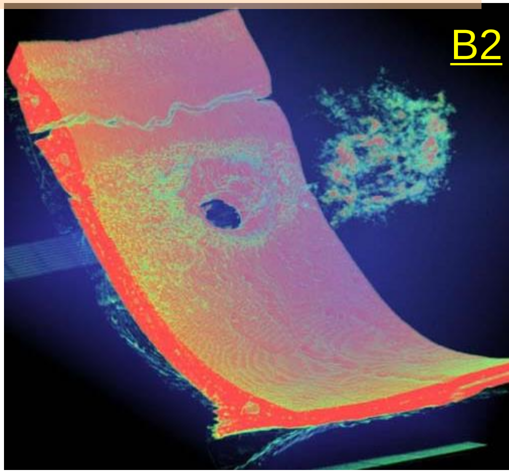

Histologies – 2 weeks after implant.

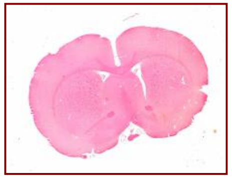

Healthy

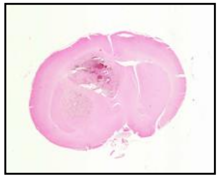

Brain with C6 cells

C,J,Hall et al., Eur. J. of Radiol., Volume 68, Issue 3 (2008)

Elettra Sincrotrone Trieste

Rat 706: Metastasis spread in the spine

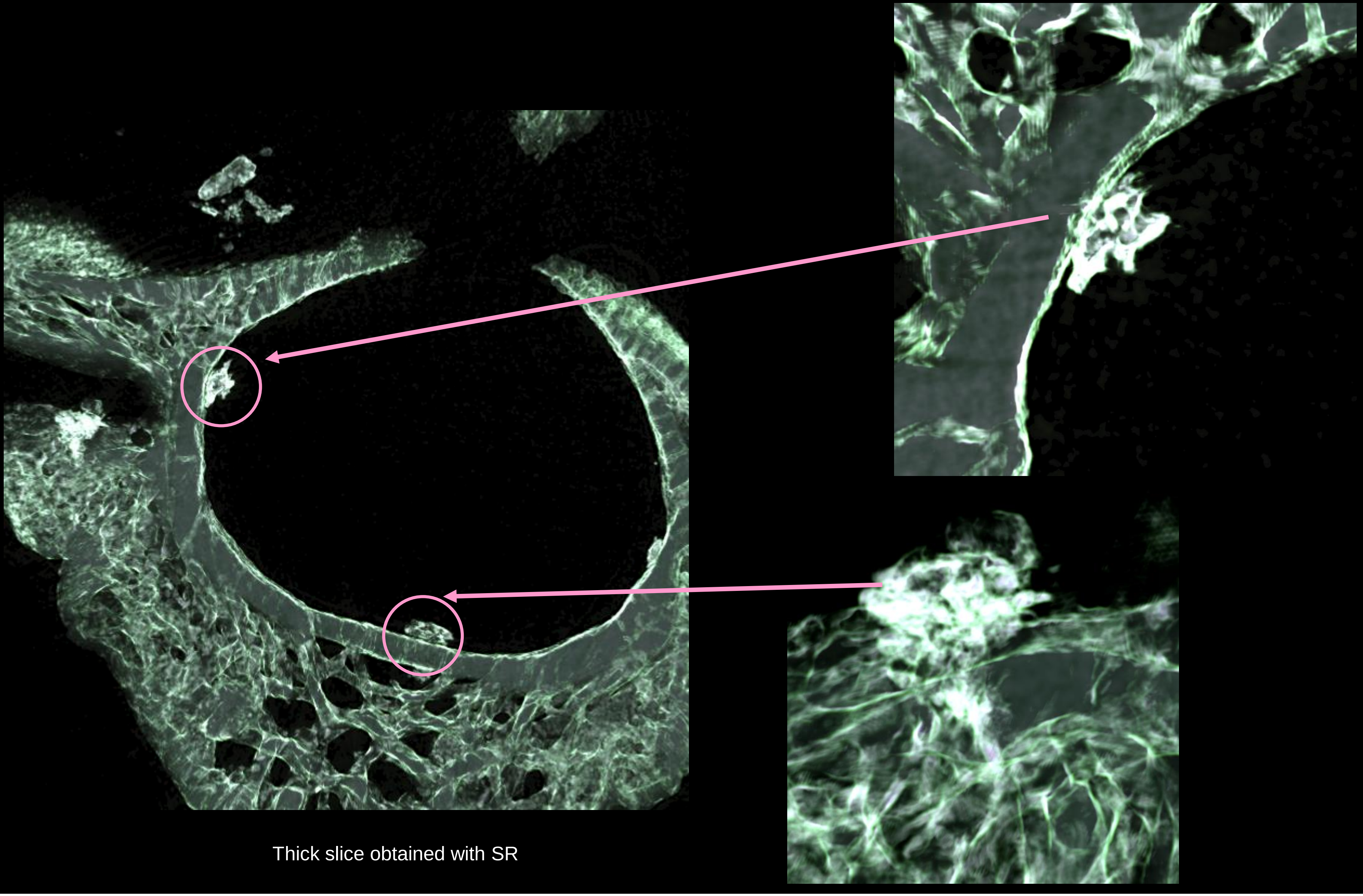

Thick slice obtained with SR

In-vivo study at low dose

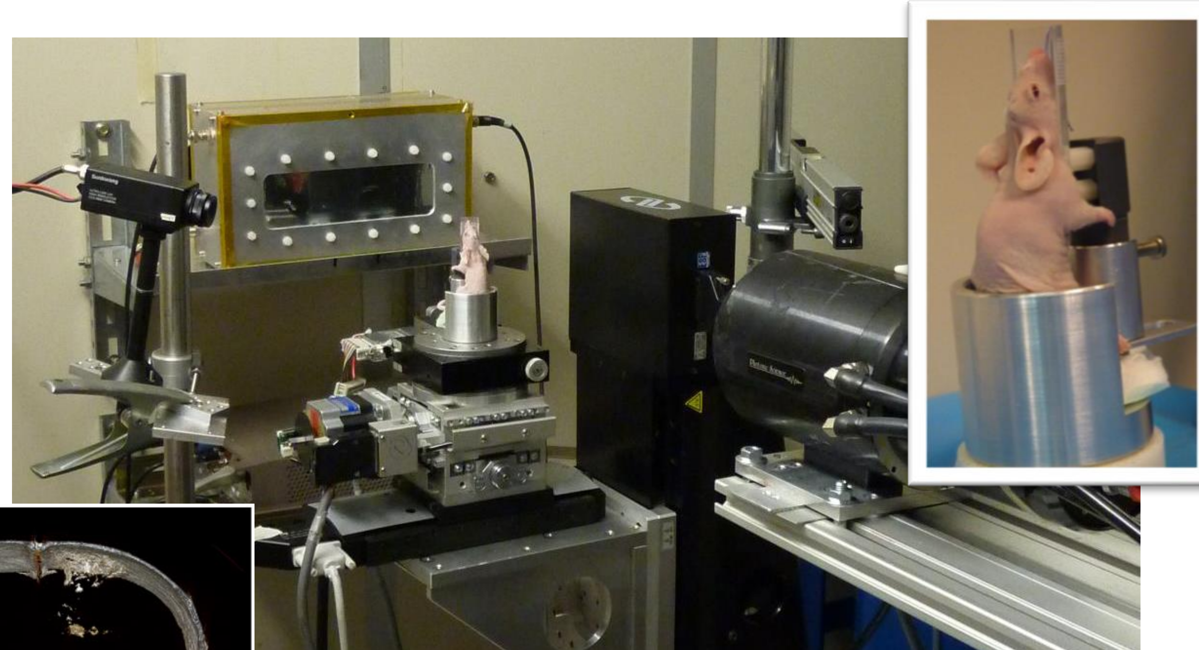

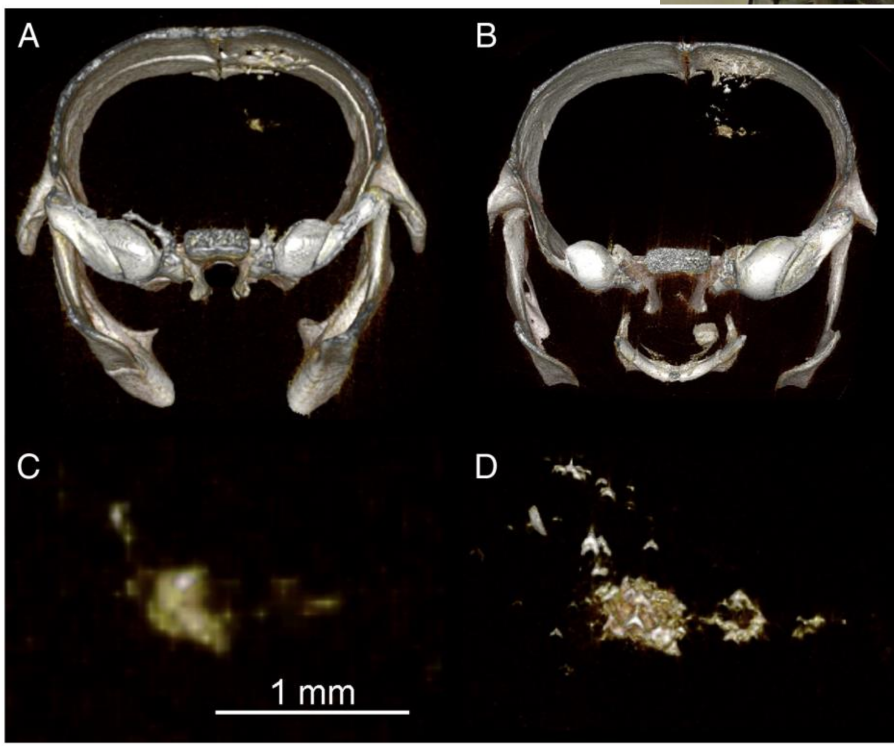

Comparison of two 3D renderings of a CT of a mouse injected with 100,000 GNP-loaded F98 cells depicts:

(A–C) - low x-ray dose *in vivo* data

(B–D) the high x-ray dose *ex vivo* data

The images in panels C and D are enlargements at full system resolution of the developed tumor depicted in panels A and B, respectively.

First experiment *in vivo*: lesions are visible also at low doses

A. Astolfo et al., Nanomedicine: Nanotechnology, Biology and Medicine, Vol. 9, Issue,2013

Clinical applications

- potential studies with patients

- *Need to **limit** radiation dose. Strict research protocol for selected patients. Find best compromise between dose and image quality, pixel sizes : 50 – 100 µm*

  - Breast imaging
  - ABI potentials for imaging of cartilage and joints
  - Feasibility study for low dose Phase contrast lung CT

Elettra Sincrotrone Trieste

Clinical Mammography

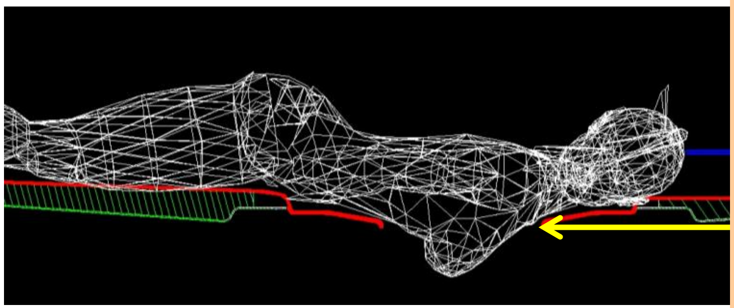

Outcomes of first protocol

Images with SR have:

- *higher specificity,*
- *better agreement with the golden standard (biopsy),*
- *improved image quality,*
- *strong reduction of X-ray doses.*

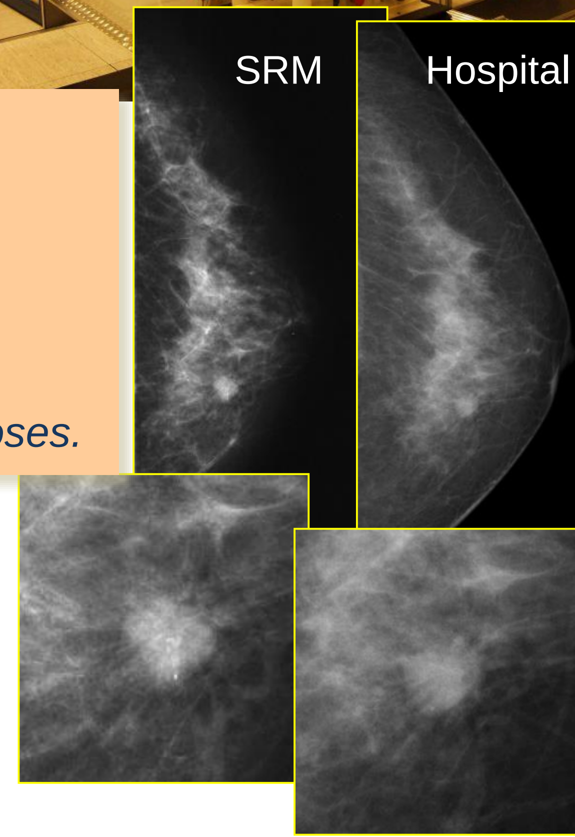

Next step: Low dose phase contrast breast CT

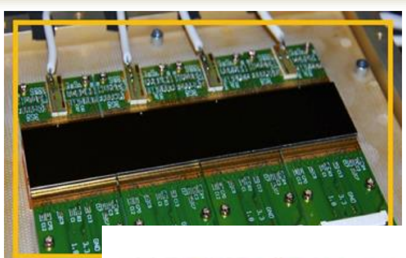

Pixirad

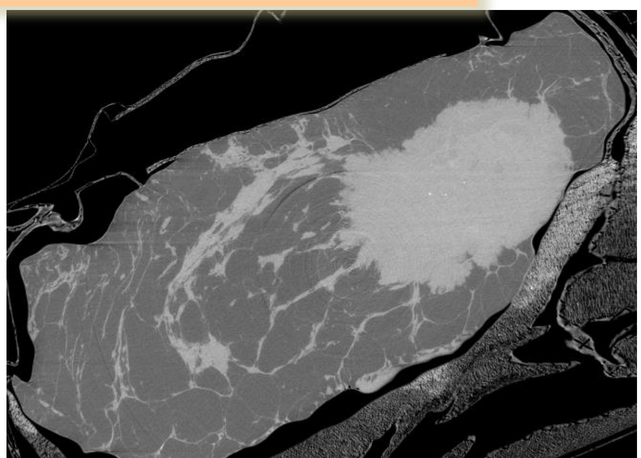

CSIRO

THE UNIVERSITY OF MELBOURNE

UNIVERSITÄTSMEDIZIN GÖTTINGEN UMG

Low dose CT - Effect of long propagation distance

9 m 3.2 m 1.8 m distance

Detail approx.
Size:1.5 x 1.5 cm
E = 32 keV
Pixirad detector
MGD ~ 20 mGy

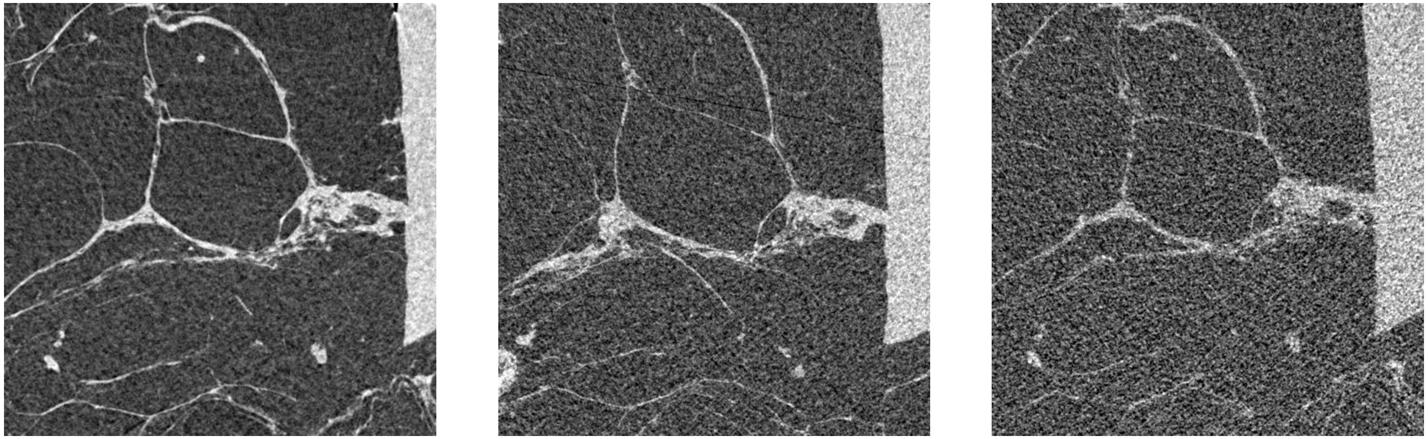

Courtesy of L.Brombal (INFN TS)
Preliminary results, unpublished

Reconstruction of low dose CT slice with application of phase retrieval pre-processing algorithm (Paganin 2002)

Mastectomy slice
Size:7 x 3 cm
E = 32 keV
XCounter detector
MGD ~ 5 mGy

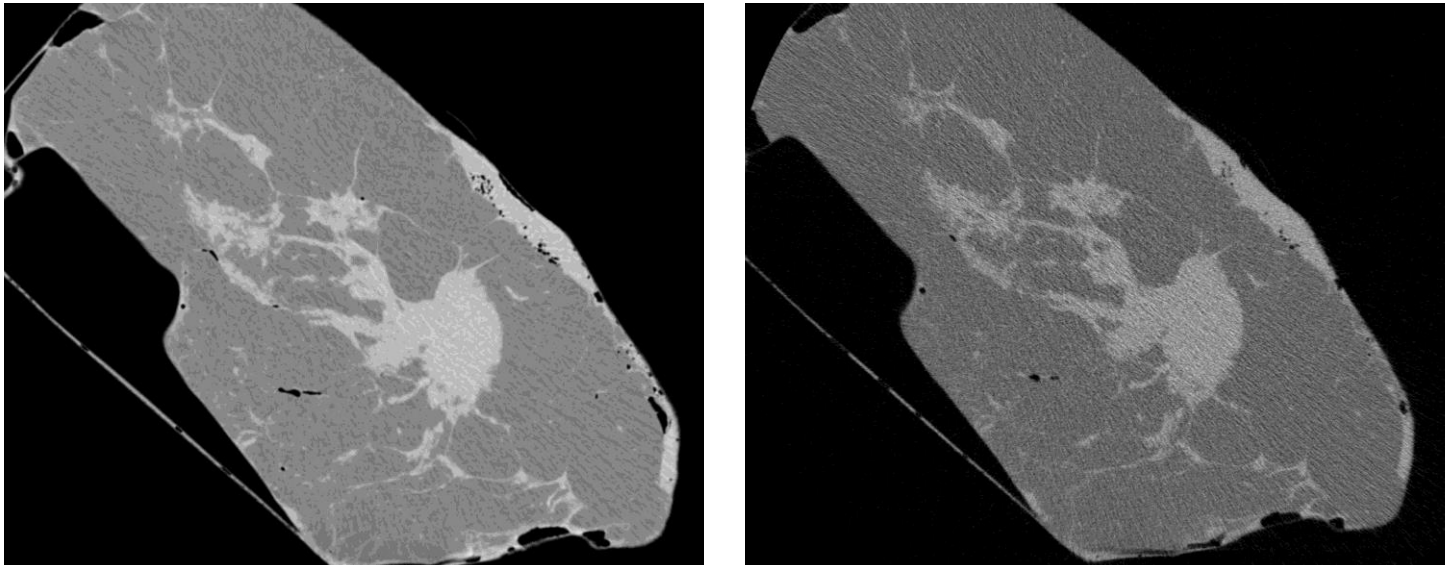

Baran et al.: Phys. Med. Biol. 62, 2017

ABI studies of Cartilage and bone interface

Osteoarthrosis (OA) is a disease characterized by the progressive degeneration of articular cartilage and the development of altered joint congruency. It has a high incidence in the adult population. Affecting mainly the elderly population, it is one of the main causes of disability worldwide. Conventional radiography detects only **important osseous changes**, at advanced OA or RA stages, when therapeutic strategies are less effective. **Early changes** in the **cartilage** and other **articular tissues** are **not** directly visible. MRI imaging works better but the maximum achievable spatial resolution is not always adequate.

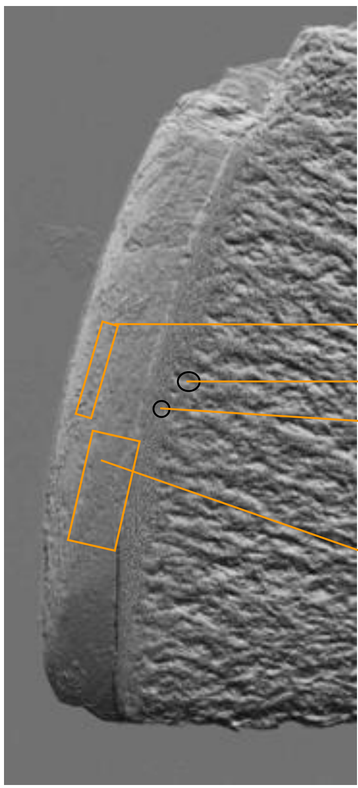

Need to study:
- cartilage
- cartilage-bone interfaces
- changes in the bone structure

Superficial Layer (Zone of horizontal collagen fibers with flat cells)

Subchondral Bone Plate (**Important for diagnostic purposes in OA**)

Tidemark (Border between normal and mineralized cartilage)

Transitional and Deep Layer (round cells, collagen fiber switches from horizontal to vertical orientation, increasing stiffness and material density)

Aim: detect the architectural arrangement of collagen within cartilage and evaluate how the cartilage degeneration affects the underlying subchondral and trabecular bone.

Elettra
Sincrotrone
Trieste

Femur head core cuts: collagen arcades structure

- The ABI technique allows to visualize the discontinuities in the sample and the inner structures invisibles by means of conventional X-Ray imaging.
- The transition bone-cartilage is emphasized.
- The articular cartilage striations are well visible due to X-ray diffraction at edges of fibers

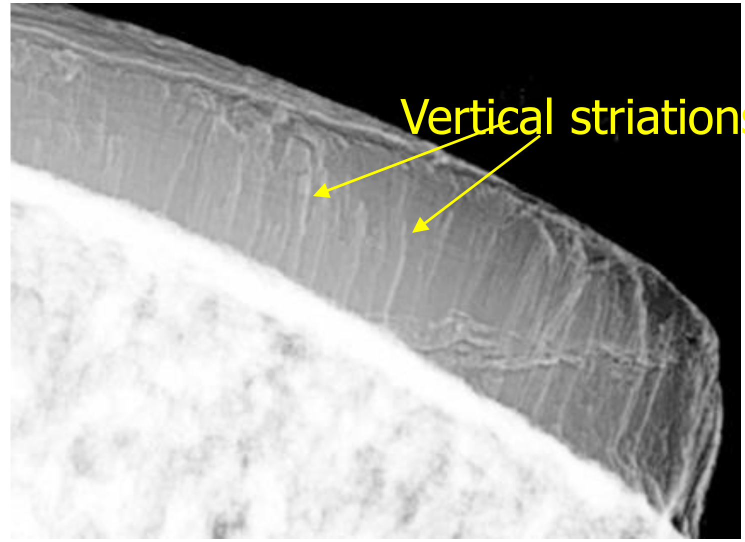

Apparent absorption image

Refraction image

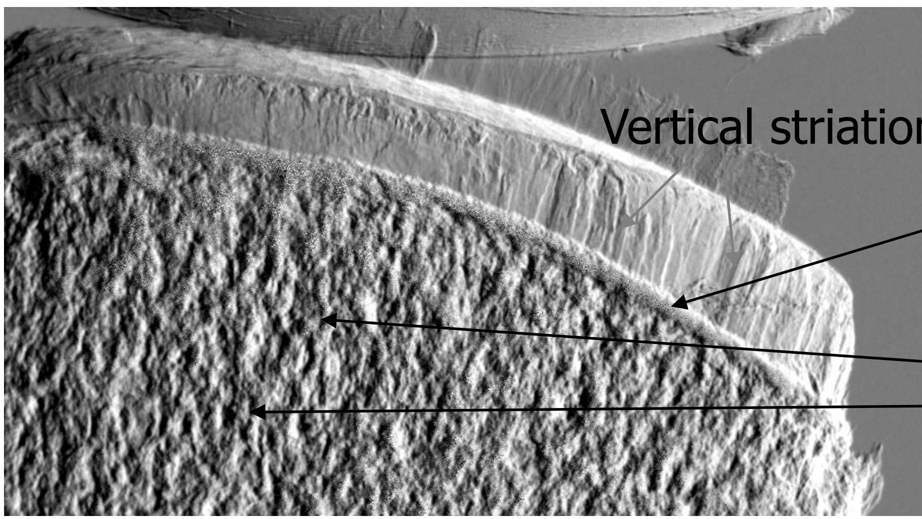

Subchondral bone

Trabecular bone

Elettra
25 keV

Muehleman C et al., J, Osteoarthritis and Cartilage 12 (2): 97-105, 2004

Femur head core cuts: comparison with MRI

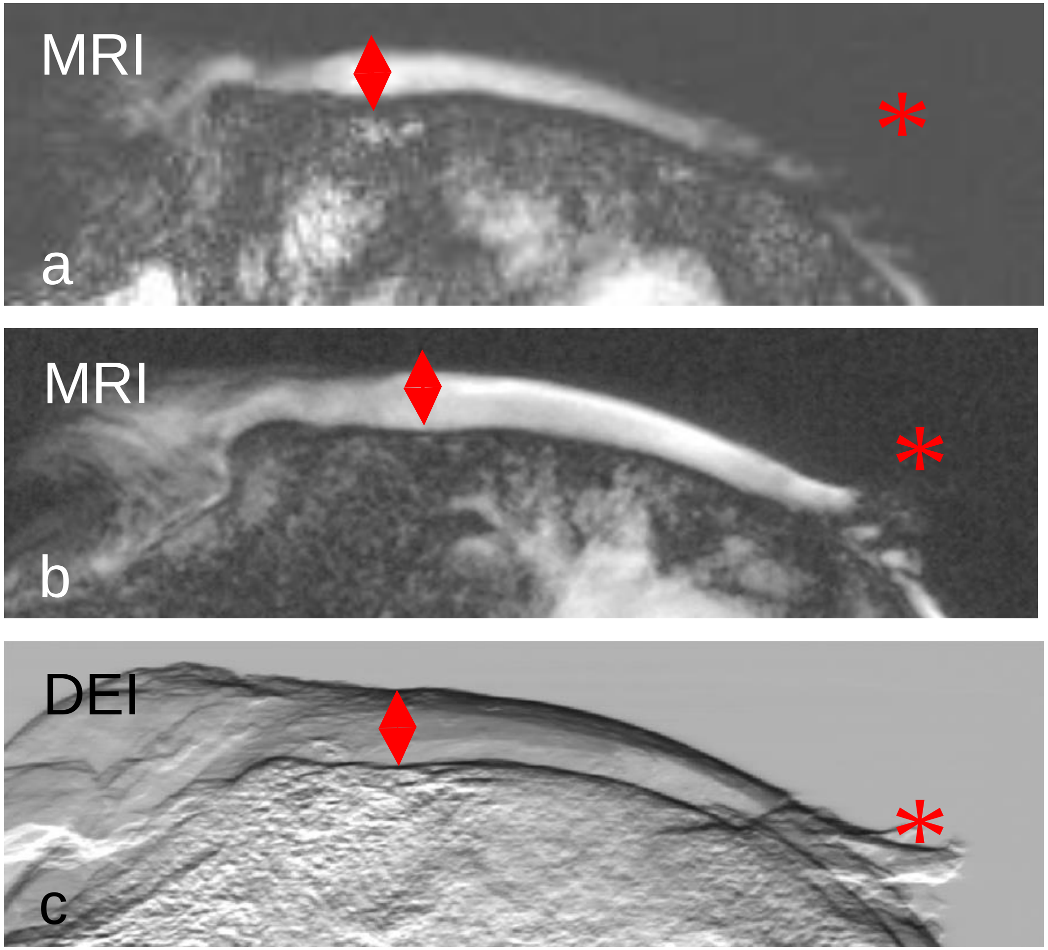

5 sec

150 sec

A.Wagner et al., Nucl. Instrum. Methods A 548, 47 (2005).

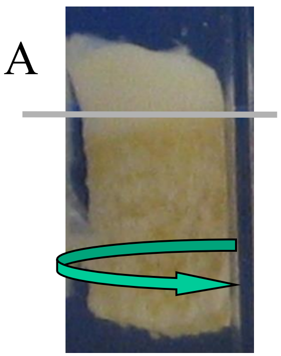

Specimen of normal cartilage (A), Coronal plane extracted from the reconstructed CT volume (B), Magnified portion identified by the ROI (C), Corresponding section from histologic preparation (D).
E = 26 keV, pixel size = 8 x 8 μm^2.

ABI in planar and tomographic modes was performed *in vivo* on articular joints of guinea pigs. Images showed the potential of technique in revealing initial lesions. Images with high spatial resolution and with an acceptable radiation dose.

Coan, P., et al., Invest. Radiology, 45(7), 437-444 (2010)

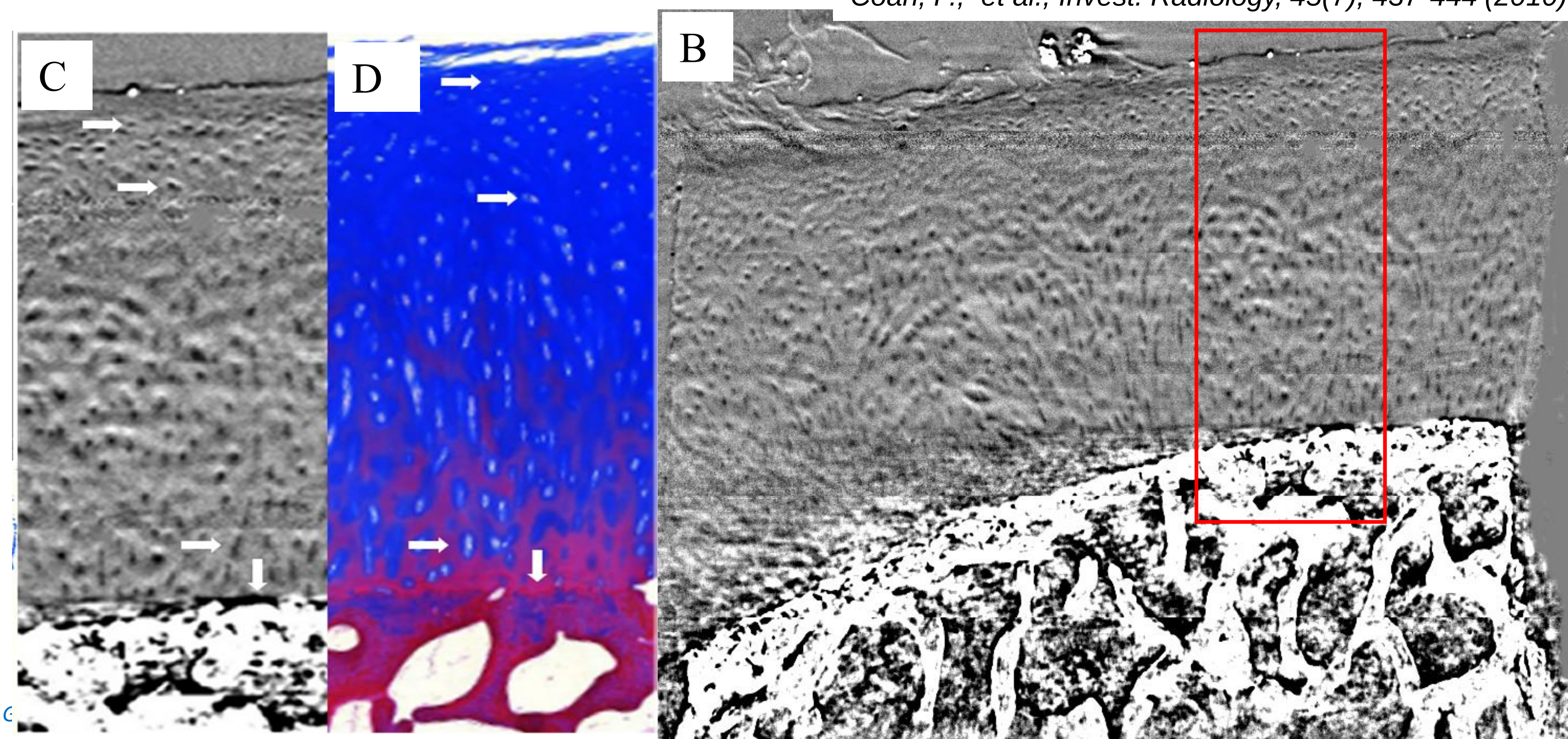

ABI studies of the finger joint

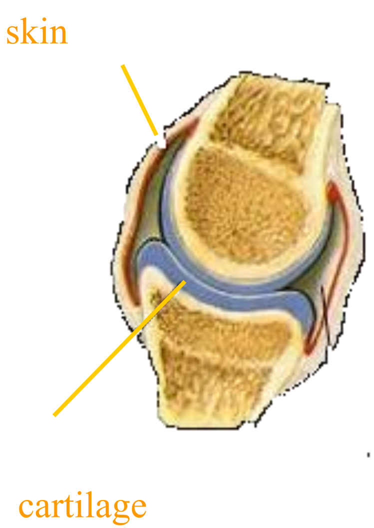

Conventional radiograph

Apparent absorption image @ 20 keV
at ELETTRA

Lewis, R. A., et al., British J. Rad., 76(905), 301-308 (2003)

Index finger proximal interphalangeal joint

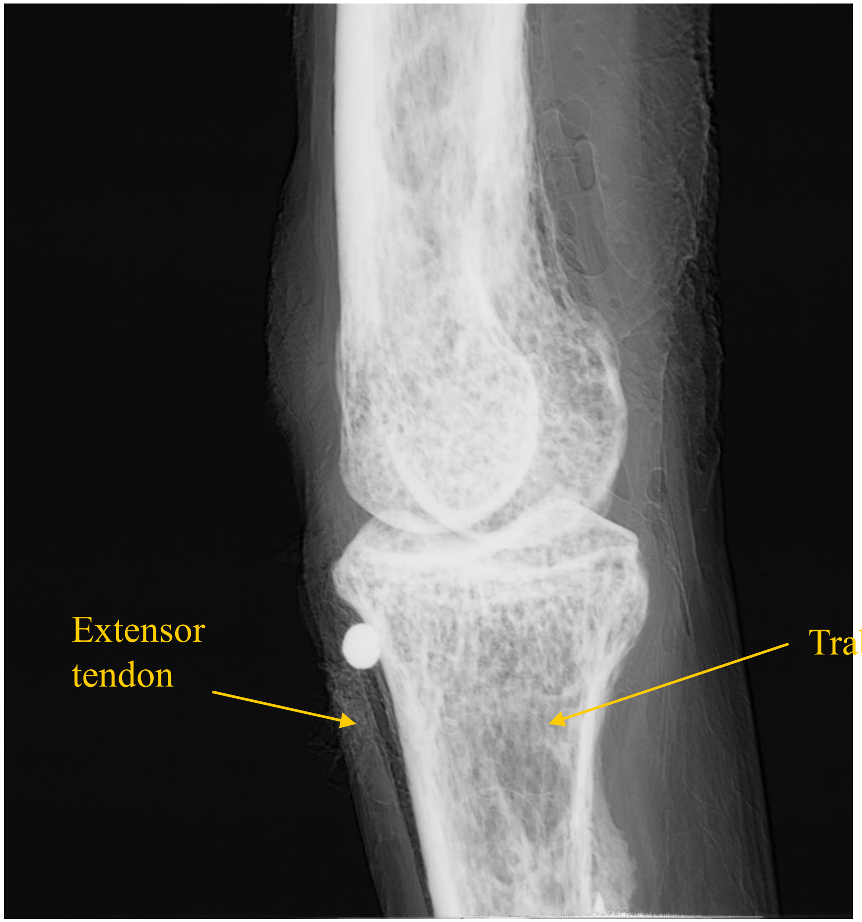

Apparent absorption Image

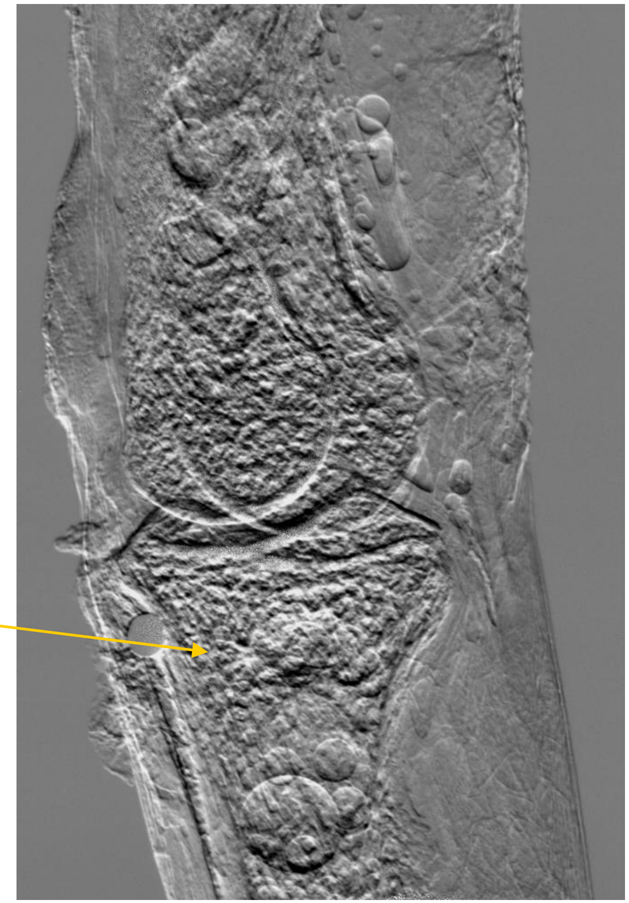

Refraction Image

Lewis, R. A., et al., British J. Rad., 76(905), 301-308 (2003)

Index finger proximal interphalangeal joint

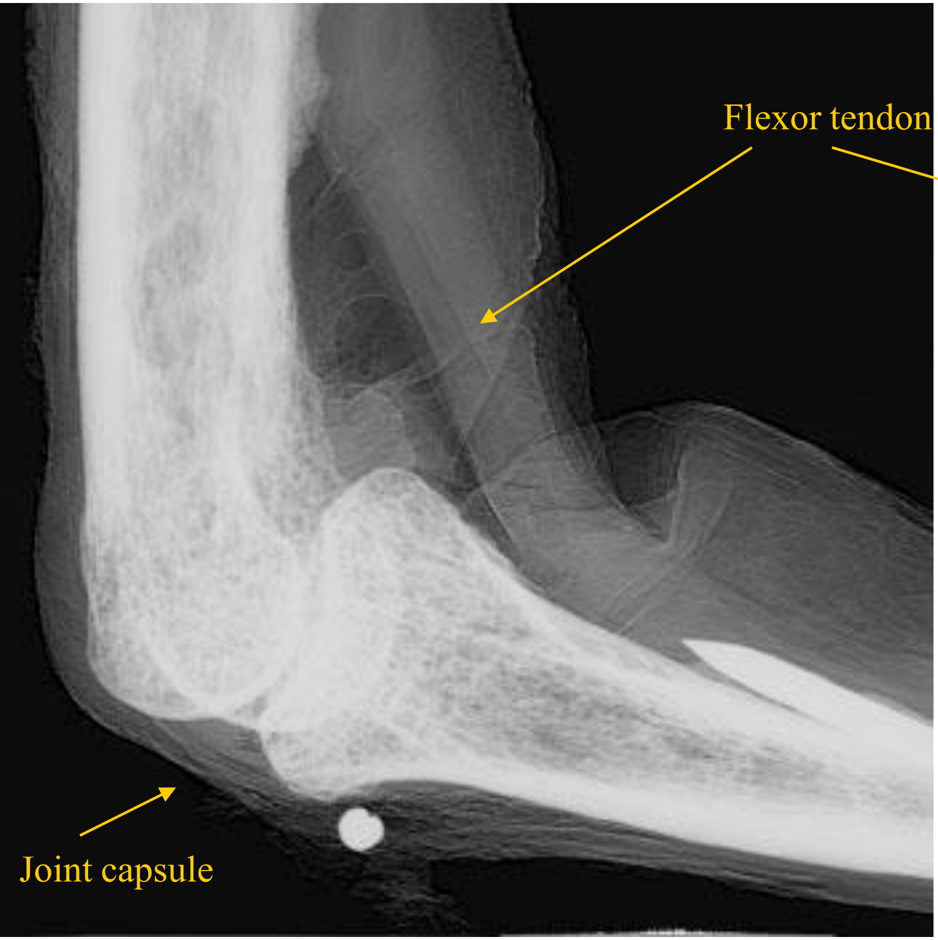

Apparent absorption Image

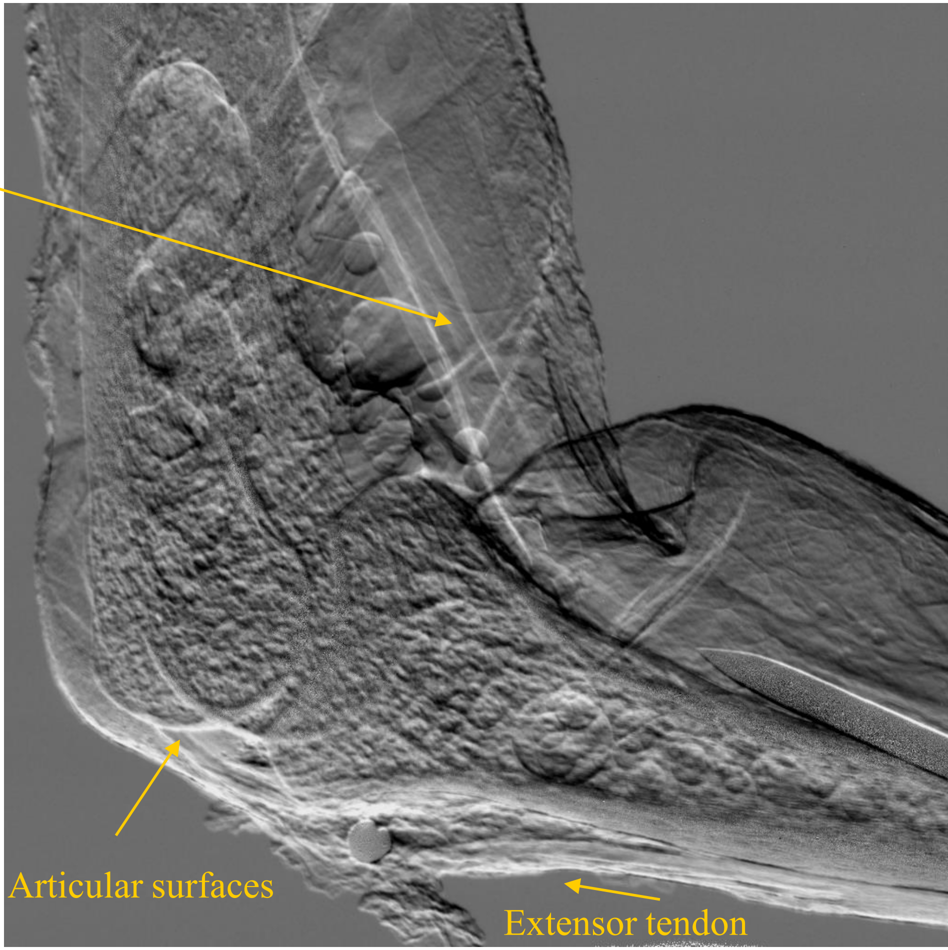

Refraction Image

Lewis, R. A., et al., British J. Rad., 76(905), 301-308 (2003)

Low dose phase contrast Lung CT - proof-of-principle study on porcine lungs

Aim: evaluate the potentials of lungs CT in humans

- samples: porcine lungs in the artiCHEST training phantom
- SR imaging: E = 40 keV, prop dist = 2.5 m, air entrance dose ~ 13 mGy
- Reconstruction: conventional FBP, phase retrieval pre-processing

SYRMEP beamline

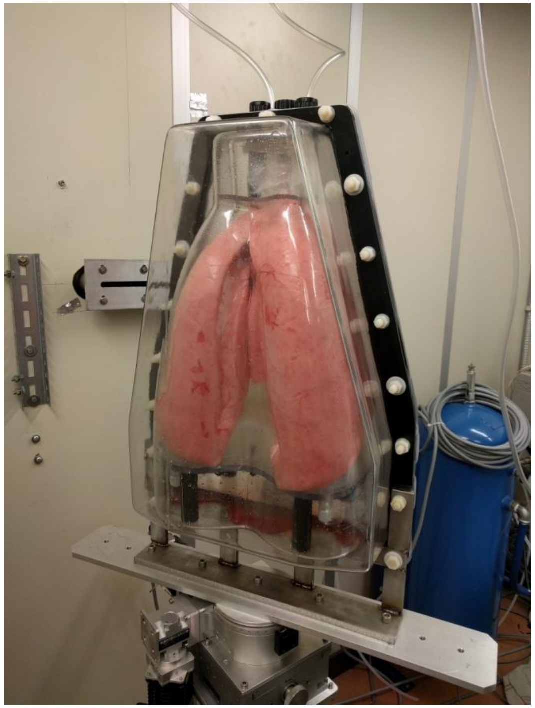

Cattinara hospital Trieste

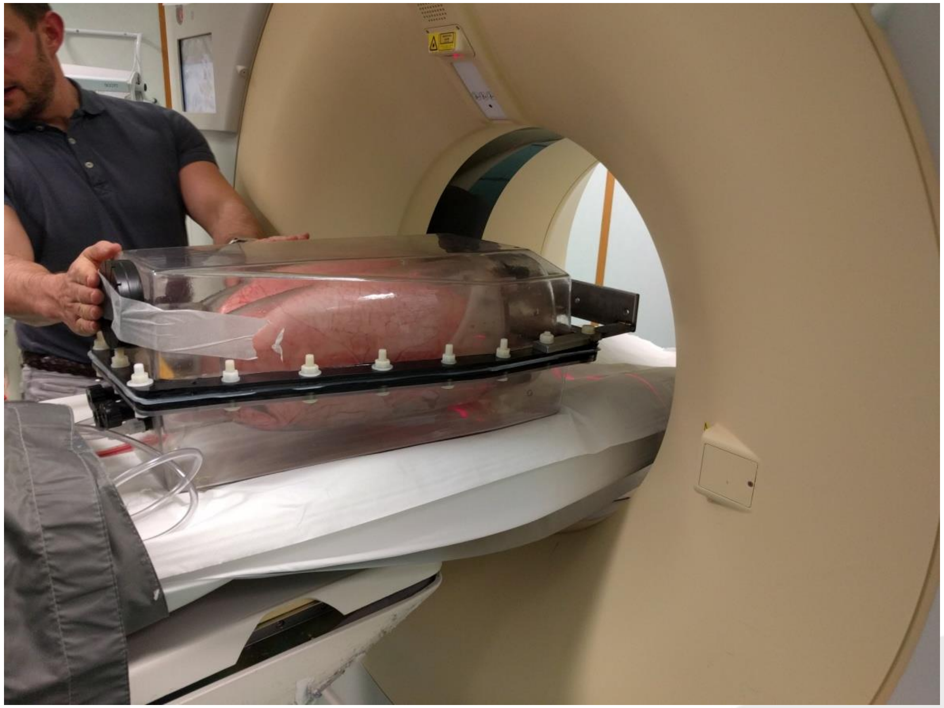

UNIVERSITÄTSMEDIZIN GÖTTINGEN UMG

DZL Deutsches Zentrum für Lungenforschung

Elettra Sincrotrone Trieste

W.Wagner et al.: J.Synchrotron Rad. 25, (2018)

Elettra Sincrotrone Trieste

Conver

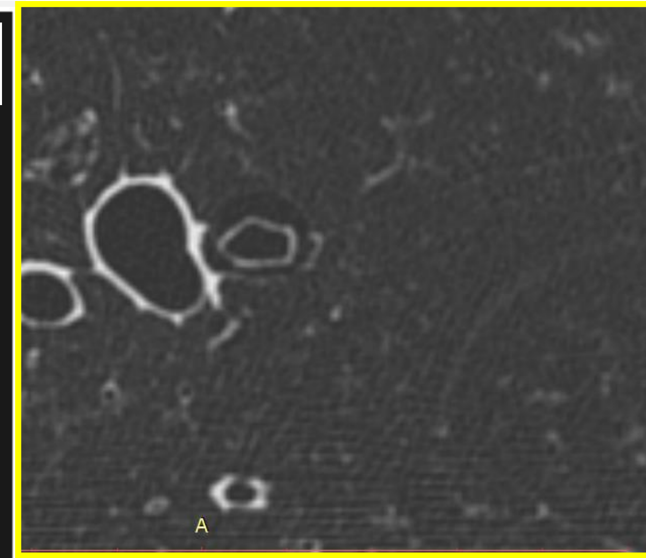

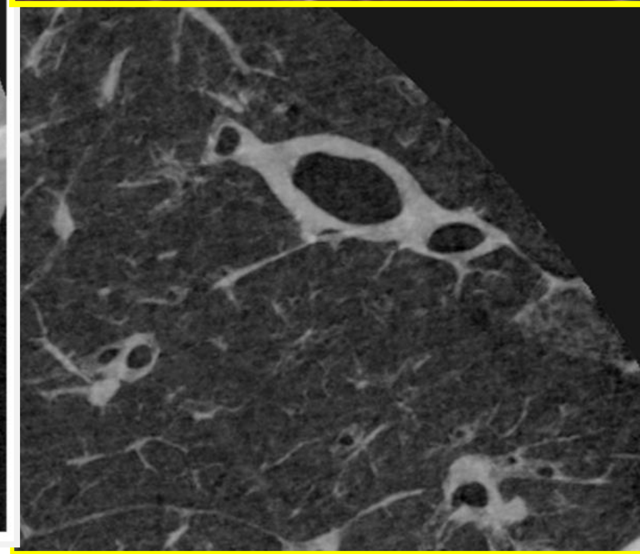

Lesions visualization

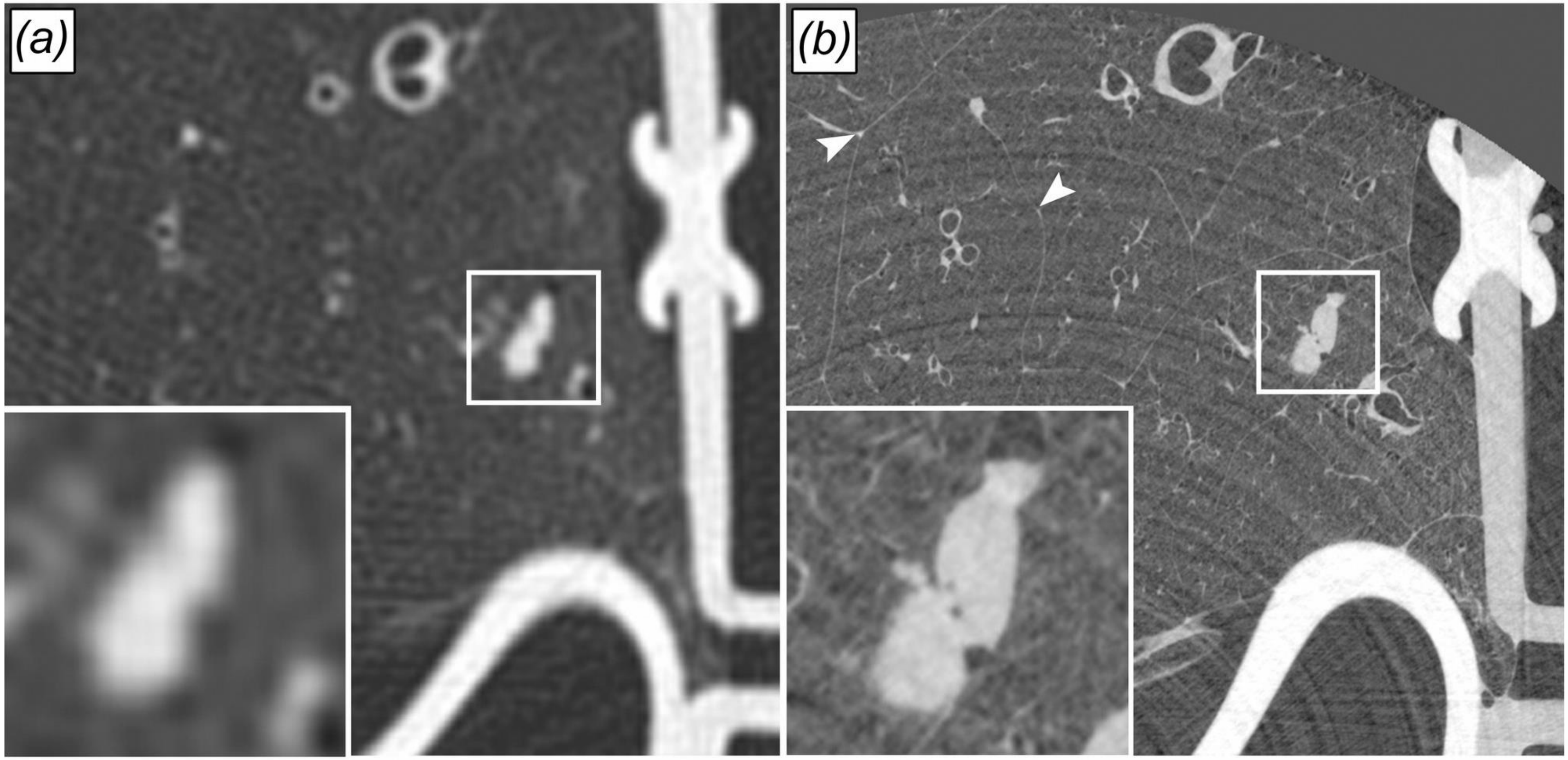

(a) clinical HRCT - air kerma ~ 33 mGy, voxel size 0.45 x 0.45 x 0.9 mm^3
(b) SYRMEP - air kerma ~13 mGy, voxel size 0.1 x 0.1 x 0.1 mm^3

W.Wagner et al.: J.Synchrotron Rad. 25, (2018)

Quantitative analysis

Pore3D: a software tool for **3D image processing** and **analysis**

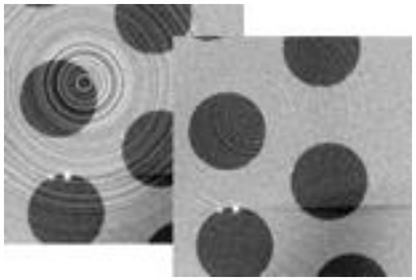

Filters
Basic (mean, median, gaussian, ...)
Anisotropic diffusion
Bilateral
Ring artifacts reduction
Binary (median, clear border, ...)

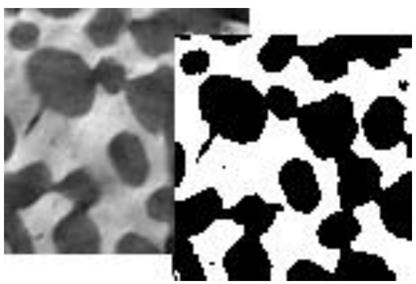

Segmentation
Automatic thresholding (Otsu, Kittler,..)
Adaptive thresholding
Region growing
Multiphase thresholding
Clustering (*k*-means, *k*-medians, ...)

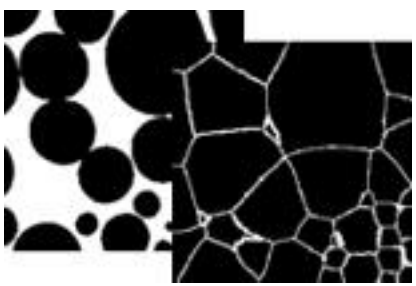

Morphological processing
Dilation and erosion
Morphological reconstruction
Watershed segmentation
Distance transform
H-Minima filter

Skeleton extraction
Thinning
Medial axis (LKC)
DOHT
Gradient Vector Flow
Skeleton pruning
Skeleton labeling

Analysis
Minkowski functionals
Morphometric analysis
Anisotropy analysis
Blob analysis
Skeleton analysis
Textural analysis (fractal dimension, ...)

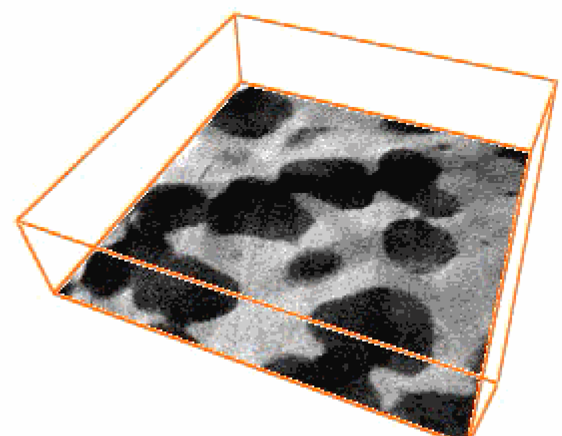

http://ulisse.elettra.trieste.it/uos/pore3d

F. Brun et al., NIM A, 615 (2010) 326–332

Bone turnover in mice exposed to micro-gravity conditions

- 3 wild type (WT) mice and 3 pleiotrophin-transgenic (PTN-Tg) mice in a special payload (MDS - Mice Drawer System). The transgenic mouse strain over-expressing pleiotrophin (PTN) in bone was selected because of the PTN positive effects on bone turnover.
- **91 days in the International Space Station (ISS) by NASA: Aug. - Nov. 2009.**
- Controls:
  - mice on Earth in the same special payload MDS (*ground* mice)
  - mice in common cages (*vivarium* mice)
- SR µ-CT experiments were performed on femurs and spines
- Being non-destructive, µ-CT is very attractive for these rare specimens

University of Genova

Elettra Sincrotrone Trieste

Università Politecnica delle Marche

University of Trieste – Dept. of Engineering

http://www.nasa.gov/mission_pages/station/research/experiments/MDS.html

Analysis of the microarchitecture of the trabecular bone in femurs

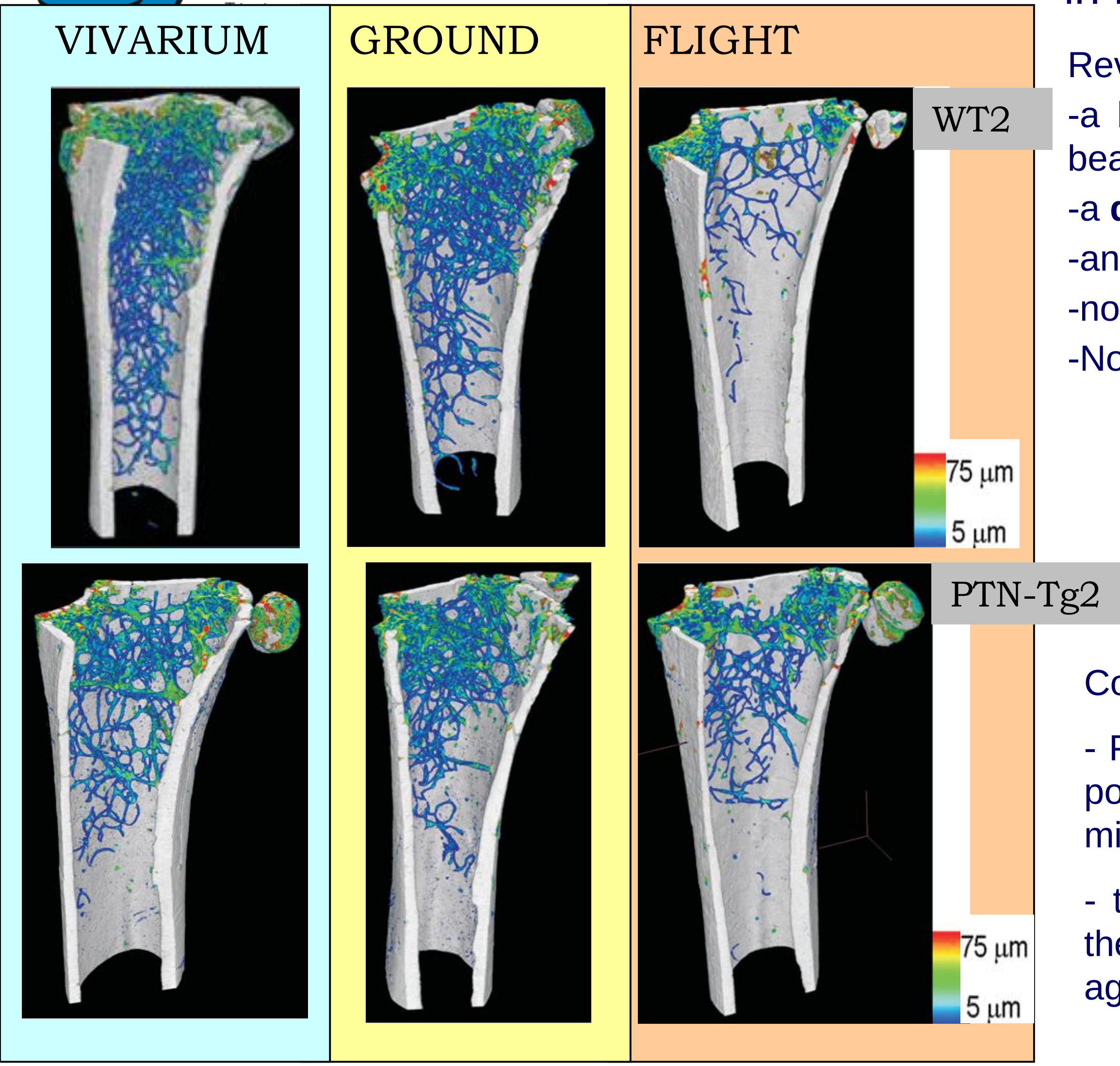

Revealed:

-a **bone loss** during spaceflight in the weight-bearing bones

-a **decrease** of the trabecular number

-an **increased** mean trabecular separation

-no significant change in trabecular thickness.

-No effects on not weight-bearing bones.

E = 19 keV
Pixel size = 9 mm
N. Proj = 900
Distance sample-ccd= 3 cm

Comparison WT vs.PTN-Tg2:

- PTN-Tg exposed to normal gravity has a poorer trabecular organization than WT mice

- the expression of the PTN gene during the flight resulted in some protection against microgravity's negative effects.

Color map represents bone trabecular thickness distribution in the femur (red = 75 µm, blue = 5 µm)

S. Tavella et al "*Bone Turnover in Wild Type and Pleiotrophin-Transgenic Mice Housed for Three Months in the International Space Station (ISS)*", *PlosONE, March 2012.*

New challenges: dynamic studies and multiscale micro-CT

- Dynamic CT studies (4DCT): repeated series of scans performed at sequential time lapses, to provide information about the microstructure evolution.
    - Application in entomology
    - Application to volcanology

- Multiscale micro-CT combines different resolution modalities on the same sample
    - Mise lungs visualzation at cellular level

4DCT: *in vivo* X-ray microscopy with projection-guided gating

- Visualizing fast micrometer scale internal movements of small animals
- Application of phase contrast microCT (~ 3.3 μm voxel size) with retrospective, projection-based gating
- 20 CT scans selected through the 150 Hz oscillations of the blowfly flight
- It is a key challenge for functional anatomy, physiology and biomechanics

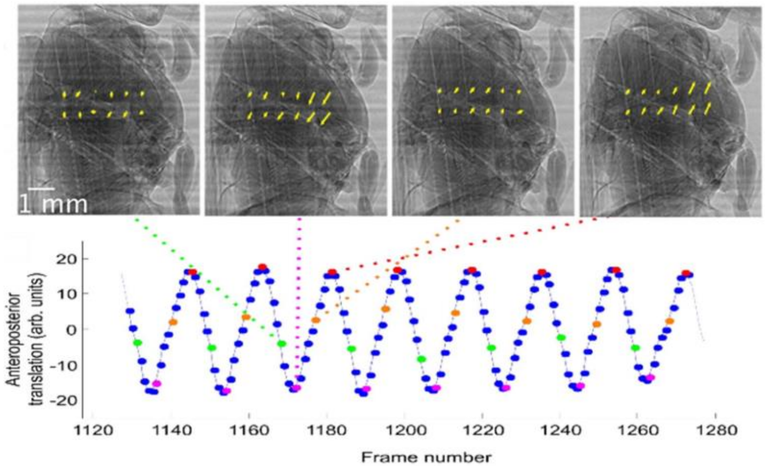

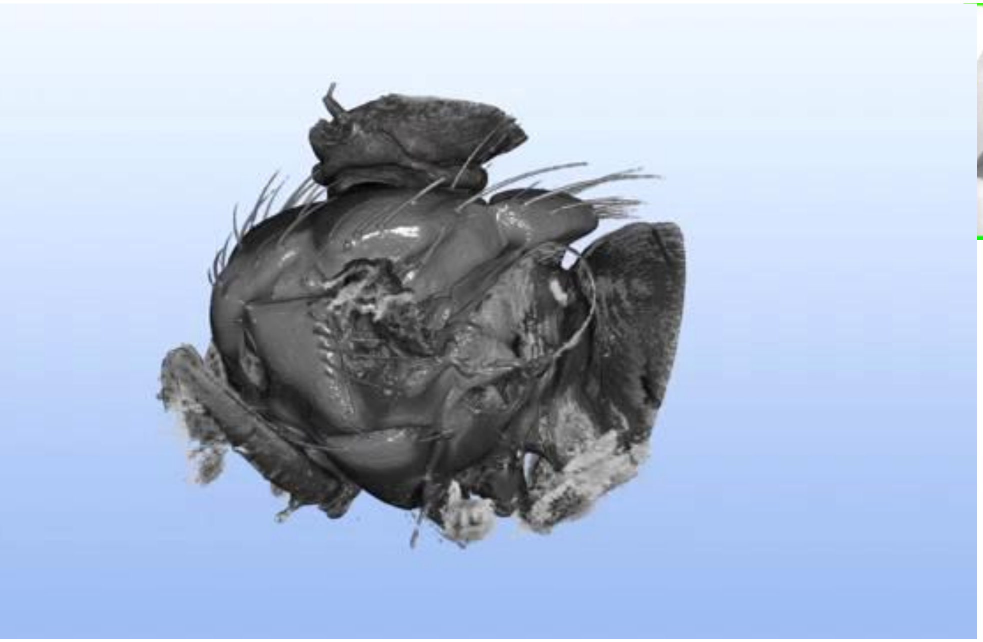

Air-filled tracheal network spanning the dorsal longitudinal muscles

Rajmund Mokso et al.: Sci. Rep. | 5 : 8727 | (2015)

4D X-ray micro-CT study of bubble growth in basaltic foams – I experiment

The study of bubble formation in magma is fundamental for understanding the volcanic eruption mechanisms

Dynamic CT studies performed *in-situ* with basaltic samples brought at 600-1200 °C – white beam

Quantitative analysis allowed to measure **bubble size, wall thickness distributions**, **connectivity**, and calculate **permeabilities** and **tensile strengths** of basaltic foams imaged during bubble growth in hydrated basaltic melts.

D.R. Baker, F. Brun, C. O'Shaughnessy, L. Mancini, J. Fife, M. Rivers, Nature Comm., 3 (2012) 1135

3D movie of the evolving sample

The study of bubble formation in magma is fundamental for understanding the volcanic eruption mechanisms

Dynamic CT studies performed *in-situ* with basaltic samples brought at 600 - 1200 °C – white beam

Quantitative analysis allowed to measure **bubbles size, wall thickness distributions**, **connectivity**, and calculate **permeabilities** and **tensile strengths** of basaltic foams imaged during bubble growth in hydrated basaltic melts.

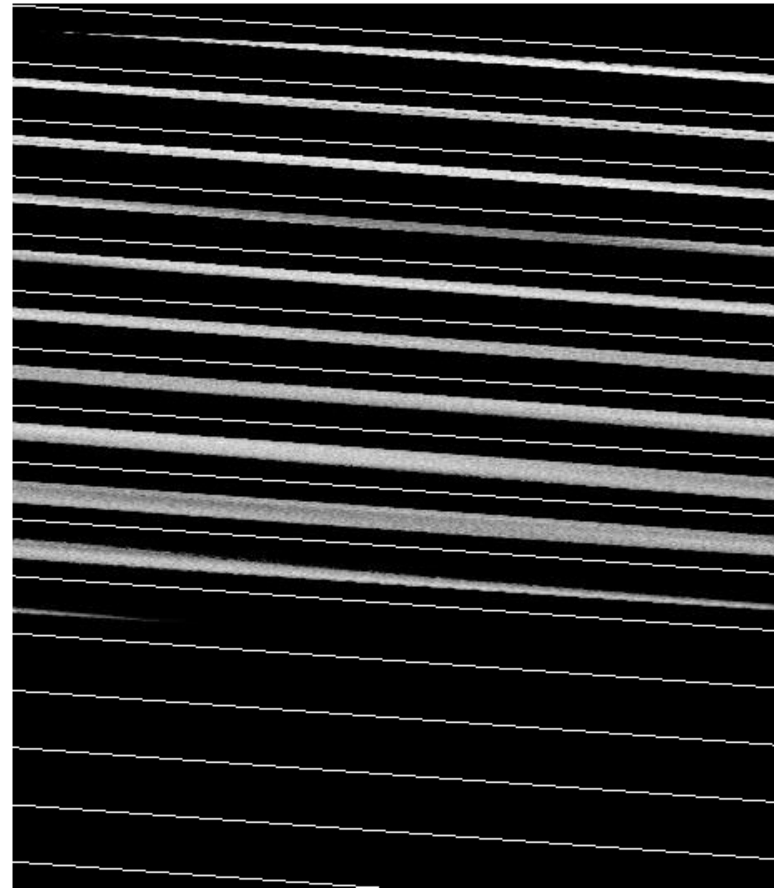

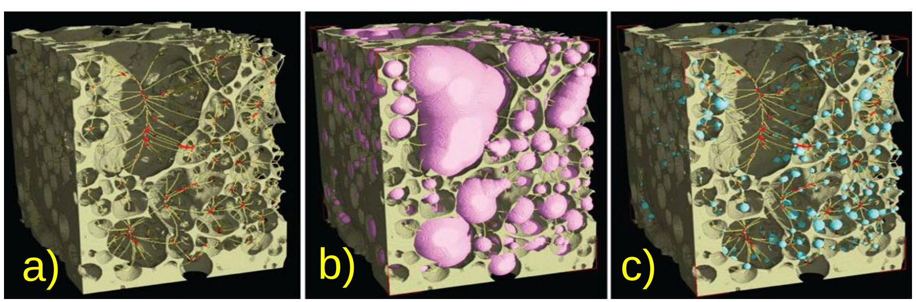

a) Topology preserving skeleton with nodes at the intersections of the branches
b) Maximal inscribed spheres to calculate bubble volumes
c) Maximal inscribed spheres to calculate pore throat diameters and wall thicknesses

D.R. Baker, F. Brun, C. O'Shaughnessy, L. Mancini, J. Fife, M. Rivers, Nature Comm., 3 (2012) 1135

Experiments vs. natural Bubble Size Distributions

4D experiments
Number of produced Vescicles vs Vescicle Volume

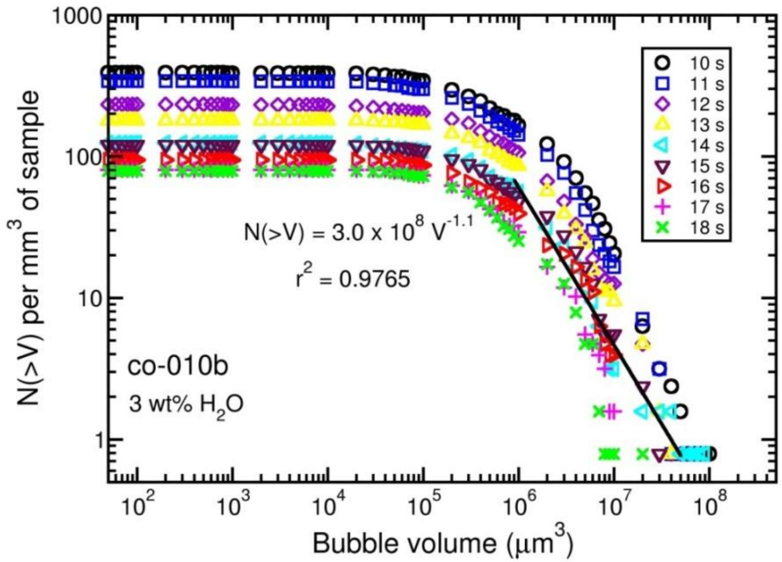

Normal Strombolian eruption

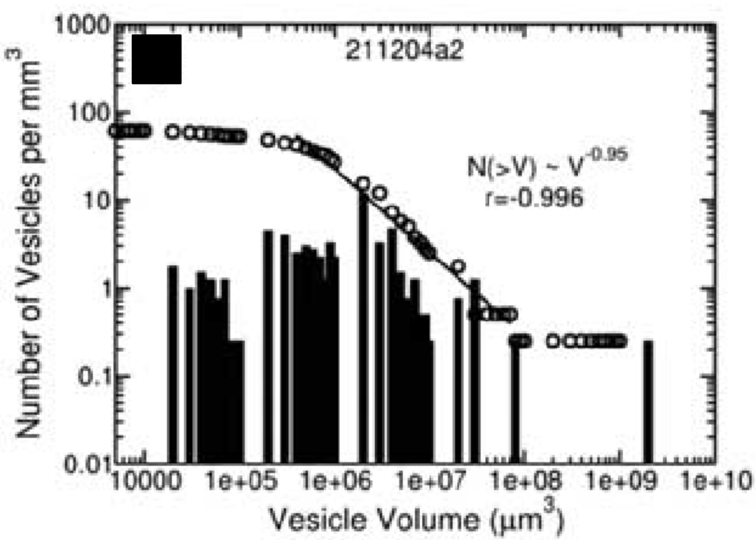

Paroxysmal eruption

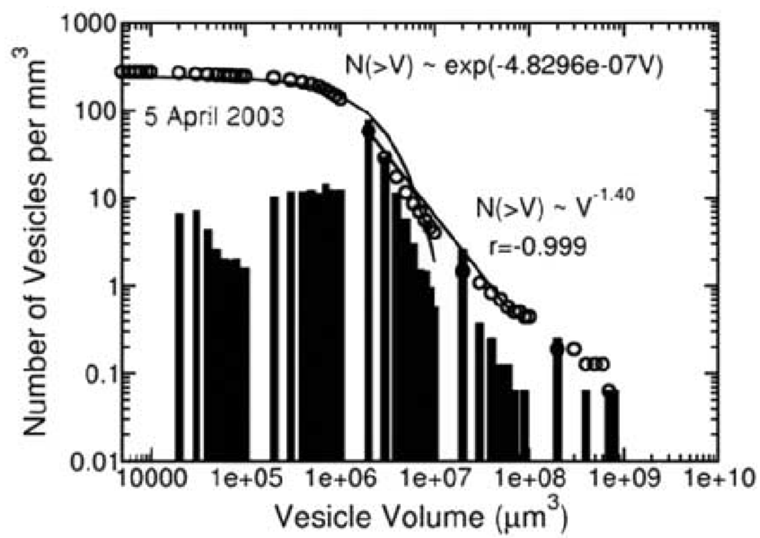

D.R. Baker, F. Brun, C. O'Shaughnessy, L. Mancini, J. Fife, M. Rivers, Nature Comm., 3 (2012) 1135

Elettra Sincrotrone Trieste

Multi-resolution CT: Zoom CT

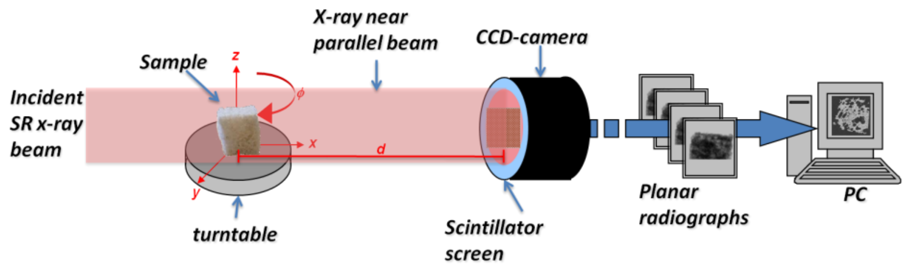

Agarose embedded mice

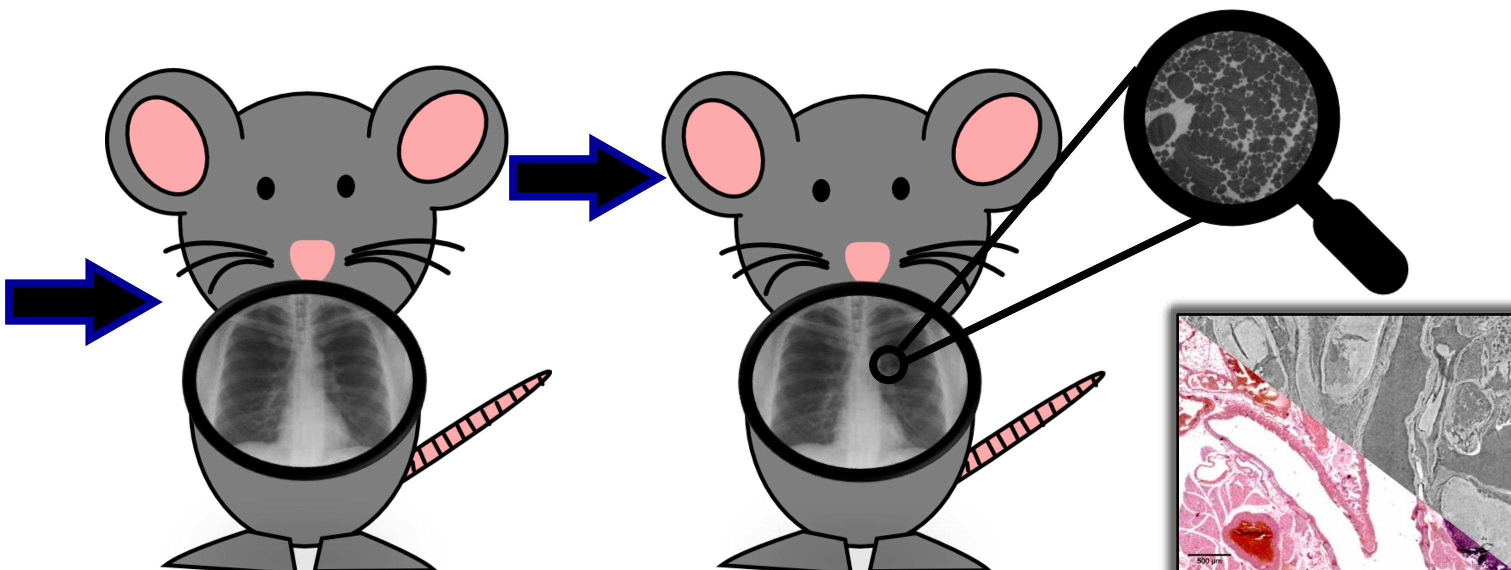

9 µm voxel size overview scan

1-2 µm voxel size region of interest scan

Combined CT / histology analysis

Zoom CT - Visualization of lung methastasis in mice

E = 22 keV,
pixel size = 9 μm
Slice of the entire lung

Lesion produced by cancer cells labeled by Ba np injected in blood stream

Pink beam,
pixel size = 2 μm
Phase retrieval,
δ/β = 1950

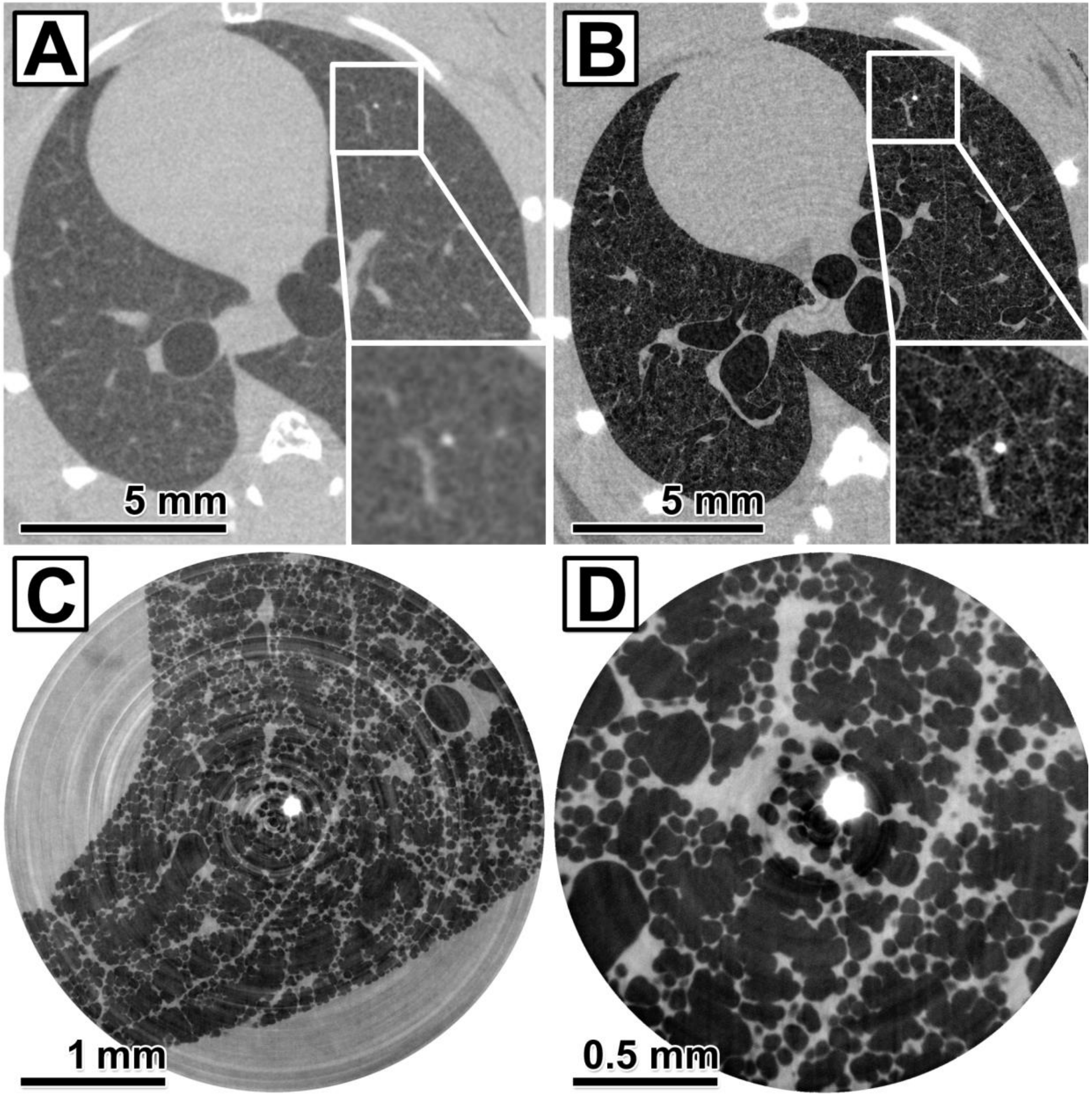

E = 22 keV,
pixel size = 9 μm
Phase retrieval,
δ/β = 1950

Pink beam,
pixel size = 1 μm
Phase retrieval,
δ/β = 1950

(Courtesy of J. Albers)

www.elettra.eu